Investigation of intra-annual glacier velocity and seasonality of White and Thompson Glaciers, Axel Heiberg Island, Nunavut

by

Lauren Samo

A thesis
presented to the University of Waterloo
in fulfillment of the
thesis requirement for the degree of
Master of Science
in
Geography

Waterloo, Ontario, Canada, 2022

Author's Declaration

I hereby declare that I am the sole author of this thesis. This is a true copy of the thesis, including any required final revisions, as accepted by my examiners.

I understand that my thesis may be made electronically available to the public.

Abstract

The Canadian Arctic Archipelago (CAA) is undergoing rapid atmospheric warming at rates that are twice that of the global average and are greater than any other time in the past four millennia. Consequently, changes in glacier behavior are being experienced due to this increase in air temperature, including longer and more intense melt seasons, modifications in glacier motion, and persistent glacier mass loss. To further understand the impacts of this warming trend on glacier flow, this study investigates seasonality and long-term changes in ice motion with a focus on two glaciers: Thompson and White Glaciers on Axel Heiberg Island, with White Glacier containing the longest in situ mass balance record in the Canadian Arctic. This study builds on previous research by creating a dense time series of glacier motion over a ~10-year period (winter 2008/2009 to winter 2021/2022), thus improving upon spatial and temporal resolution of earlier work. The main objectives of this study are to (1) utilize a large catalogue of previously unused SAR (R2 and TSX) data to produce velocity maps of White and Thompson Glaciers, (2) perform a comparison of different SAR datasets and (3) investigate seasonality and long-term changes in velocity structure.

Acknowledgements

I would like to thank Dr. Wesley Van Wychen for his guidance, supervision, support, and encouragement throughout this process. I also greatly appreciate my lab colleagues, Danielle Hallé, Courtney Bayer, Natalija Nikolić and Monika Wagner as they are a wonderful support system.

I would also like to acknowledge and thank Anna Wendleder at DLR for providing the TSX data that will allow for a high spatio-temporal analysis, Luke Copland (University of Ottawa) and Laura Thomson (Queen's University) for providing GPS results, the Canada Foundation for Innovation (John Evans Leadership Fund), the Natural Science and Engineering Research Council of Canada, ArcticNet (Student Travel Fund), Environment and Climate Change Canada (Climate Research Division), the New Frontiers Research Fund and the University of Waterloo.

I would also like to thank my family for their support.

Lastly, I would like to thank my dog, River, for the companionship, moral and emotional support and joy she provided throughout this process.

Contents

List of Figures

List of Tables

List of Abbreviations

AHI	Axel Heiberg Island
asl	Above Sea Level
CA	Canadian Arctic
CAA	Canadian Arctic Archipelago
dGPS	Differential Global Positioning System
ELA	Equilibrium Line Altitude
EM	Electromagnetic
QEI	Queen Elizabeth Islands
R2	RADARSAT-2
SAR	Synthetic Aperture Radar
SLC	Single Look Complex
S1	Sentinel-1
TSX	TerraSAR-X

Chapter One - Introduction

1.0 Introduction

Rapid atmospheric warming is occurring within the Canadian Arctic (CA), with warming rates twice the global average currently being observed (Derksen et al., 2019). This rate of warming is anomalous and is the greatest observed in the past four millennia (Fisher et al., 2012). In particular, warming surface air temperatures, which are amplified in the Arctic, and changes in summer air circulation patterns, are the main driving forces of increases in glacier mass loss in the CA (Fisher et al., 2012). Arctic warming can affect glaciers in key ways, including longer and more intense melt seasons leading to persistent glacier mass loss as well as modifications in glacier motion (Medrzycka et al., 2019). As such, glaciers are important climate indicators, as they respond well to climate forcings - especially smaller glaciers and those at lower elevations which are more sensitive to climate changes compared to larger glaciers (Thomson et al., 2011, Cogley et al., 2011). Given this, having inventories of past glacier dynamics is important for understanding how the current climate is modifying ice motion specifically and glaciers more generally (Cogley et al., 2011).

Over the past few decades, the Canadian Arctic Archipelago (CAA) has experienced a negative mass balance regime (Figure 1-1) which has led to the region becoming the third largest contributor (aside from Antarctica and Greenland) to global sea level rise (Derksen et al., 2019). Additionally, this warming has also led to the retreat of glaciers and decreased velocities due to less movement of ice down-glacier, resulting in the thinning and receding of glacier ice in response to a negative mass balance (Heid and Kääb, 2012; Medrzycka et al., 2019; Thomson and Copland, 2017b). About 26% of glaciers on Axel Heiberg Island (AHI) in the CA (Figure 2-1A) are mountain or valley glaciers, and, as they are smaller, are much more sensitive to a warming climate (Dowdeswell et al., 1997; Thomson and Copland 2017b). As a result of this general warming over the past five decades, glaciers in the CA and alpine glaciers in Canada have experienced thinning due to increased surface air temperatures (Derksen et al., 2019).

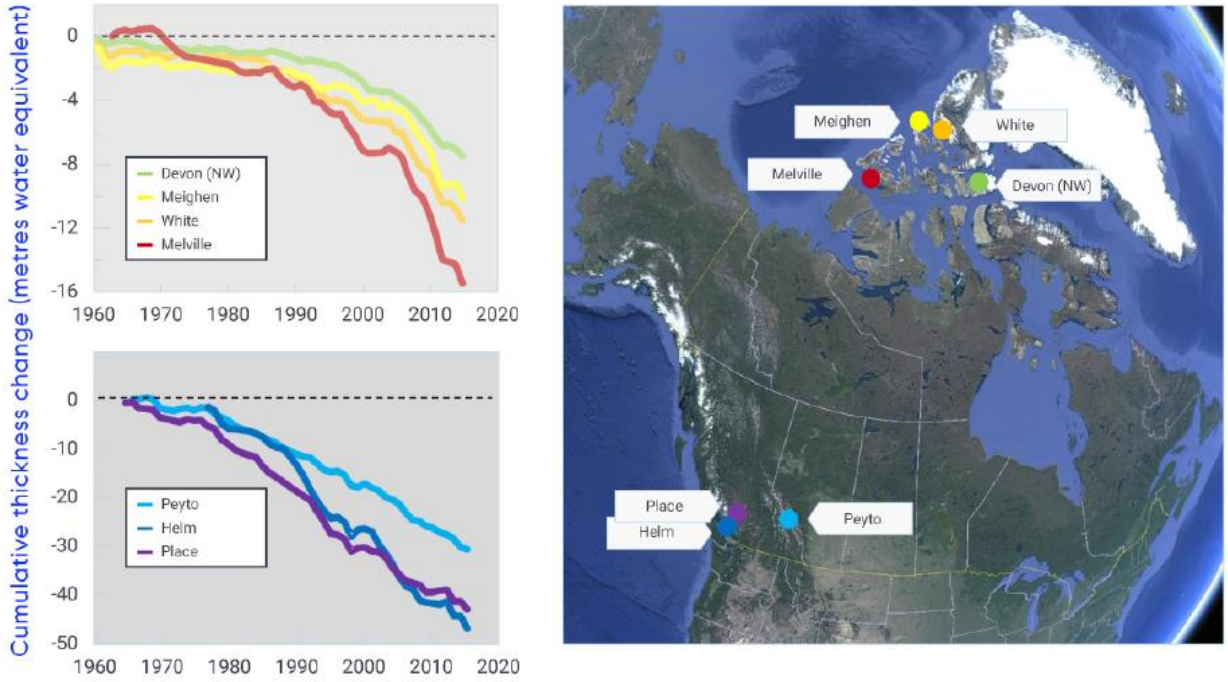

***Figure 1-1**. Changes in ice thickness at long-term glacier monitoring sites across Canada. Graphs of sites in the CAA (top left) and Western Cordillera (bottom left) show changes to a negative mass balance regime, since the 1960s (Derksen et al., 2019).*

In the coming decades, snow cover duration is likely to continue to decline under all current climate scenarios (Derksen et al., 2019). In northern Canadian regions, there are only small changes projected for snow accumulation in the next century which are not expected to counter the expected enhancement in meltwater runoff (Lenaerts et al., 2013; Derksen et al., 2019). Indeed, climate projections that use a moderate climate warming scenario model run until 2100 indicate a persistently negative surface mass balance across the CAA, contributing to a possible rise of 0.35 ± 0.24 mm per year to global sea level rise and the disappearance of smaller ice caps and ice shelves (Lenaerts et al., 2013; Derksen et al., 2019). As such, the current negative mass balance trend that glaciers are currently experiencing is likely to be a long-term trend. Understanding the rate of mass loss is important due to subsequent sea-level rise and other important issues associated with glacier loss, such as; natural hazards for communities, changes in water resources and ecosystems and impacts of calving glaciers on travel by boat in the Arctic.

Müller and Iken (1973) collected in situ data, including annual, winter and summer velocities, melt season duration, ablation and mass balance measurements, from 1959-1969 on a few glaciers on AHI, but had a particular emphasis on White Glacier (Figure 2-1B). This study also collected repeat stake measurements at three different profiles along White Glacier: Upper, Middle and Lower profiles (Müller and Iken, 1973). This research was significant in the field of glaciology as it was the first to identify

seasonality of an Arctic glacier, since it was previously accepted that glacier movement in polar regions was constant throughout the year and that seasonal variations only occurred on alpine glaciers. This seminal research that measured surface movement, ablation and run-off of a large part of the ablation zone on White Glacier and its findings on the impact of meltwater on velocity fluctuations is further discussed in section 3.3.

More contemporary research of ice flow in the CA has largely used remote sensing data (optical and radar data) or limited in situ data to determine variability in glacier velocities within the Canadian Arctic. These studies have been useful to identify glacier surging (a cyclical dynamic instability that causes a drastic increase in glacier velocity for a short period of time; further discussed in section 3.4), quantify ice motion from year to year (Van Wychen et al., 2016; Thomson and Copland 2017a) and measure seasonality in ice flow (Williamson et al., 2008).

Previous research that has investigated interannual change of glacier velocities in the Arctic has primarily relied on only a single set of Synthetic Aperture RADAR (SAR) image pairs to represent an entire year of ice motion and largely neglected any investigation of seasonality (Van Wychen et al., 2014; 2016; 2021). These results allowed for the detection and quantification of changes in ice dynamics at annual time steps, with some glaciers in the CAA undergoing cyclic surge-type flow, newly identified pulse-type flow and the constant acceleration of Trinity and Wykeham Glaciers (located outside of AHI; Figure 1-2; Van Wychen et al., 2016). Figure 1-2 shows glaciers that experienced a change in velocity structure as well as the classification type of the glaciers in the study. Van Wychen et al. (2020), showed that, in the CAA, dynamic variability is much more widespread compared to what was previously thought. However, research that specifically investigates variability of ice motion that occurs within a year (i.e. intra-annual variability) remains relatively sparse. Previous research that has investigated seasonality in the Canadian Arctic primarily using remote sensing methods includes:

Williamson et al., (2008) that studied temporal changes in calving rates on Ellesmere Island;
Van Wychen et al., (2016; 2017) that investigated intra-annual changes in ice dynamics, and;
Dalton et al., (2022) that studied seasonal and multiyear dynamic variability.

Williamson et al. (2008), found that four of the tidewater glaciers studied experienced a major increase in velocity during the summer months compared to the annual velocities. Van Wychen et al. (2016) found that the winter velocities of glaciers in the study were lower than annual velocities. Van Wychen et al. (2017), showed that many of the smaller, land terminating glaciers showed no significant

change (>20 m a^{-1}) in motion, but larger glaciers experienced a decrease in mass flux between years. The most recent study that explored seasonality, Dalton et al. (2022), focussed on the processes controlling glacier motion and ice discharge, with findings suggesting that temporal variability is controlled by subglacial topography and surface meltwater flux to the glacier bed and the possibility of a dynamic switch between seasonal flow and flow dominated by dynamic thinning in response to external forcings, particularly for Trinity and Wykeham glaciers. Collectively, these papers do capture seasonality but have focused on larger, tidewater terminating glaciers and there is a gap in research when it comes to investigating seasonality on smaller, land terminating glaciers using remote sensing methods, like White and Thompson Glaciers on AHI.

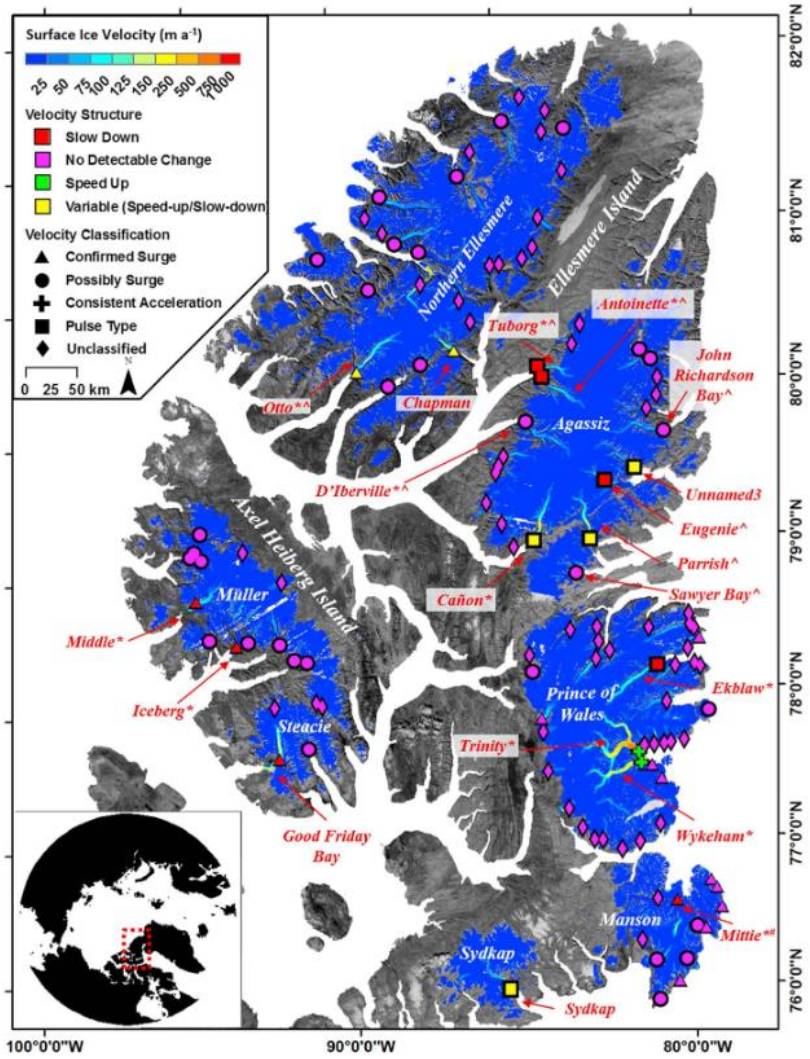

Figure 1-2. *Distribution of velocity classifications and dynamic changes over the QEIs. Asterisk indicates glaciers with previously derived velocities from Short and Gray (2005), circumflex accent from Williamson et al., (2008), and pound from Copland et al., (2003). (Figure from Van Wychen et al., 2016).*

Additionally, now that R2 data that has been used in previous research (Van Wychen 2014; 2016; 2021) is no longer readily available for glacier velocity research in the Canadian Arctic, a new dataset will need to be used for continuing the long-term record of glacier ice motion and research of glacier dynamics in the CA. As such, the comparison of the results derived from different SAR datasets is important as the results of this research will determine if data from the European Sentinel-1 (S1) or TSX missions can provide the same information as R2 and if there is any data loss due to the lower spatial resolution products. S1 is an openly available SAR data product that can provide long-term continuous year to year monitoring of glacier motion. However, a comparison must be performed to determine if any major differences between the outputs exist and if the products can be used interchangeably. Furthermore, over the last two years, a large archive of TSX data over Thompson and White Glaciers has been collected, which will allow for a comparison between the TSX and R2 derived velocity results and provides an opportunity to compare the results derived from these two datasets.

1.1 Research Objectives

Given all this background, this project will utilize a large catalogue of under-utilized TSX and R2 SAR datasets to complete an intercomparison of the velocity products derived from a variety of different SAR image inputs and then use the outputs from this effort to investigate how glacier motion of Thompson and White Glaciers on Axel Heiberg Island have evolved (with a specific emphasis on seasonality) over the last decade, during a period of significant mass loss in the Canadian Arctic. As such, the main research objectives of this project are as follows:

1. 'Rescue' a large catalogue (71 images) of Synthetic Aperture RADAR (R2 and TSX) datasets and process these to a dense record of velocity maps for Thompson and White Glaciers over the 2008 – 2022 period;
2. Provide an assessment of different SAR datasets for deriving glacier motion of Thompson and White Glaciers on Axel Heiberg Island (R2 vs S1 vs TSX);
3. Use the derived velocity data (created to satisfy objective 1) to investigate long-term and shorter-term (seasonality) variability of ice motion for Thompson and White Glaciers on Axel Heiberg Island and explore the drivers of these changes.

Seasonality, in the context of this study, refers to how glacier motion evolves throughout the year, or how it follows the seasons. In the future, it is anticipated that the results of this research will be openly

available to facilitate future research and upon the completion of the project will be placed in the Polar Data Catalogue for long-term preservation and dissemination.

1.2 Thesis Structure

This thesis follows a traditional thesis formatting and consists of six chapters. The first chapter introduces this research and provides motivation for the work. Chapter 2 provides background to the study site, Chapter 3, provides a literature review relevant for understanding how glacier velocities vary over time and Chapter 4 provides the methodology used in this research. Chapter 5 provides the results and discussion of how the research satisfies the main objectives, and lastly, Chapter 6 recaps the main findings and discusses the significance of this research.

Chapter Two – Study Site

2.0 Axel Heiberg Island

Axel Heiberg Island is located in the Canadian Arctic Archipelago and, along with Devon Island and Ellesmere Island, makes up the Queen Elizabeth Islands (QEI; Figure 2-1 inset). Excluding Antarctica and Greenland, the QEI contains approximately 14% of global glacier and ice cap mass (Sharp et al. 2014). AHI is covered by close to 35% permanent ice, while the remaining area is mostly bare ground. The island has over 1,100 glaciers, covering an area of ~11,700 km^2 (Thomson et al., 2011). These glaciers range from large outlet glaciers to smaller niche glaciers, with the majority of the glacierized area (55%), drained by outlet glaciers (Ommanney, 1969; Thomson et al., 2011). AHI has two major ice masses, Müller and Steacie Ice Caps, as seen in Figure 2-1. Climatically, AHI receives around 200 mm of precipitation annually, with little variation between years and has a regional mean annual temperature of around -20˚C (Sharp et al., 2011). The CAA experiences short, cool summers and longer, colder winters that allow for glacier formation and persistence (Van Wychen et al., 2020). The cooler temperatures combined with lower atmospheric moisture conditions do not create optimal conditions for input, via precipitation, to these glacier systems and the little snow accumulation received by these glaciers does not vary much interannually (Sharp et al., 2011).

Glaciological research started on the island in 1959 and was led by Fritz Müller of the McGill University Arctic Research Expedition. At this time, an in-situ mass balance program was initiated and is still ongoing (Thomson and Copland, 2017b). There is an Arctic research station in Expedition Fjord, which supports ongoing glaciological research which measure annual and seasonal velocities, mass balance and other variables (Cogley et al., 2011; Thomson and Copland, 2017a). The first glacier inventory of AHI which used aerial photographs collected between 1958 and 1959 was created by Ommanney (1969) and a large-scale inventory of surge-type glaciers, based on the analysis of imagery from 1959/60 and 1999/2000 identified three surge type glaciers on AHI: Iceberg, Good Friday Bay and Airdrop (also known as Middle) Glacier (Figure 2-1; Copland et al., 2003). Overall, the glaciers of AHI have experienced a negative mass balance and during the 42-year study period of Thomson et al.'s (2011) study, 90% of smaller ice masses, with an area less the 0.2 km^2, completely disappeared.

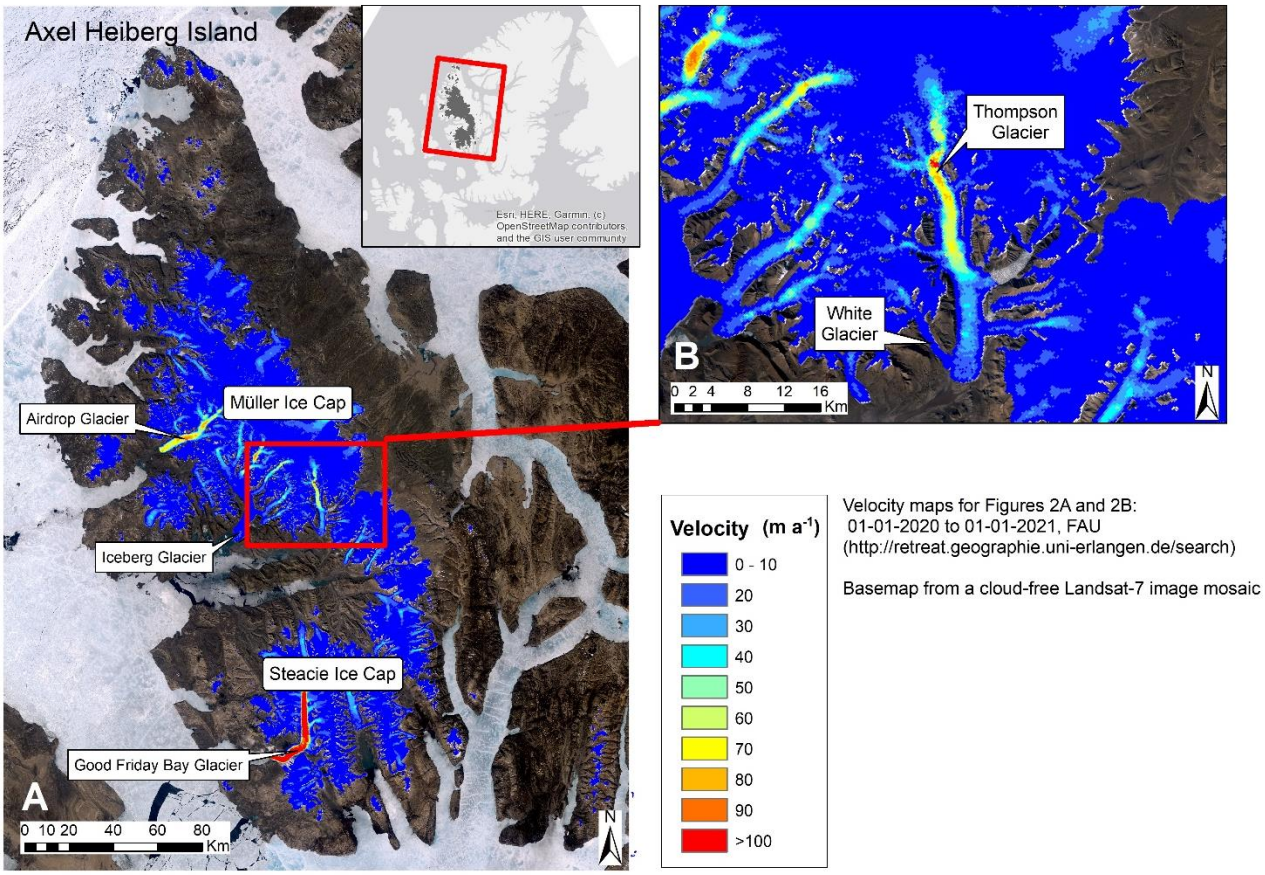

Figure 2-1*. Glacier motion on AHI using pre-derived yearly mosaic from the FAU portal. The velocity values represented in the legend are the same for both A and B. The inset map on the upper right of A, shows the location of AHI in the CA in relation to the QEIs. The velocity maps of A and B are on a cloud-free Landsat-7 image mosaic.*

2.1 White and Thomson Glaciers

White and Thompson Glaciers are two of the most intensely studied glaciers on AHI and within the Canadian Arctic as a whole. Both glaciers are centrally located on the island, in the Expedition Fjord area (Figure 2-1B). Thompson Glacier is one of the largest outlet glaciers on Müller Ice Cap. It is ~35 km in length and ~3 km wide along the main trunk and terminates on land. The glacier extends from ~140 m a.s.l. at the tongue to ~1400 m a.s.l. into the ice cap. Earlier studies (Ommanney, 1969; Müller and Iken, 1973) of these glaciers provide a baseline of glacier dynamics, before a negative mass balance trend, for current and future research.

White Glacier has an area of 38.7 km^2 and extends about 15 km in length (Cogley et al., 1996). The glacier's thickness ranges between 200 m and 400 m, spans between 100-1800 m a.s.l. and has a glacier tongue ~1 km wide (Cogley et al., 1996; Thomson and Copland, 2017a). The equilibrium line altitude (ELA) rose from around 1000 m a.s.l. in the 1960s to 1270 m a.s.l. between 2006 and 2015 (Thomson and Copland, 2017a). White Glacier is a polythermal glacier, with a cold upper shell and a temperate ice zone near the glacier bed (Cogley et al., 1996, Thomson and Copland, 2017a). The peak velocity magnitude and duration of White Glacier has evolved since the 1960s at all three profiles, mostly associated with basal sliding (Thomson and Copland, 2017a). White Glacier is of particular interest in the glaciological community, as it is the first location where evidence of seasonality in ice motion of a high Arctic glacier was observed (Müller and Iken, 1973). Cogley et al. (2011), with over 50 years of mass balance observations, shows a negative mass balance of White Glacier that started in the 1970s.

In general, land terminating glaciers in the Arctic follow a general pattern of slow velocities extending from the ice cap interior or accumulation basin area, of < 20 m a^{-1}. This slow flow is due to the cold glacier bottom being frozen to the bed, so the movement is solely by internal deformation (Short and Gray, 2005; Van Wychen et al., 2016). Van Wychen et al. (2016), found that in the Canadian Arctic most land terminating glaciers did not exceed 75 m a^{-1}, while tidewater terminating glaciers did not exceed 400 m a^{-1}, with exceptions of glaciers exceeding this velocity located elsewhere and not on AHI. Increased velocity along the main trunk typically indicates changes in bedrock topography, sediment type or thermal regime – from cold to warm based. Both Thompson and White Glaciers conform with this expected velocity structure of land terminating glaciers in the CA and neither glacier has been previously identified as surge type (described in Chapter 3).

Thompson and White Glaciers were selected as the glaciers of interest for this study because of an extensive catalogue of R2 and TSX data that has been collected over these two glaciers since 2008, which can be used to derive an extensive record of glacier flow rates. In addition to this, there is available

in situ (dGPS) data that can be used in comparison with the SAR data used in this study for White Glacier. Finally, previous research that has investigated seasonality has heavily studied large glaciers that were typically tidewater terminating. White and Thompson are considered small and medium sized glaciers, respectively, and thus represent an opportunity to determine if the seasonality of smaller, land terminating glaciers can be derived only using remote sensing data. Despite its small size, White Glacier has been the focus of many studies since the 1960s and there is the previous benchmark of data that can be used from Müller and Iken's work (Müller and Iken, 1973). Although Thompson Glacier has not been studied as extensively as White Glacier, there is still contemporary research that have investigated this glacier (for example Van Wychen et al., 2016; 2020).

Chapter Three – Literature Review

This chapter provides the relevant background necessary regarding glacier mass balance, glacier dynamics and the causes of fluctuations on glacier dynamics at both seasonal and multi-annual scales. It will also specifically discuss glacier hydrological changes throughout the year and the impacts that this has on glacier velocity (seasonality). Glacier surging (i.e. multi-annual changes in glacier dynamics) will also be briefly discussed, although this mechanism is not known to play a part in the dynamics of White and Thompson Glaciers, however, it is a process that is known to occur for other glaciers on AHI. Finally, a review of SAR remote sensing will be provided (a full description of how SAR data is utilized in this study is provided in the methodology chapter).

3.1 Glacier Mass Balance

The 'health' of a glacier can be determined by the measurement of its mass balance (Koerner, 2005). Mass balance is the difference between the accumulation (different forms of precipitation, rime and redistribution processes like wind-blown snow and avalanching) and ablation (melt, evaporation, sublimation, and removal of snow through wind and avalanching, with calving and sub-aqueous melt playing an important role for tidewater glaciers) processes (Figure 3-1; Benn and Evans, 2010). A positive mass balance means that more accumulation occurred than ablation, while a negative mass balance means more ablation occurred. Typically, positive mass balances over a long period of time means that glaciers become thicker and advance, while persistent negative mass balances mean that glaciers thin and retreat. Within the CA, accumulation (largely snowfall) mainly occurs during the winter season and ablation (largely driven by surface melt and run-off) mainly occurs during the short summer season (Koerner 1979; Van Wychen et al., 2020). Mass is gained throughout the winter season and is at its maximum in the spring before the melt season starts, with the strongest melt occurring between June and August (Benn and Evans, 2010).

The amount of precipitation an area receives depends on its proximity to a moisture source, with the primary moisture source of the CAA being Baffin Bay and the Arctic Ocean acting as a secondary moisture source (Koerner 1979; Van Wychen et al., 2020). In the Canadian Arctic, ice masses typically form closer to the moisture source and in areas with higher elevation with the largest amounts of snowfall occurring in more maritime regions (Van Wychen et al., 2020). The largest amounts of snowfall occur in maritime regions, where there is a higher moisture content in the air compared to colder, drier polar regime of the CA. This results in most glaciers on AHI forming on the west coast of the Island (Sharp et al., 2014). Mass balance can be measured or inferred in several ways, including: direct measurements that

are extrapolated over large areas, hydrological methods, geodetic methods, and gravimetric methods. Direct or glaciological measurements are from field measurements of accumulation and ablation (Benn and Evans, 2010). Hydrological methods use components of the annual water balance, such as precipitation, runoff and evaporation, to calculate the net balance for smaller glaciers < 10 km^2 (Benn and Evans, 2010). The geodetic method uses aerial photographs or satellite data to calculate changes in ice volume which are then converted to mass. Limitations of this method come from the unknown of changing snow and ice densities (Benn and Evans, 2010). The newer gravimetric method uses Gravity Recovery and Climate Experiment (GRACE), which takes direct mass measurements from space and can detect seasonal variations but with relatively coarse resolution (Benn and Evans, 2010).

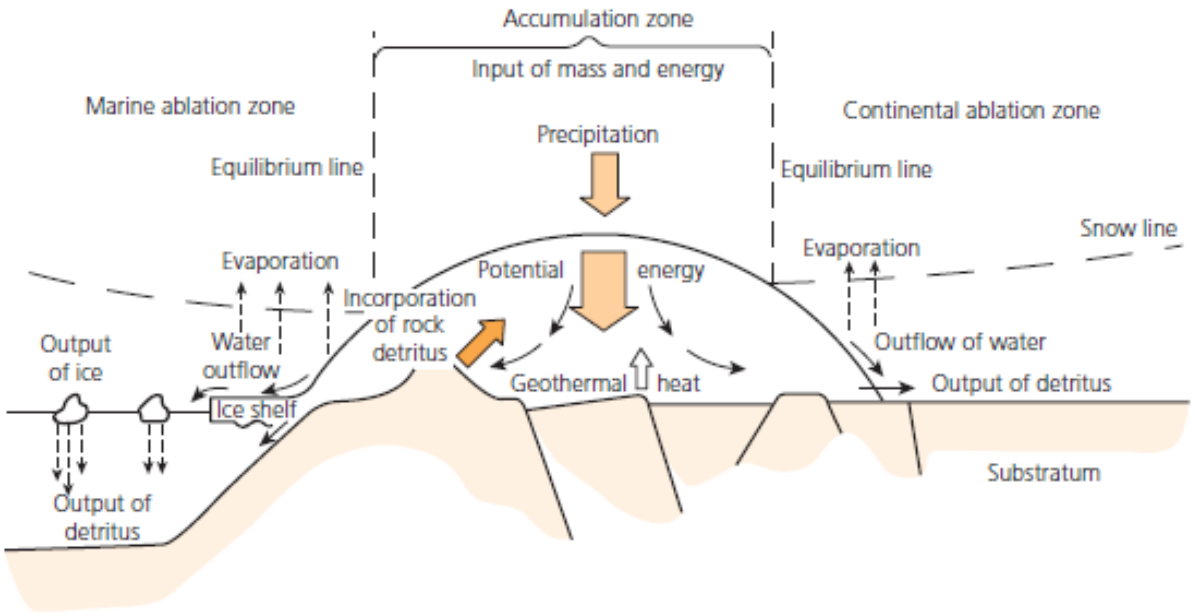

***Figure 3-1**. Accumulation and ablation zones of glaciers (Benn and Evans, 2010).*

AHI, along with the rest of the CA, is experiencing an overall negative mass balance (Derksen et al., 2019; Thomson et al., 2011). White Glacier has been experiencing a negative mass balance since the 1970s; with a -175 w.e. m a^{-1} mass loss rate that increased to -580 w.e. m a^{-1}, between 2005/06 and 2008/09 (Cogley et al., 2011). Thinning and retreat of these glaciers due to the negative mass balance is occurring, with current mass loss being dominated by surface melt and runoff (Van Wychen et al., 2014). Between 1948 and 1995, White Glacier experienced thinning, narrowing and a retreat of 250 m (Cogley et al., 1996).

3.2 Glacier Dynamics

As glaciers have significant mass, they flow under their own weight via a process called 'ice creep' (the internal deformation between ice crystals due to stress of the mass of the ice), with ice moved from higher areas of accumulation to lower areas of ablation (Benn and Evans, 2010; Figure 3-1). In addition, glaciers can also move by a process called 'bed deformation' whereby the bed on which the glacier sits deforms allowing it to move or through a process called 'enhanced flow' which is the sliding of ice overtop its bed (Chandler and Evans, 2021). Many factors influence flow rate, like temperature, debris content of ice, bed topography and water pressure, although a lot is still unknown as it is difficult to obtain information from within and below a glacier (Benn and Evans, 2010). As basal sliding is important for seasonal changes in ice motion and is controlled by water inputs, glacier hydrology is therefore important and reviewed in Section 3.3. The main processes of White and Thompson Glaciers are ice creep and basal sliding (Thomson and Copland, 2017a).

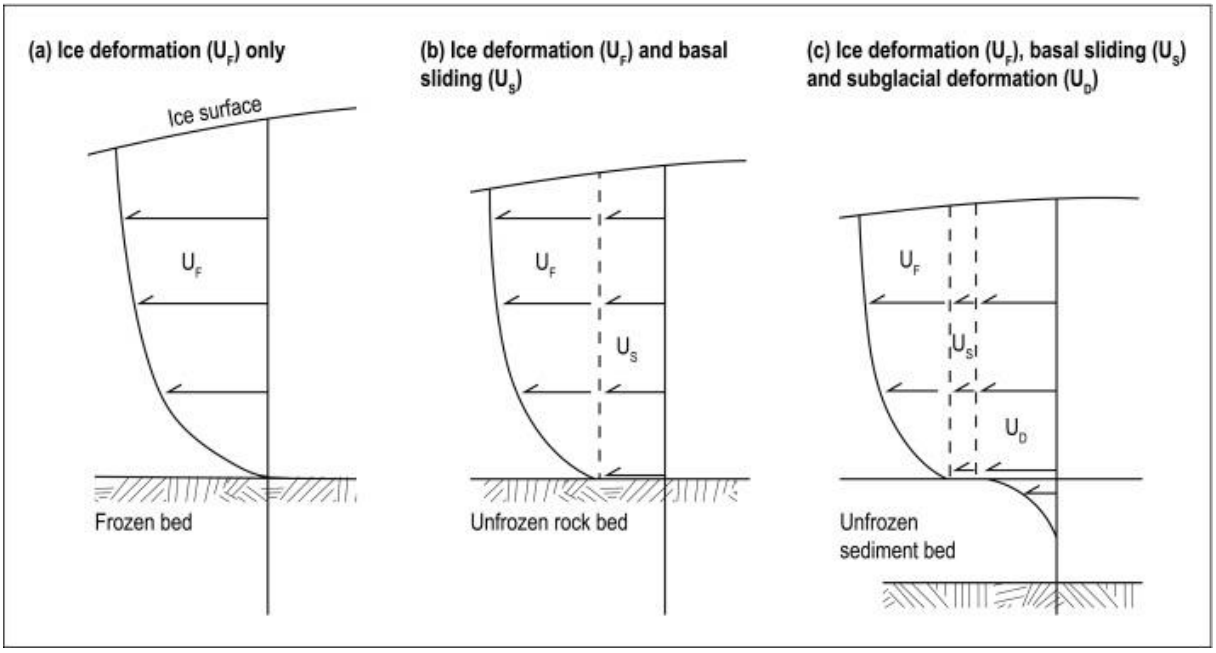

Figure 3-2. *Schematic diagram that shows the vertical distribution of velocity based on the different types of glacier motion. (A) Ice deformation alone. (B) Ice deformation and basal sliding. (C) Ice deformation, basal sliding and subglacial deformation together. (From Chandler and Evans, 2021).*

3.2.1 Ice Creep

Ice creep, the movement within and between ice crystals, can occur along cleavage planes, or weakened planes due to the crystalline structure or along crystal defects, causing recrystallization at

crystal grain boundaries (Benn and Evans, 2010). The rate of this internal deformation of ice crystals can change due to temperature and other influencing factors like water content, ice crystal size and orientation and the presence of impurities (Benn and Evans, 2010). Water content is usually highest close to the glacier bed, where the ice is also usually the softest. Stress is also greatest at this ice bed interface, impacting flow rates and dynamics of glacier ice (Benn and Evans, 2010). Deformation occurs much more easily along cleavage planes, particularly when cleavage planes are aligned parallel to the shear stress (Benn and Evans, 2010). Impurities that can be found in glacier ice are dissolved ions, gas bubbles and solid materials (i. e. rock particles). The type of impurity that is present can have different effects, like hardening or softening the ice, or having no impact (Benn and Evans, 2010). The velocity from ice creep is a gradient due to the cumulative effect of strain rates. The velocity is zero along the bed and increases with height from the bed (Benn and Evans, 2010; Figure 3-2A). The increase in velocity is more drastic closer to the bed to due to higher pressure and velocity gradient lessens closer to the surface of the glacier (Figure 3-2A). Importantly, ice creep is present in all glaciers, unlike bed deformation and basal sliding.

3.2.2 Basal sliding and bed deformation

Basal sliding occurs when the presence of water, as a thin film, at the glacier bed reduces friction between glacier ice and the bed, facilitating glacier motion. Water from surface melt that enters the ice-bed interface through the englacial system (section 3.3) can contribute to an increased velocity. Subglacial melting of water, when ice reaches its pressure melting point, can be another water source that contributes to basal sliding. If the bedrock topography is irregular, a high point along the bed, can also cause ice to compress, introducing pressure and allowing ice to reach its pressure melting point. The water created will help the glacier ice get over the obstacle and once the ice has passed over it, regelation occurs, refreezing, as the pressure lifts and the meltwater continues down-glacier (Chandler and Evans, 2021). Figure 3-2B displays the impact on velocity from the combination of creep and basal sliding.

Some glaciers sit atop unlithified sediments or poorly consolidated sedimentary rocks. These softer glacier beds can deform as a response to the stress from the weight of the overlying glacier, playing a role in glacier ice velocity. Till deformation is much more complex than what was found in initial studies that explored till rheology (Benn and Evans, 2010). Shear strength, effective pressure and voids ratio are three variables that can be used to describe till deformation. Water content is an important factor in bed deformation if the glacier bed is unlithified sediment. Figure 3-2C shows the combination of the three types of motion and the impact on velocity.

3.3 Seasonality in Glacier flow

The change from efficient to inefficient hydrological glacial drainage networks typically occurs cyclically, with the seasons. Research as early as the 1960s linked seasonal changes in hydrology with increased glacier velocities in the Canadian Arctic (Figure 3-3; Cress & Wyness, 1961; Müller and Iken, 1973; Van Wychen et al., 2020). The connection between surface melt and ice motion leads to a greater surface velocity with the start of a melt season, like two times greater on Sverdrup Glacier on Devon Ice Cap (Cress & Wyness, 1961; Van Wychen et al., 2020). Sharp et al., (2009), notes that seasonal penetration of surface meltwater to the glacier bed is a key driver of changes in seasonal velocity. Danielson and Sharp (2013), linked seasonal velocity variations to surface melt and showed that rapid lake drainage can lead to a short-term increase in velocity.

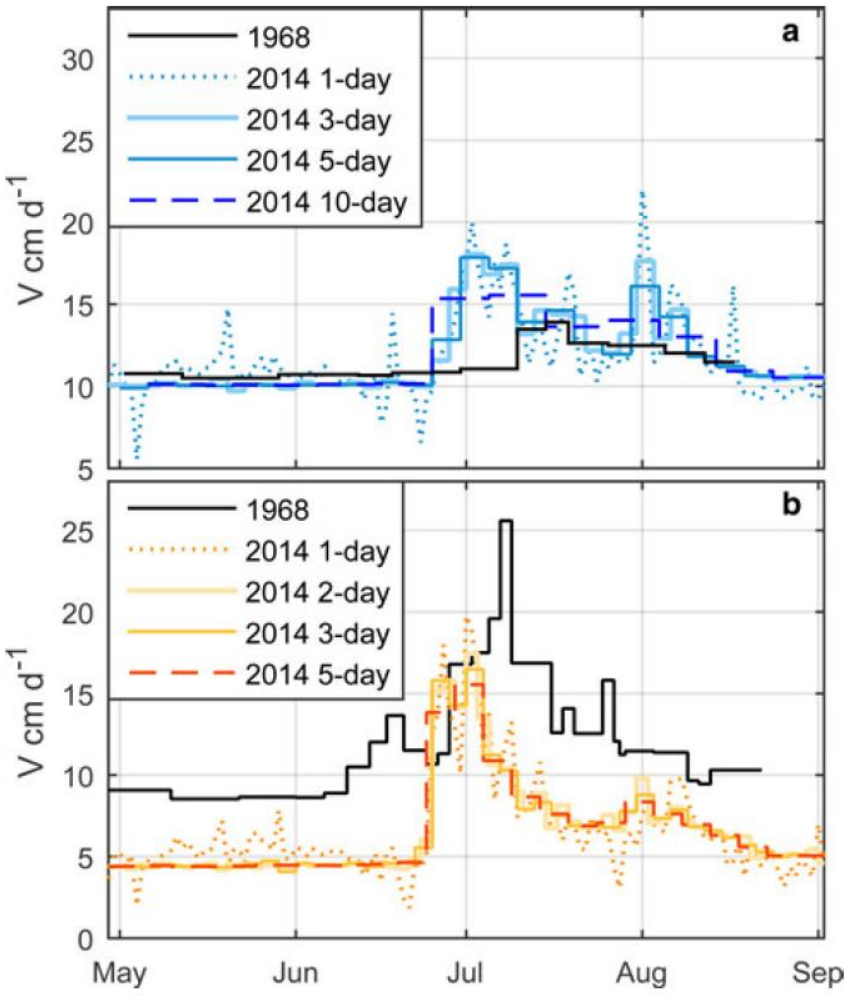

***Figure 3-3**. Comparison of recent (Thomson and Copland, 2017a) and earlier (Iken, 1974) velocity profiles at the upper (870 m a.s.l.) and lower (370 m a.s.l.) transects on White Glacier (Thomson and Copland, 2017a).*

As summer velocities and net summer displacement are influenced by the duration of the melt period (Thomson and Copland, 2017b), it is expected that in the future, basal motion in the summer will become a main factor in the total glacier motion at White Glacier (Thomson and Copland, 2017a). As the ice thins, there will be less pressure and likely less internal deformation, or ice creep, causing the ice to stagnate. If this occurs, the efficient drainage network that appears in the summer may persist through the winter, resulting in less basal sliding the following summer (Thomson and Copland, 2017a). This process has already been proposed as altering the dynamics of White Glacier.

Müller and Iken (1973) collected in situ data over a decade, from 1959-1969, in the ablation area of glaciers at different time intervals: short, medium intervals and annual or seasonal, with White Glacier being the main glacier of interest. Previously, it was thought that Arctic ice masses moved at a constant velocity throughout the year. Over a daily period, researchers concluded a connection between glacier motion and water input that caused the observed variations. Longer term, seasonal changes mostly occur due to changes in ice mass thickness and are also affected by changes in the longitudinal stress (Müller and Iken, 1973). Longitudinal stress is how the glacier is pushed or pulled due to internal force in relation to the direction of flow (Benn and Evans, 2010). It was concluded that, during the summer months, the frequency and amount of melt water are the most important controls on glacier movement (Müller and Iken, 1973). The distribution of melt over time is also important. For example, if there are fewer but larger melt events in the summer, this would result in a greater change in velocity than constant meltwater discharge throughout the summer, which is related to the water pressure in melt channels (Müller and Iken, 1973). At the beginning of the melt season, it will take more time for surface melt to make its way to the glacier bed compared to later in the melt season, when channels that route water from the surface, through the englacial system, are well established (Müller and Iken, 1973). Müller and Iken (1973) also concluded that alpine glaciers considered to be of medium and large sizes are not frozen to the glacier bed during the summer months. Müller and Iken's (1973) research on AHI was the first time seasonality of an Arctic glacier was identified, observing changes in velocity on both shorter (days) and longer (weeks to months) timescales. Thomson and Copland (2017a) revisited the work of Müller and Iken's (1973) with more in situ data and dual frequency differential GPS (dGPS), observations (Figure 3-3). Thomson and Copland (2017a) compared their results from the summers of 2013-2015, to previous observations and their results showed that the glacier had thinned over 20 m and had a decreased annual surface velocity by 15-35%. Almost half of the total annual displacement of White Glacier occurs in less than 2 months during the summer (Thomson and Copland, 2017a).

3.4 Glacier Hydrology

Water is a key control in glacier movement for glaciers experiencing basal sliding because it reduces friction at the glacier/bed interface and promotes motion. As such, a review of glacier hydrology is necessary to understand how hydrology causes variations in glacier sliding (Figure 3-4). There are three major components (Figure 3-5) of glacier hydrology:

1) the supraglacial network (the flow and storage of water on the glacier surface),
2) the englacial network (the flow and storage of water within the glacier),
3) and the subglacial network (the flow and storage of water beneath the glacier).

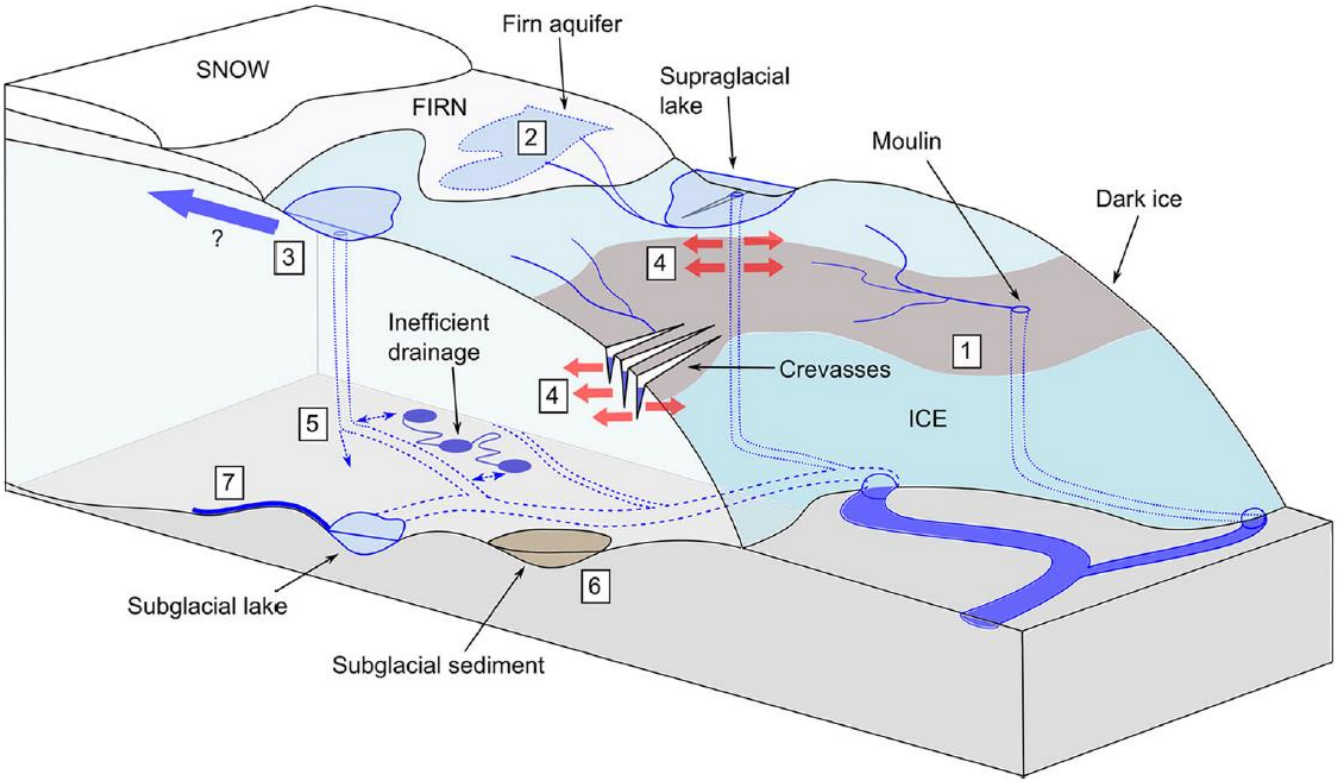

Figure 3-4*. Three major components of glacier hydrology: supraglacial, englacial and subglacial hydrology networks (Nienow, et al., 2017).*

The supraglacial hydrological system can both store and drain water. If the surface is snow covered, meltwater can percolate down into the snowpack and refreeze – releasing latent heat while forming in ice lens, or superimposed ice (Nienow et al., 2017). Latent heat release can increase the temperature of the snowpack to above the melting point temperature, if this occurs, refreezing stops, and the meltwater accumulates in firn aquifers (Nienow et al., 2017). Some of this water may drain laterally until surface channels form (Nienow et al., 2017). Glacier ice acts as an impermeable solid, as such, if the

surface is bare ice, meltwater travels over the surface, either through sheet flow or surface channels. Supraglacial channels can meander and are influenced by englacial structures (i. e. crevasses, moulins, etc.) and foliation and can sometimes form channel networks (Nienow et al., 2017).

The englacial system is a network that can transport surface meltwater through the glacier to the ice-bed interface. Glaciers in the High Arctic have efficient channels that can cause dynamic responses to surface melt (Müller and Iken 1973; Danielson and Sharp, 2013). Channels can form by cut and closure, hydrologically enhanced ice fracturing and the use of pre-existing structures. For cut and closure channels to form, the rate of incision downwards needs to be greater than the ablation rate of the surrounding ice. As the channel continues to cut down from the movement of meltwater, roof closure can occur above the level of the water due to ice creep (Benn and Evans, 2010). Water filled crevasses can lead to water transport through a glacier; enough water can cause the crevasse to extend down towards the bed through a process called hydro-fracturing. Hydro-fracturing requires a substantial amount of water and glacier ice that is subject to tensile stress (Benn and Evans, 2010). Glacier lakes are commonly associated with hydro-fracturing. This process allows for the rapid transport of surface meltwater to the bed in both temperate and polythermal glaciers (Benn and Evans, 2010). Water can also move upwards through the glacier towards the surface if the water is under enough pressure. This upwards hydro-fracturing is common along glacier beds where there is a change from warm to cold ice in polythermal glaciers (Benn and Evans, 2010). Movement of water through a glacier can also occur with pre-existing structures, like debris. Water can flow along the debris, a more permeable pathway unlike impermeable glacier ice. As the water flows, the conduit becomes larger, allowing more water to pass to the glacier bed – a positive feedback loop of increased water flow and a larger conduit for that water to flow through. When the amount of water diminishes, the channel will begin to close due to the decreased water pressure (Nienow et al., 2017).

The state of the subglacial system is important as this is what has the most impact on glacier velocity, although input and drainage of water from the supraglacial through the englacial system is a key component in delivering water to the glacier bed to facilitate basal sliding. There are two classes of subglacial drainage systems:

1) channelized or efficient systems and,

2) distributed or inefficient systems.

With efficient systems, water moves through and out of the system quickly due to well developed drainage channels (Röthlisberger, Hooke or Nye channels or tunnel valleys) underneath the glacier (Figure 3-6). As a consequence of this, when an efficient drainage network is present there is little impact on glacier velocities because the amount of sliding is negligible (Nienow et al., 2017). Alternatively, when an inefficient drainage network is present under a glacier, water moves over a larger part of the bed in a slow and torturous manner (Figure 3-6; Nienow et al., 2017). In these situations, fluctuations in the amount of water underneath the glacier has a large impact reducing basal friction and facilitating glacier sliding.

A glacier typically switches between these two different subglacial systems over time, generally through the summer as the melt season progresses. At the beginning of the melt season, the glacier tends to have an inefficient subglacial system as channels can close over the winter due to decreased water

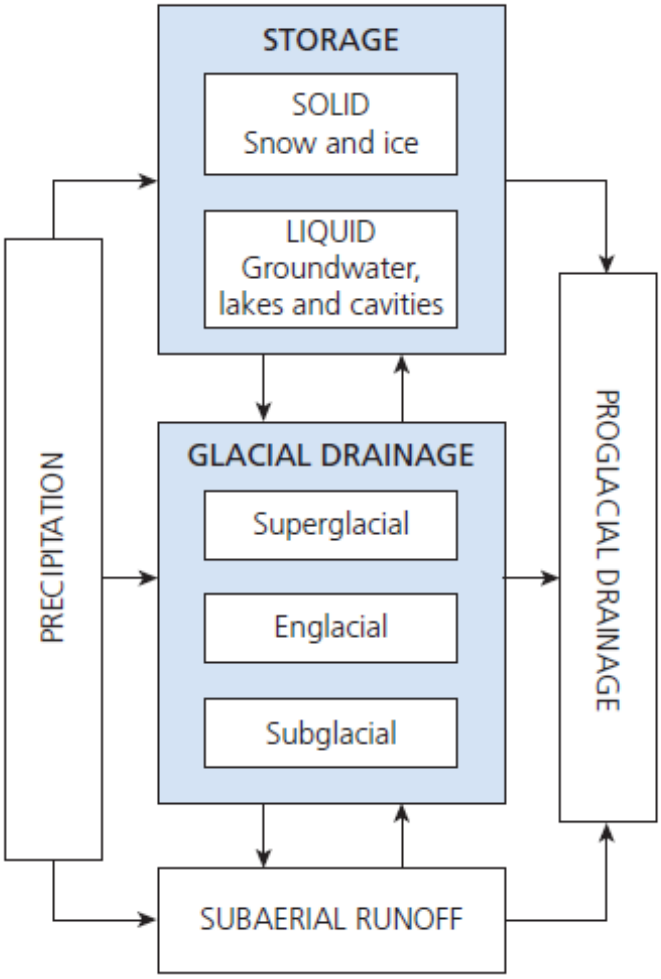

Figure 3-5. *Water routes, sources, and storage in a glacier system (Benn and Evans, 2010).*

pressure and the overburden mass of the glacier closes in these conduits. However, as air temperatures rise in the summer, more melt water is produced at the glacier surface and then transferred from the glacier surface, through the englacial system and to the glacier bed. When this occurs and the water is delivered to a subglacial drainage network that is inefficient, basal friction is reduced, thereby allowing glacier sliding to occur. Essentially, water acts as a lubricant, reducing friction and allowing faster movement of the ice down-glacier. Typically, the greatest amount of sliding occurs in the lowermost portion of the glacier as this is where melt occurs first and is where most meltwater drains to. As the melt season progresses and increasingly large amounts of water are transferred to the glacier bed, the subglacial system will switch from an inefficient system to an efficient as channels are preferentially created, thereby allowing water to move through the system more easily. In this situation, the water pressure underneath the glacier diminishes, basal sliding correspondingly slows or ends, and glacier velocities will be reduced (Nienow et al., 2017). These processes imply that there will be a seasonal change in glacier flow rates as a direct result of changes in melt that is delivered to the bed and the state of the subglacial drainage network through the ablation season.

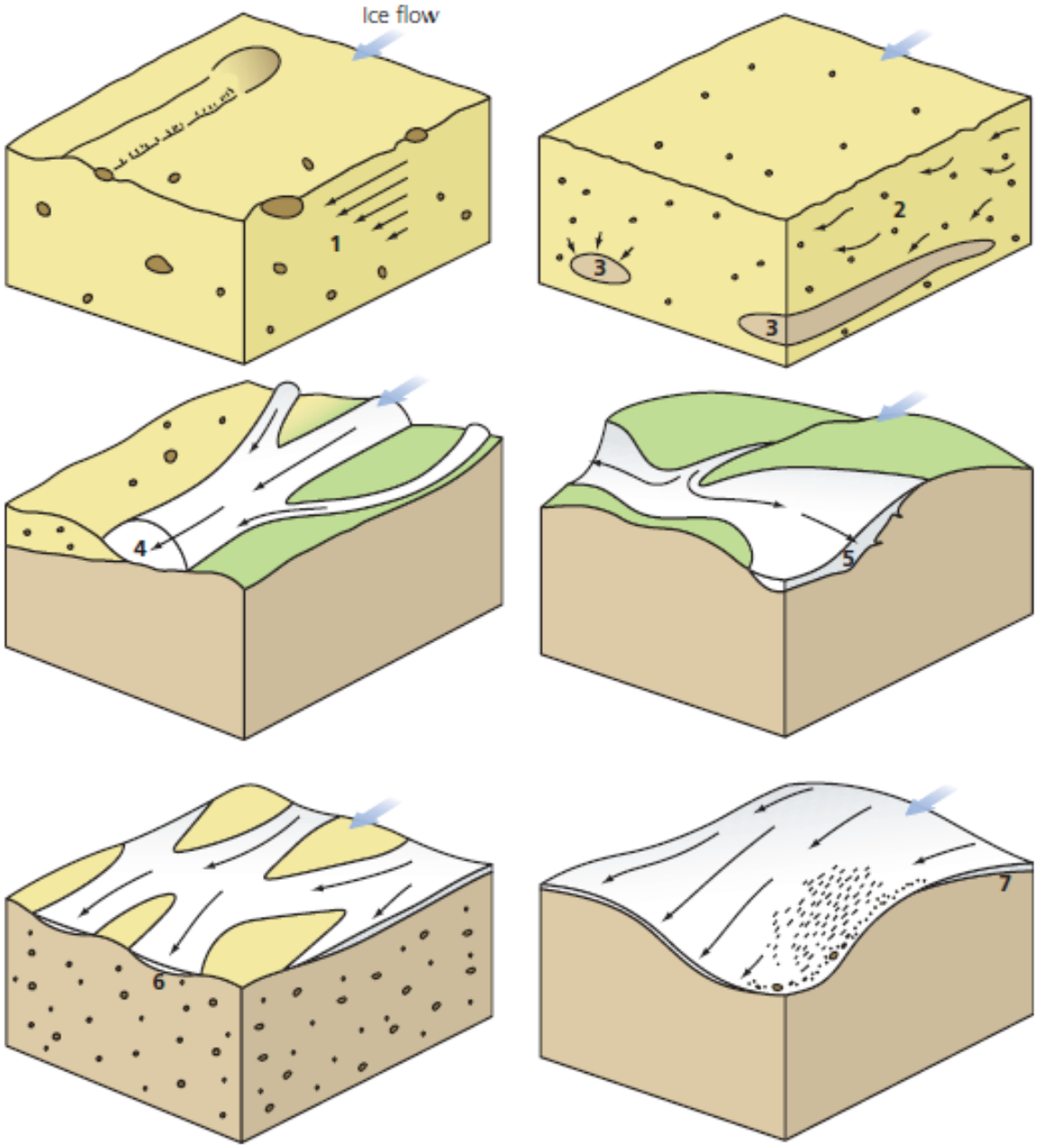

Figure 3-6. *Water movement through subglacial drainage networks. Efficient drainage systems include pipe flow (3) and channelized networks (4). Movement of water from till deformation (1), water flow through pores (2), linked cavities (5), braided channels (6) and a thin film at the glacier bed (7) are all a part of inefficient systems (Benn and Evans, 2010).*

3.5 Glacier Surging

The previous sections focused on changes in glacier flow within a year, this section discusses how glacier flow can change from year to year due to flow instabilities. Few glaciers, less than 1% in the Canadian Arctic, undergo a dynamic instability or experience irregular flow regimes, such as surge or pulse events (Sevestre and Douglas, 2015; Van Wychen et al., 2016). Glaciers that undergo surging events typically experience lengthy quiescent periods, velocity slowdowns, that can last decades or centuries and coincide with glacier retreat (Copland et al., 2003; Medzrycka et al., 2019; Van Wychen et al., 2016; Sevestre et al., 2018; Jiskoot et al., 2000). At these times, glacier velocities are quite low, and are less than what would be expected due to mass balance conditions. Active surge periods are much shorter intervals where glacier velocities increase by a 10 - 1000 order in magnitude from the quiescent phase (Meier and Post, 1969; Medrzycka et al., 2019). These drastic increases in velocity typically start up-glacier and propagate down-glacier, causing a rapid transport of mass down-glacier, resulting in changes in ice thickness and "rapid terminus advances" (Raymond 1987; Van Wychen et al., 2017; Medrzycka et al., 2019; Jiskoot et al., 2000). The following features are signs that, when combined, may indicated a surge-type glacier: looped or deformed moraines, widespread crevassing, stagnant ice, potholes, over steepened termini (Meier and Post, 1969; Sturm, 1987; Sharp et al., 2009), and significant surface increase in flow velocities (Copland et al., 2003; Medzrycka et al., 2019). Pulse events are different compared to surging as they are isolated to the lower portion of the glacier (Van Wychen et al., 2016; Medrzycka et al., 2019). Pulse events are identified by fast flow starting at the glacier terminus that does not extend past where the glacier bed is grounded below sea level in tidewater terminating glaciers (Van Wychen et al., 2016; Medzrycka et al., 2019).

Surging glaciers in the CA have typically been classified as "Svalbard-type" as they have a similar behavior of longer active and quiescent phases, ~7-15 and ~50-100 years, respectively, as the glaciers found in Svalbard (Van Wychen et al., 2016). Svalbard-type surge glaciers are thought to be linked to changes in the basal thermal conditions at the bed of the glacier (Murray et al., 2003; Van Wychen et al., 2016). In the QEI, 51 surge-type glaciers have been identified (Copland et al., 2003; Medrzycka et al., 2019), most of which are larger tidewater glaciers (Sharp et al., 2009). Copland et al., (2013), confirmed that 3 glaciers on AHI are of the surge-type: Good Friday Bay, Iceberg and Airdrop (or Middle) Glacier. However, as Good Friday Bay Glacier has been advancing for the last 70 years, it is debatable that it is surging (Medrzycka et al., 2019). Iceberg Glacier has been studied twice during its quiescent phase and has experienced surging events lasting 10-30 years (Medrzycka et al., 2019). Importantly, the two glaciers that will be intensively studied here, White and Thomson Glaciers, have not been identified as surge-type.

3.6 Glacier Thermal Regimes

Glaciers can be classified and described by their thermal regime, or temperature of the glacier ice. Glaciers can be cold (polar), warm (temperate) or a combination of both – polythermal (Figure 3-7). Initially, alpine areas were thought to contain only temperate glaciers, which proved to be untrue, as White Glaciers is a mostly cold, polythermal glacier with a temperate ice zone along the glacier bed (Iken 1974; Thomson and Copland, 2017a). A range of thermal regimes, from completely cold, entirely warm ice and differing combinations, exists (Figure 3-7; Blatter and Hutter, 1991). Temperate ice is likely to have water content and can exist due to both internal and external factors. Snow on the glacier surface acts as an insulator and can preserve heat gained over the summer (Wohlleben et al., 2009). Meltwater that refreezes in the glacier can release latent heat and ice creep and basal friction along the glacier bed, along with water flow can create enough heat for temperate ice to exist (Wohlleben et al, 2009). Ice reaching the pressure melting point near the bed can also cause warm ice (Wohlleben et al., 2009).

Understanding the thermal regime of a glacier can be beneficial for understanding and identifying where sliding might occur. Cold ice is frozen to the bed and the only movement would be by internal deformation. Temperate or warm ice is at a temperature close to 0°C, or the melting point of ice, indicating water is present and it is possible for the glacier ice to move via basal sliding. White Glacier is a mostly cold polythermal glacier, with temperate ice along the bed near the terminus (Blatter, 1987; Thomson and Copland, 2017b). White Glacier is likely to experience shorter term variability in velocity in the terminus region where there is temperate ice along the bed (Blatter, 1987).

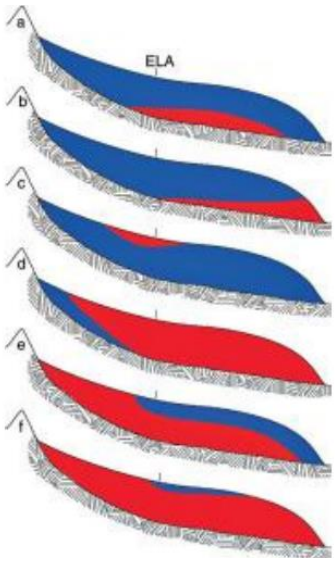

Figure 3-7. *Types of polythermal glaciers, ranging from (A) mostly cold polythermal, like White Glacier, to (f) mostly temperate polythermal. (Benn and Evans, 2010). Blue represents cold ice, while red represents temperate ice.*

3.7 Synthetic Aperture Radar (SAR) Data

In the CA, optical data is only available for 6 months of the year during the late-spring, summer and early-fall periods because of the 'Polar night'. However, it is often unusable for remote sensing analysis due to persistent cloud cover. As such, Synthetic Aperture Radar imagery has become a preferred dataset for studying glaciers within the region. This is because an advantage of RADAR is that the microwaves are largely unaffected by atmospheric particles, like ozone, water vapor and pollution and does not rely on solar illumination, which makes it an ideal tool for Arctic remote sensing projects (McNairn, 2021a). SAR uses energy from the microwave region of the electromagnetic (EM) spectrum, with wavelengths generally between 1 cm and 1 m, depending on the sensor (McNairn, 2021a). Both R2 and S1 are C-band sensors, with a wavelength ranging between 3.8 – 7.5 cm (McNairn, 2021a). TSX is an X-band sensor, with wavelengths ranging between 2.4 – 3.8 cm (McNairn, 2021a). Active SAR sensors create and emit energy from their own source then detects the energy scattered back to it from the target – backscatter. The backscatter provides key information and characteristics on the target, like roughness and moisture content of the surface and is useful in detecting changes in snow and ice (McNairn, 2021b).

The wavelength and elapsed time between images impacts coherence, or the difference in backscatter between acquisitions. Low coherence indicates a greater change between acquisitions. High coherence indicates less change between acquisitions. Longer wavelengths tend to propagate deeper into materials while shorter wavelengths tend to scatter more readily in the upper portion of a material (McNairn, 2021b). As X-band (TSX) has a shorter wavelength than C-band sensors (R2 and S1), X-band data will lose coherence more quickly than C-band data. However, this can be offset by the difference in the acquisition interval between images. Therefore, the shorter the amount of time that elapses between TSX images may mean there is a greater change that coherence between images is maintained. Water content also has an impact on SAR. A water molecule is a dipole with a net positive charge, that interacts with an electric field, like SAR, by rotating and aligning to electric field (McNairn, 2021b). Higher water content reduces the depth of penetration of the wavelength into the target material and can discontinue the propagation of the wavelength (McNairn, 2021b). During the ablation season, there can be a great amount of meltwater on the glacier surface, reducing the coherence between images as the water content reduces the capability of SAR to resolve motion using displacement matching techniques (discussed further in the next chapter).

In EM fields, cycles of electric and magnetic fields are synchronized and travel at the speed of light. Radars can have different polarizations, or orientations, of the electric field. There are vertical and

horizontal components to the electric field and can result in linear, circular, or elliptical polarizations. Phase refers to the position of a wave at a particular point in time or space and is impacted by the structure of a target and can be offset (McNairn, 2021a). Radar data can have different polarization configurations of both transmitted and received polarizations, for example, HH, VV, HV or VH (Banks, 2021). Where the first letter describes the polarization of the transmitted wave and the second for the received wave of the backscatter, with H meaning horizontal and V for vertical orientation. When the energy arrives at the target, the wave is completely polarized and the target may cause partial or complete depolarization. The R2 and TSX data used in this study both have HH polarization, as this is the best polarization for looking at relatively flat objects (Banks, 2021), the S1 monthly velocity mosaics are also derived from HH polarized data.

Radar geometry is important in understanding how the data is acquired by the satellite (Figure 3-10). Radars are side-looking in the range direction, either to the left or right, which is perpendicular to the flight path or azimuth direction (Figure 3-8; McNairn, 2021a). Slant range is the distance between the radar and the target and is considered the natural radar viewing geometry, while ground range is the slant range projected onto the surface of the Earth (McNairn, 2021a). Range resolution is equal to half the pulse length of the pulse of energy transmitted by the radar (McNairn, 2021a). The azimuth direction depends on the length of the satellite antenna (McNairn, 2021a). An 'image swath', the area that is 'looked at' by the sensor in a pass, is the distance on the ground from the near range to the far range (McNairn, 2021a).

The R2, S1 and TSX satellites all function in this general way, with slight differences in their imaging characteristics, like beam mode, swath width and repeat pass, to name a few. Specifics of the sensors used in this study are summarized in Table 4-1. R2 is a Canadian satellite with a 24-day revisit period that was launched in 2007 (Schellenberger et al., 2016). R2 data is not openly available to the public and generally must be obtained from the Government of Canada. R-2 has been the primary data source for glacier monitoring in the CA (Van Wychen 2014; 2016; 2021). The R2 data for this velocity mapping research over AHI has been provided by Environment and Climate Change Canada. There are different Fine Beam modes that are used in this study (F1, F1F, F1N, F2, F4, F5, F6F and F6N). R2 Spotlight is a different beam mode from the R2 sensor that is also used in this study. The R2 data obtained for this study covers all of AHI and will be used to create a dense record of glacier motion of Thompson and White Glaciers. TSX is a German satellite with an 11-day repeat pass (McNairn, 2021a). S1 has a 12-day repeat orbit, however there are two S1 satellites that, when used in tandem, shortens the 12-day repeat orbit to a 6 day repeat pass (McNairn, 2021a).

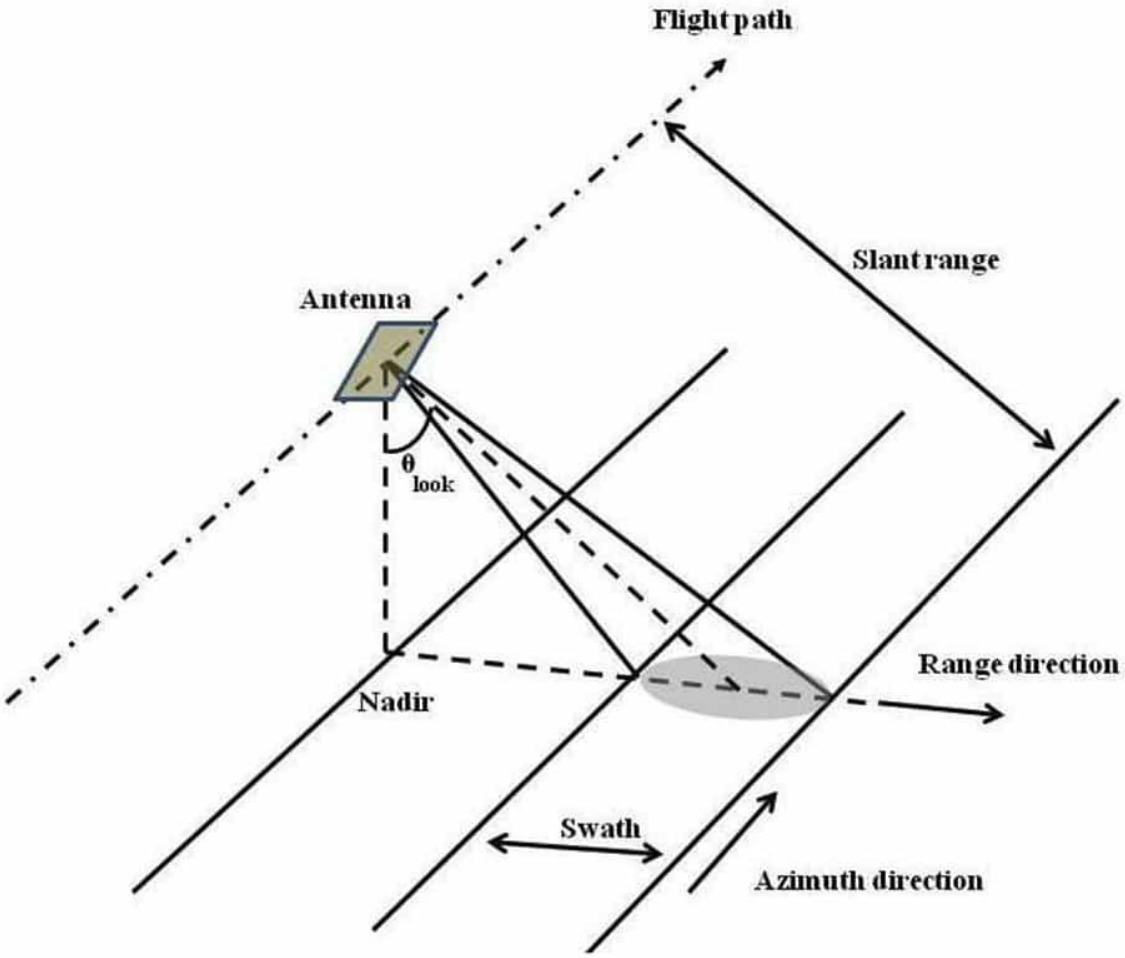

***Figure 3-8**. Radar geometry of a side-looking radar which is perpendicular to its flight path. Range direction is to the side, while azimuth direction is the same as the flight path. (ASF, n.d.)*

Chapter Four – Methodology

4.0 Overview

The previous section described variations in glacier motion and introduced SAR datasets. This chapter provides an overview of how SAR data will be processed in this study to derive glacier velocities, compare velocity outputs from different sensors, quantify error limits and detect seasonality.

4.1 SAR Data

A combination of different SAR datasets and sensors, R2, S1 and TSX sensors, were used to derive velocities of White and Thompson Glaciers. R2 Fine Beam data were provided by Environment and Climate Change Canada from winter 2008/2009 to winter 2010/2011. Previously processed R2 Fine Beam and Fine Wide Beam data from 2008/2009 through to 2019/2020 (Van Wychen et al., 2016; 2021), was then used for further velocity analysis and comparisons between datasets. As the R2 data provided by Van Wychen et al., (2016; 2021) used one or averaged two image pairs to represent glacier velocity for the entire year, it is referred to as "R2 Yearly" in this thesis to differentiate it from the R2 Fine Beam and R2 Spotlight data processed for this research. TSX data were acquired and provided by DLR (German Aerospace courtesy of Anna Wendleder) and is available for the study site every 11 days from February 17th, 2020 to April 30th, 2022 Pre-derived S1 monthly velocity mosaics are readily available through the FAU university portal (http://retreat.geographie.uni-erlangen.de/search). Unlike the S1 datasets which are already delivered as velocity map products, the R2 Fine Beam and TSX datasets were processed to derive velocity products. The following section will describe how the SAR data is processed through to the end velocity map product. Table 4-1 summarizes the SAR data characteristics available for this project.

4.2 Offset Tracking and GAMMA SAR software

Offset tracking of SAR data is a common approach to determine glacier motion from pairs of imagery and the implementation of offset tracking in the GAMMA SAR software has been effectively proven by previous research (Schellenberger et al., 2016).

The offset tracking procedure in GAMMA works in the following manner (summarized in Figure 4-1). First, the SAR images are loaded and converted from their proprietary SLC format to a more generic version that the GAMMA SAR software expects; the 'GAMMA SLC' format. This process creates a single-look complex (SLC) data file as well as an accompanying parameter (.PAR) file, that contains image parameter information like path direction, beam mode, pixel size etc. Once all the files are converted into the expected GAMMA file format, all matching image pairs are identified. For the TSX image data the pairs

are separated by 11 days and for R2 image pairs are separated by 24 days, determined by the repeat pass time of the respective sensor. The orbital information in the metadata file of the images is used for the co-registration of the reference and secondary image, which is necessary before offset tracking can be completed.

Before offset tracking begins, the user decides the appropriate window sizes (i.e., the real-world size that the group of pixels will represent). Typically, pixel window sizes that represent ~500 m in both azimuth and range directions have been shown to be effective for deriving glacier motion in the CA (Van Wychen et al., 2017; 2020). For this study, TSX had a window size of 256 pixels x 500 pixels and R2 Fine Beam used a window size of 128 pixels x 256 pixels. There is a trade off between increased size of pixel windows and processing time, as larger window size generally obtains better results due to a more unique backscatter signal, however, processing time will also increase. It is also possible that larger windows may result in capturing areas outside of the glacier of interest.

Table 4-1. *Summary of SAR datasets characteristics used in this study; Radarsat-2 (Government of Canada, 2022), S1 (The European Space Agency), and TSX (GERMAN ERAOSPACE)*

Sensor	Beam mode	Band	Orbital repeat pass period (days)	Polarization	Input image resolution (m)	Output velocity product resolution (m)	Date range (years)	Pre-processed
R2 Fine Beam	Fine Beam	C-band	24	HH	~5 m x ~5 m	~35 m x ~95 m	2008-2011	No
R2 Spotlight	Spotlight	C-band	24	HH	1 m x 1 m	~35 m x ~95 m	2012-2015	Pre-processed
R2 Yearly	Fine and Fine wide	C-band	24	HH	~5 m x ~8 m	~100 m x ~100 m	2009-2020	Pre-processed
S1	IW	C-band	6 or 12	HH	~3 m x ~25 m	~210 m x ~210 m	2015-2020	Pre-derived monthly mosaic
TSX	StripMap	X-band	11	HH	~1.5 m x ~1.8 m	~35 m x ~95 m	2020-2022	No

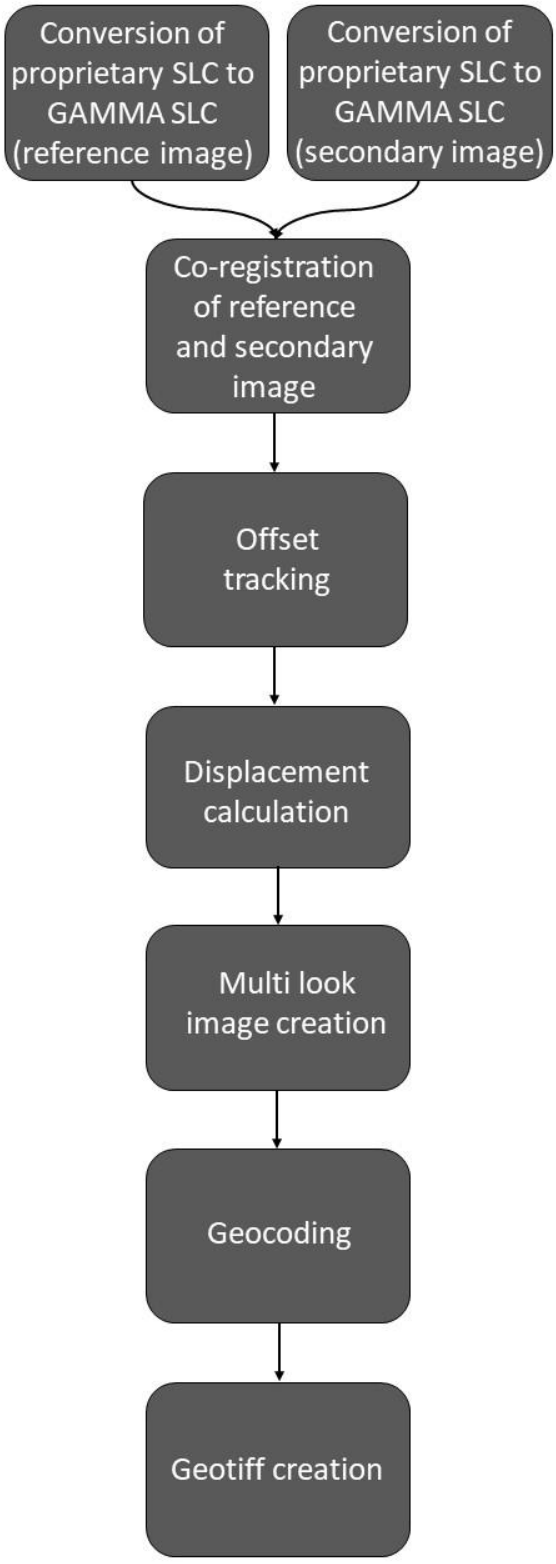

Figure 4-1. *Simplified GAMMA processing steps as a flow chart, starting with the conversion of both reference and secondary images from proprietary SLC to the GAMMA SLC format used in GAMMA processing, followed by co-registration of reference and secondary images. Offset tracking, displacement calculation, creation of the multi-look image and geocoding follow, resulting in a geotiff file.*

The offset tracking algorithm works by taking the two co-registered images and looking for sets of matching pixels between each image using a cross correlation algorithm. The algorithm uses a group of pixels defined by the window determined by the user in the first image (the reference image), then systematically searches for the best match in a group of pixels in the second image (secondary image). Both images need to have been acquired with the same imaging geometry and maintain coherence between acquisitions, i.e., the target surface should stay the same such that nearly the same backscatter values are returned to the sensor in both images (McNairn, 2021a). Coherence is lost if there is too much of a difference between scenes, typically from melt or extreme precipitation resulting in poor displacement calculation between acquisitions. Offset tracking calculates the distance between the center of the group of pixels by tracking how many pixels it moves from one image to the next in both azimuth and range directions. The magnitude of displacement, which is then inferred to be a representation of glacier surface velocity, between the two co-registered images is automatically calculated using equation 1.

Equation 1: Total Displacement = SQRT((Azimuth displacement^2) + (range displacement^2))

The final output of the GAMMA processing scheme is a series of geotiff files, which include rasters of the total displacement between the two images and the orientation of the calculated displacement. The GAMMA processing scheme automatically removes poor displacements above a defined threshold, of a cross correlation peak coefficient below 0.8 (Friedl et al., 2021), that eliminates the need for later manually filtering. The magnitude geotiff was then imported into ArcMap for further manipulation (described below).

4.3 ArcMap

ArcMap 10.8.1 was used to post-process the data and create a final glacier velocity map from the geotiff output from GAMMA through the following steps (see Figure 4-2). Once the geotiff file was imported to ArcMap, it was normalized to displacements of meters per year (m a^{-1}) using the raster calculator tool. Standardizing the values in m a^{-1} allows for comparisons across multiple datasets and conforms with previous glacier velocity records (Van Wychen et al., 2016; 2017; Medrzycka et al., 2019). For the TSX and R2 data, the geotiffs were normalized by equations 2 and 3, respectively. The geotiff is divided by the number of days in the revisit period, then multiplied by 365.25, which is the number of days in a year that accounts for leap years.

Equation 2: TSX Normalization = $\left(\frac{Geotiff}{11}\right) * 365.25$

$$\textit{Equation 3: R2 Normalization} = \left(\frac{Geotiff}{24}\right) * 365.25$$

In all cases, regardless of the input data, the final velocity output is represented in m a^{-1}. The normalized geotiff was then clipped to the glacier extent using the Arctic Canada North file of the standardized Randolf Glacier Inventory (Pfeffer et al., 2014; version 6.0: GLIMS: Global Land Ice Measurements from Space).

To compare glacier velocity across a series of images to determine seasonality, a common approach is to compare the centreline glacier velocities at various times. To do this, the pixel values from the derived velocity maps were extracted along the center of the length of the glacier. First, a centreline was manually digitized along the centerline of both White and Thompson glaciers (Figure 4-3), from the terminus to an arbitrary point at the top of the glacier, which is an approximation of the glacier's centerline. The centerline was then converted to point values with a distance of 100 m and 50 m for Thompson and White Glaciers, respectively, which were then extracted and plotted as line graphs to visually analyze the velocity values.

***Figure 4-2**. ArcMap workflow starting with adding the GAMMA output geotiff to ArcMap. The tiff file was the normalized to meters per year and clipped to the RGI (version 6.0) of AHI. The velocities were then classified into 10 groups, resulting in the final velocity maps. The centerlines of both Thompson and White Glaciers were then extracted from the velocity products.*

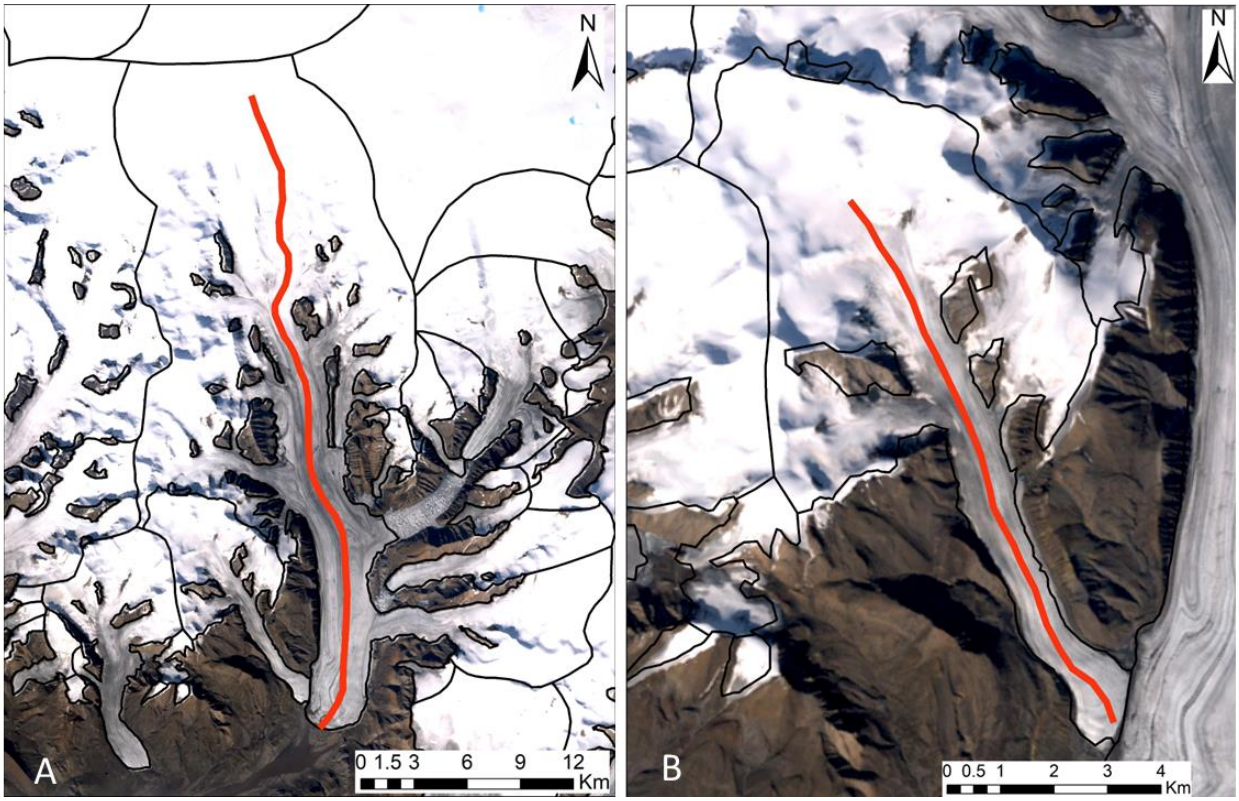

Figure 4-3*. The red line represents the digitized centerline used to extract glacier velocities along the estimated centerline. (A) shows Thompson Glacier and the centerline used for velocities. (B) shows White Glacier with the red line representing the centerline used in this study. Background image is a cloud free Landsat image.*

4.4 Error and uncertainty in the offset tracking method

Errors in the offset tracking procedure can occur due to decreased accuracy from physical characteristics of the glacier itself, the SAR data and offset tracking, co-registration, and geocoding errors (Schellenberger et al., 2016; Rohner et al., 2019). Physical features of the glacier or ground surface, like topography, roughness and feature stability can impact the SAR data (McNairn, 2021b). A common way to verify the uncertainty of the offset tracking method is by calculating the mean velocity over non-moving regions (i.e., bedrock outcrops) (Short and Gray, 2005; Van Wychen et al., 2014; Schellenberger et al., 2016). If the area in question is an ice cap interior, with no visible bedrock outcrop to measure displacement, ice divides can be used in their place as the surface velocity should be close to zero (Raymond, 1983; Van Wychen et al., 2014). Ice divides can be derived from the RGI (Van Wychen et al., 2014; 2016).

Short and Gray (2005), have shown that the use of speckle tracking (a form of offset tracking) applied to Radarsat-1 imagery with good coherence in the Canadian Arctic with a 24 day repeat pass will

result in velocity errors of 2-10 m a^{-1}. In areas that are faster flowing (to hundreds of meters per year) with heavy crevassing, errors of 10 – 20 m a^{-1} are more likely due to a possible loss of coherence between images from the increased velocity (Short and Gray, 2005; Van Wychen et al., 2016). The error from both the bedrock and ice divide can be calculated for each year to quantify uncertainty (Short and Gray, 2005; Van Wychen et al., 2012; 2014; 2016; 2017). The best velocity results are achieved when minimal change occurs between images, so little to no melt or snowfall, which in the CAA is typically between January and April (Medrzycka et al., 2019). Based on all the previously published literature, it is expected that the error margins of the method will be similar to those of previous work (i.e. uncertainty of 10-20 m a^{-1}). This means that to determine variations in glacier flow related to seasonality changes in ice flow of at ~20-40 m a^{-1} are likely to be needed to determine if real change is occurring.

The error for this study was calculated from the velocity determined over bedrock regions adjacent to White and Thompson Glacier, by extracting velocity values over bedrock (Figure 4-4) and converting the raster file to a point shapefile. A polygon was created around White and Thompson Glaciers in ArcMap, covering the glacier termini, while excluding areas that extended to the fjord with sea ice. If these were to be included, error values would subsequently increase, as sea ice and the fjord are dynamic features. The area of the RGI was removed from this polygon and the velocity rasters were then clipped to the bedrock polygon, creating rasters that represent the velocities over the stationary bedrock areas. The polygon was used for the error analysis over velocity over bedrock (Figure 4-4). The velocity over non-moving area rasters were converted to a point shapefile. The statistics were calculated directly in ArcMap from the point shapefile by running the ‘calculate statistics’ tool on the ‘grid code’ (velocity value) attribute of each shapefile. The statistics resulted in the mean and SD for displacement over non-moving areas. This was performed on every velocity map generated image and then averaged for each sensor.

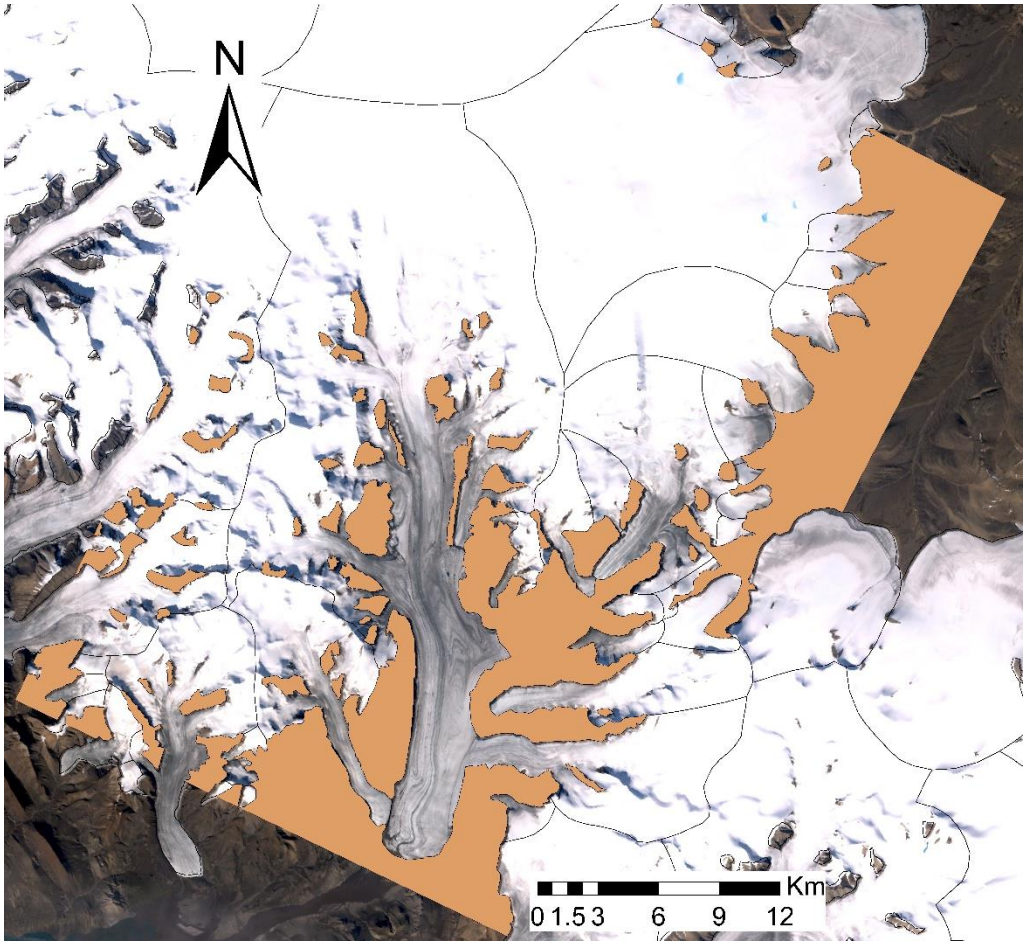

Figure 4-4. *The orange polygon represents the bedrock shapefile used to determine area for error via motion over bedrock. Background image is a cloud free Landsat image.*

4.5 Data Volume

In total, 148 SAR image pairs (TSX and R2 Fine Beam) were processed to velocity maps in this study. However, of this 148, 31 did not cover the area of interest and 34 were summer acquisitions. Therefore, 83 image pairs were acquired during the accumulation season and covered Thompson and White Glacier (summarized in Table 4-2). Of these 83 image pairs, 13 were removed from velocity analysis of Thompson Glacier and 12 removed from White Glacier. One image from TSX and the remaining 12 (Thompson Glacier) or 11 (for White Glacier) from R2 Fine Beam, as the error was above the 10 m a^{-1} error limit of this study or there was a noticeable loss in coherence can be seen by the bolded dates in Table 4-2. R2 Fine Beam F4 for May 14th to June 7th, 2009 (red image pair in Table 4-2), had an error lower than 10 m a^{-1}, but had little data over Thompson Glacier. However, the velocity data of this image pair over White Glacier was consistent with other image pairs in the dataset and was included in the velocity analysis.

***Table 4-2**. Summary of the available R2 Fine Beam and TSX velocity data processed in this study during the accumulation season that covered the area of interest. The dates of image pairs that are bolded were removed from further analysis of velocity structure due to error above 10 m a-1 or a visual loss of coherence. The date in red was removed from further analysis on Thompson Glacier due to minimal velocity data over the centerline but was included for White Glacier.*

Accumulation year	Sensor	Beam mode	Reference image date	Secondary image date	Reference image date	Secondary image date	Reference image date	Secondary image date	Reference image date	Secondary image date
2008-2009	R2 Fine Beam	F1	**2008-09-22**	**2008-10-16**	**2008-10-16**	**2008-11-09**	2008-11-09	2008-12-03	2008-12-03	2008-12-27
			2009-02-13	2009-03-09	2009-03-09	2009-04-02	2009-04-02	2009-04-26	2009-04-26	2009-05-20
		F1F	**2008-09-29**	**2008-10-23**	**2008-10-23**	**2008-11-16**	2008-11-16	2008-12-10		
		F1N	2009-03-02	2009-03-26	2009-03-26	2009-04-19	2009-04-19	2009-05-13	2009-05-13	2009-06-06
		F2	2009-04-16	2009-05-10	2009-05-10	2009-06-03				
		F4	2009-03-03	2009-03-27	2009-03-27	2009-04-20	2009-04-20	2009-05-14	**2009-05-14**	**2009-06-07**
		F5	**2008-09-30**	**2008-10-24**	**2008-10-24**	**2008-11-17**	2009-04-10	2009-05-04	2009-05-04	2009-05-28
		F6F	2009-03-07	2009-03-31	2009-03-31	2009-04-24	2009-04-24	2009-05-18	**2009-05-18**	**2009-06-11**
		F6N	2009-03-24	2009-04-17	2009-04-17	2009-05-11	2009-05-11	2009-06-04		
2009-2010	R2 Fine Beam	F4	2009-10-05	2009-10-29	2009-10-29	2009-11-22	2009-11-22	2009-12-16	2009-12-16	2010-01-09
			2010-01-09	2010-02-02	2010-02-02	2010-02-26	2010-02-26	2010-03-22	2010-03-22	2010-04-15
			2010-04-15	2010-05-09						
		F5	2009-09-25	2009-10-19	**2009-10-19**	**2009-11-12**	**2009-11-12**	**2009-12-06**	**2009-12-06**	**2009-12-30**
			2009-12-30	2010-01-23	2010-01-23	2010-02-16	2010-02-16	2010-03-12	2010-03-12	2010-04-05
			2010-04-05	2010-04-29	**2010-04-29**	**2010-05-23**				
2010-2011	R2 Fine Beam	F4	2010-09-06	2010-09-30	2010-11-17	2010-12-11				
2019-2020	TSX	StripMap	2020-02-17	2020-02-28	2020-02-28	2020-03-10	2020-03-10	2020-03-21	2020-03-21	2020-04-01
2020-2021	TSX	StripMap	**2020-09-02**	**2020-09-13**	2020-09-13	2020-09-24	2020-09-24	2020-10-05	2020-12-10	2020-12-21
			2020-12-21	2021-01-01	2021-01-01	2021-01-12	2021-01-12	2021-01-23	2021-02-14	2021-02-25
			2021-02-25	2021-03-08	2021-03-08	2021-03-19	2021-03-19	2021-03-30	2021-05-02	2021-05-13
			2021-05-13	2021-05-24	2021-05-24	2021-06-04				
2021-2022	TSX	StripMap	2021-08-31	2021-09-11	2021-09-11	2021-09-22	2021-09-22	2021-10-03	2021-10-03	2021-10-14
			2022-01-10	2022-01-21	2022-01-21	2022-02-01	2022-02-01	2022-02-12	2022-02-12	2022-02-23
			2022-02-23	2022-03-06	2022-03-28	2022-04-08	2022-04-08	2022-04-19	2022-04-19	2022-04-30

4.6 Pre-derived velocity products

This section will briefly discuss the methodologies used on the pre-derived SAR datasets used in this study; R2 Yearly, R2 Spotlight and S1.

4.6.1 Pre-derived R2 Yearly velocity products

To create regional maps of ice motion across the Canadian Arctic, R2 data from 2008-2015 were obtained from Natural Resource Canada, with the acquired image pairs being between November and April (mid-autumn to spring; Van Wychen et al., 2016; 2021). These studies used the velocity products to investigate ice dynamics over a regional scale and determine if glaciers were undergoing dynamic instability, surge or pulse behavior. Glacier velocity was determined by processing the R2 data with a MATLAB speckle tracking code that uses a cross-correlation algorithm to determine displacement between images, a similar method of determining ice motion as the GAMMA offset tracking method (Schellenberger et al., 2017). Bedrock, areas of no motion, were used to determine biases in the calculated offsets and there were subsequently removed. The velocity outputs were normalized to meter per year. In ArcMap, manual filtering was performed by Van Wychen et al. (2016; 2021), to remove any mismatches based on criteria in Van Wychen et al. (2012; 2014) from the dataset. Individual image pairs were mosaicked if there was more than one image pair for that accumulation year and clipped to the extent of RGI version 3.2. Van Wychen et al., (2021) added to the previous dataset by processing R2 Wide Fine from 2015/16 to 2019/20 with the same speckle tracking methodology as Van Wychen et al., (2016). This 2021 study used the parameters of ~450 m in the azimuth direction and ~370 m in the range direction as the 2016 study to determine displacement and maintain consistency between the datasets. Manual filtering was performed to remove mismatches from the cross correlation. These glacier velocities processed in Van Wychen et al., (2021) were clipped to the extent of the RGI version 6.0. The error was calculated using the similar method of motion over non-moving areas of bedrock. The velocity maps created by Van Wychen et al. (2016; 2021) were made available for this study as a comparison dataset. These pre-derived R2 velocity products are known as R2 Yearly in this study to differentiate them from the R2 Fine Beam processed in this study. The R2 Yearly data will be presented for accumulation years where other data is available for a comparison and will be used in a direct comparison with TSX and S1 velocity products for a similar time frame, March 2020. This will allow for a comparison between data derived in this study and velocity data that has already been published.

4.6.2 Pre-derived R2 Spotlight velocity products

A few R2 Spotlight image pairs from 2012 to 2015 were provided by Luke Copland of the University of Ottawa (and originally obtained through a Canadian Space Agency SOAR-E project agreement #5106

and processed by W. Van Wychen). These data were processed in the same general procedure as described in section 4.2, however window sizes of 200 pixels (~266 m) in range and 600 pixels (~248 m) in azimuth were used. Step sizes were set to ~25m in both range and azimuth directions. Of the twelve image pairs provided, two were from the winter of 2012 to 2013, six image pairs were from the 2013 to 2014 accumulation season and 4 image pairs were provided for spring of 2015. The months that are covered by the obtained R2 Spotlight data are as follows: January 2013, January to May 2014 and March to June 2015.

4.6.3 Pre-derived S1 velocity products

Friedl et al. (2021) used S1 interferometric wide (IW) swaths from the European Space Agency's Sentinel-1 constellation to determine ice motion for many glacier regions worldwide. SAR data that had been archived were downloaded from the Alaska Satellite Facility's Distributed Active Archive Center, with new data continuously being downloaded from there, as well. The S1 IW imagery was acquired with the terrain observation with progressive scans in azimuth, allowing larger swath widths than the typical strip map mode. This is due to the antenna being steered back and forth in both the azimuth and range directions. This acquisition type requires more processing than strip map mode. The orbital vectors of the IW SLC images need to be recalculated using Precise Orbit Determination service to ensure a high level of geolocation accuracy. Then co-registration of image pairs can be performed followed by the GAMMA intensity offset tracking algorithm. During the offset tracking process, mismatches of image pairs are rejected if the cross correlation peak coefficient is below 0.8, while a value of 1 indicates a good cross correlation. This is the same process used for this research on the TSX and R2 data (section 4.2). Following the automatic removal of mismatches, the methodology of Friedl et al. (2021) used a DEM to geocode and orthorectify the data, with the use of different DEMs for different regions. The product of the previous processing steps are rasters (GeoTIFF). Additional post-processing filtering and corrections were performed to remove any remaining co-registration errors. The pre-derived S1 data will be presented for accumulation years where other data is available for a comparison and will be used in a direct comparison with TSX and R2 Yearly velocity products for the same time frame. The S1 data will allow for a comparison between the velocity products derived in this study and velocity data that has already been published.

4.7 GPS data comparisons

In situ GPS data, provided by Laura Thomson of Queen's University, was used as an additional validation dataset to compare with the SAR derived glacier velocities of White Glacier. The processing of the GPS data from a raw RINEX format between 2013-2016 was completed by Dr. Thomson and shared as

text files. This time-period of the pre-processed field data overlaps with 9 image pairs of R2 Spotlight. The dates of the reference images of R2 Spotlight data that overlapped with the GPS data resulted in three image pairs that overlapped with GPS data from the Upper/Moraine profile, two image pairs with the Middle/Wind profile and four overlapping at the Lower/Anniversary profile (Figure 4-5; Table 4-3). The next step was to convert the latitude and longitude coordinates to UTM coordinates using an online latitude – longitude to UTM coordinate conversion tool (Convert Geographic Units - Montana State University). The decimal degree latitude and longitude coordinates of the GPS data were converted to UTM coordinates using UTM zone 15 N. The UTM latitude and longitude values were then saved as a CSV file (comma delineated).

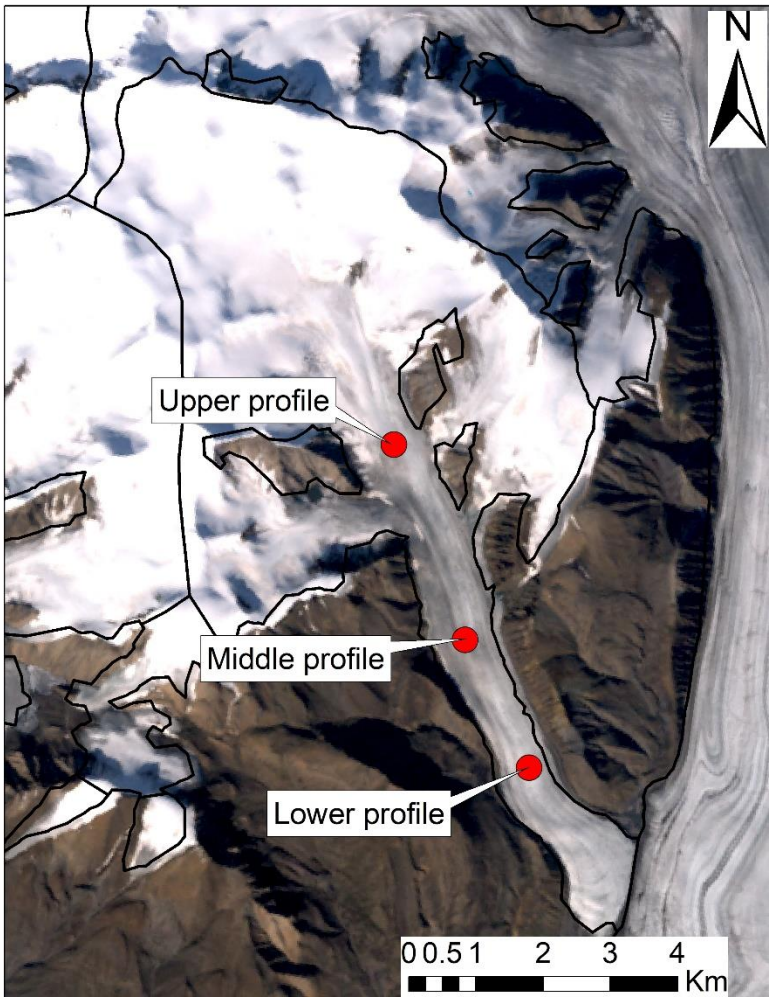

Figure 4-5. *The locations of GPS station profiles: Upper/Moraine, Middle/Wind, and Lower/ Anniversary. The red dots represent the locations of each GPS station on May 4th, 2015. Background image is a cloud free Landsat image.*

The CSV file with coordinate data was added to an ArcMap project, displaying the X and Y data, resulting in the location of the GPS station for that respective timestamp. The geographic coordinate system was set to GCS WGS 1984. The location of the GPS station displayed on the glacier in ArcMap is then able to be directly compared to the SAR image pair, providing the reference image acquisition date matches the GPS data date. The 'Identify' tool in ArcMap was used after zooming in to the point of the GPS location, allowing for the selection of a pixel close to the GPS point from the appropriate glacier velocity map.

The data was then stored in an MS Excel file, and was used to calculate the difference between the provided in situ GPS data and the R2 Spotlight data. The Easting and Northing values of the GPS locations that matched the reference and secondary SAR image dates were used to calculate the displacement using equation 4.

$$\textit{Equation 4: Displacement} = Sqrt((Northing1 - Northing2)^2 + (Easting1 - Easting2)^2)$$

Where the Northing1 and Easting1 represent the Northing and Easting coordinates, respectively, of the GPS station on the date that matches the reference SAR image pair date. Northing2 and Easting2 represent the respective Northing and Easting coordinates of the GPS station with the same date as the secondary SAR image pair.

The displacement value was then normalized to m a^{-1} in the Excel file. The SAR offset tracking velocity was then added to the Excel file to compare the calculated displacement of the UTM coordinates of the GPS with the offset tracking results from matching dates. The difference in meters per year and percent between the in situ and SAR data were then calculated. These steps were repeated for all R2 Spotlight data that overlapped with the provided GPS data, resulting in the difference between the GPS and offset tracking of the 9 overlapping R2 Spotlight dates. If SAR velocity data was missing below the GPS location, the closest available SAR velocity data was used and the distance from the GPS station was noted. This was the case for one SAR image pair from May 28th to June 21st, 2015 at Middle profile, resulting in a 30 m distance between GPS and available SAR data.

Table 4-3. *The R2 Spotlight image pairs with corresponding GPS data available for the in-situ comparison with SAR data. The asterisk is the profile and date where R2 Spotlight data was not available below the GPS location, but 30 m away.*

White Glacier Profile	R2 Spotlight image pair dates with corresponding dGPS data	
	Reference image	Secondary image
Upper	2014-05-16	2014-06-09
Upper	2015-05-04	2015-05-28
Upper	2015-05-28	2015-06-21
Middle	2015-05-04	2015-05-28
Middle*	2015-05-28	2015-06-21
Lower	2014-04-22	2014-05-16
Lower	2014-05-16	2014-06-09
Lower	2015-05-04	2015-05-28
Lower	2015-05-28	2015-06-21

Chapter Five – Results and Discussion

This chapter provides the results and discussion for each of the three research objectives stated in Chapter 1. First, the velocity results and error values over Thompson and White Glaciers will be presented and described for the 2009-2020 period (thus satisfying research objective 1). This will be followed by an assessment of the quality and comparability of glacier velocity maps from the different sensors (thus satisfying research objective 2). Finally, the results will be compared to determine if any seasonality or long-term velocity changes with these datasets are observed (thus satisfying the third research objective).

For the purposes of this study, the calendar year was divided into four segments which follow the seasons: fall (September – November), winter (December – February), spring (March – May) and summer (June – August). This better allows for the investigation of seasonality while keeping the timeframes for comparisons consistent throughout the study. The summer months coincide with the highest melt, causing loss of coherence with SAR data and was excluded from the comparisons between sensors and investigations of long term and seasonal changes in velocity structure. The investigation into multi-annual velocity structure change and seasonality use "non-summer" velocities, a combination of fall, winter and spring velocities for analysis and comparisons.

5.1 Derived Glacier Velocity Products

Results of the derived velocity products of this project for R2 Fine Beam and TSX for Thompson and White Glaciers will first be presented. The velocity product maps from R2 Spotlight will focus on White Glacier, as the data only extends about 10 km upglacier from the terminus of Thompson Glacier. While the R2 Yearly and S1 velocity products were not derived in this study, they were used as comparisons when there was data available during the same accumulation year as the data derived in this study (R2 Fine Beam, R2 Spotlight and TSX). The centerline velocities were extracted from the velocity products found in Table 4-2 and Figures 5-1 to 5-24. The glacier velocity products will be presented in sections of accumulation years. The first accumulation year of 2008 – 2009, that is, fall 2008 through to spring 2009, displays R2 Fine Beam velocity products of different beam modes (F1, F1F, F1N, F2, F4, F5, F6F, F6N only, as other beam modes that were acquired did not cover the area of interest). The last accumulation year presented is 2021 – 2022, which displays TSX derived velocity products. The accumulation years in between will consist of a combination of R2 Fine Beam, Yearly and Spotlight, as well as, TSX and S1 velocity

products. There are some accumulation years that are not represented due to R2 Fine Beam, Yearly or TSX data not being available (2011 – 2012, 2015 – 2016 to 2018 – 2019). Velocity products were omitted from further analysis if the calculated error of the image pair was greater than 10 m a^{-1} or if the velocity product visually looked like there was a significant loss of coherence. There were occasions where the error was below 10 m a^{-1}, but the velocity product visually looked like it lost coherence to an extent where it did not seem as though the centerline velocities would be beneficial for further analysis. When the velocity products of image pairs had an error above 10 m a^{-1}, they were removed, this cut off has been used previously (Van Wychen et al., 2016; 2021).

R2 Spotlight data available for this study only covers about 10 km up glacier from the terminus of Thompson Glacier, as the primary purpose of this data when it was acquired was to derive motion for White Glacier. As such, only velocity maps of R2 Spotlight data for White Glacier are presented in the thesis. A more in depth analysis of the long-term and short-term variations in glacier velocity variability for each glacier will be in a following subsection (continued in section 5.3, after the velocity maps and error (section 5.2) are presented).

5.1.1 Accumulation year 2008 – 2009

Figure 5-1, provides the derived velocity products of R2 Fine Beam F1 imagery from early fall 2008 to end of spring 2009. The first kilometer extending up from the terminus of Thompson Glacier has a velocity that is consistently under 25 m a^{-1}. At a distance of 3 km from the terminus, the glacier reaches velocities of 35 m a^{-1}, and increases further upglacier, reaching a maximum velocity around 85 m a^{-1} around 24 km from the terminus.

The R2 Fine Beam F1 velocity data for White Glacier covers the length of the glacier. The first 0.6 km from the terminus experiences velocity under 20 m a^{-1}. Between 0.6 km and 3 km from the terminus, the glacier motion slows to under 10 m a^{-1}. From 3 km and further up glacier, the velocity increases to around 30 m a^{-1}, then reaches a maximum velocity of 50 m a^{-1} around 8.5 km from the terminus. The velocity then slows to below 20 m a^{-1} with increasing proximity to the accumulation basin.

Particularly good results were recorded in Figure 5-1 C to 5-1 H where there was better coherence between image pairs. Figure 5-1 A experienced a loss of coherence with a mean error of 11 m a^{-1} and standard deviation of 9 m a^{-1} and was removed from further analysis of short and long-term velocity structure changes. Less useable results were determined in Figure 5-1B, from October 19th to November 9th, 2008, where there is less coherence and an error of 10 m a^{-1} and a standard deviation of 10 m a^{-1} and

was also removed from further velocity analysis. This pattern of poorer results in the September to November timeframe can be expected as winter (December to February) is typically when better results are obtained (Van Wychen et al., 2016).

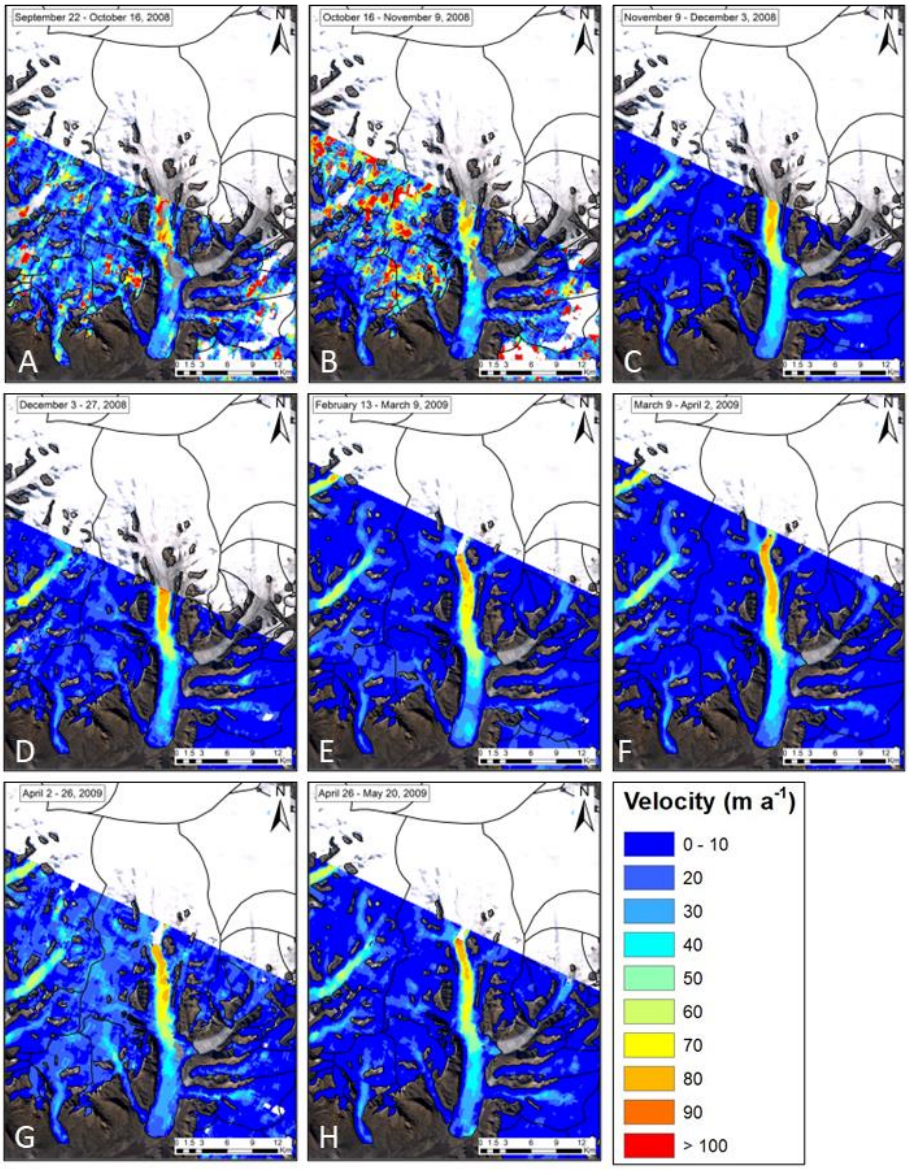

Figure 5-1. *Velocity structure of White and Thompson Glaciers derived from RADARSAT-2 Fine Beam F1 imagery from September 22nd, 2008 to May 20th, 2009. Deep black lines on the figure indicate the glacier extents provided by version 6.0 of the Arctic Canada North shapefile of the Randolf Glacier Inventory. Background image is a cloud free Landsat image.*

R2 Fine Beam F1F, Figure 5-2, is the next beam mode available for the 2008 to 2009 accumulation season. There was only one useable image pair, from November 16th to December 10th, 2008, available for this year. The velocity product over the glaciers of interest looks visually comparable to good results

of other beam modes and has comparable velocities along the centerlines of both glaciers to other beam modes. The first kilometer from terminus of Thompson Glacier experiences velocity below 15 m a^{-1} then increases to 30 m a^{-1} at a distance of 3 km from the glacier tongue. The velocity slowly increases from 30 m a^{-1} and reaches a maximum of 80 m a^{-1} at 19 km from the terminus. The SAR data for this image pair only extends 19.7 km from the terminus.

White Glacier experienced slow velocities around 5 m a^{-1} from the terminus to 4 km upglacier where the velocity shortly increased to 15 m a^{-1}. The velocity decreased to under 10 m a^{-1} around 5 km from the terminus. At 6.5 km from the terminus, the velocity increased to 15 m a^{-1} then increased further upglacier, reaching a maximum velocity, at 9 km from the glacier tongue, of 35 m a^{-1}. The velocity slowed to under 20 m a^{-1} closer to the accumulation basin, 10.7 km from the terminus.

Figure 5-2 A and B provide less useable results with errors of 13 m a^{-1} and 10 m a^{-1} and standard deviations of 13 m a^{-1} and 11 m a^{-1}, respectively. A and B were removed from further analysis of short- and long-term changes in velocity structure. Figure 5-2 C provides better results than A and B.

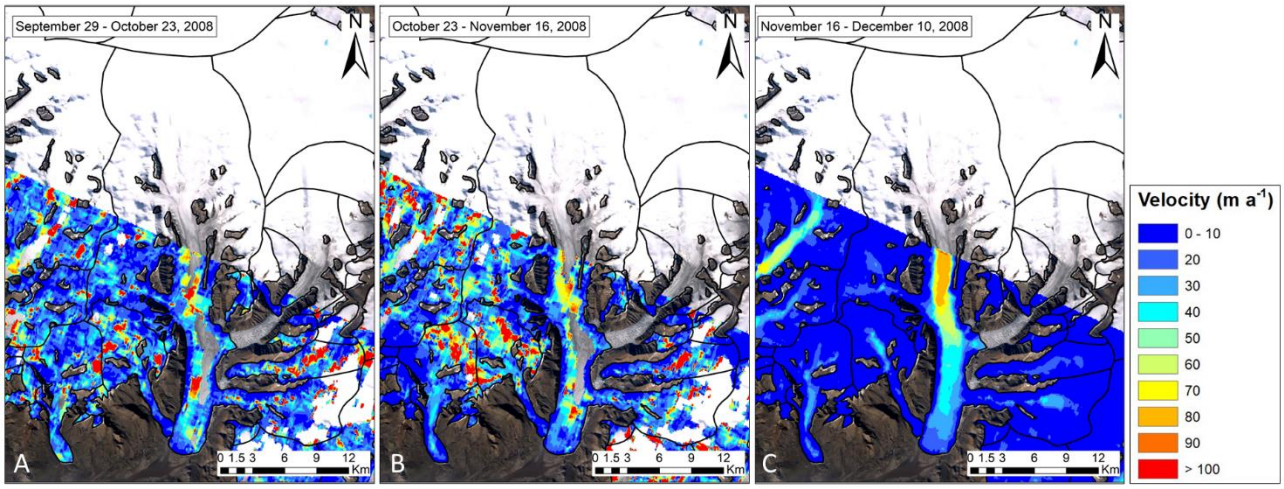

***Figure 5-2**. Velocity structure of White and Thompson Glaciers derived from RADARSAT-2 Fine Beam F1F imagery from November 16th to December 10th, 2008. Deep black lines on the figure indicate the glacier extents provided by version 6.0 of the Arctic Canada North shapefile of the Randolf Glacier Inventory. Background image is a cloud free Landsat image.*

The velocity product of R2's F1N beam mode, Figure 5-3, include four image pairs from spring 2009. The area covered by this beam mode extends over 23 km from the terminus of Thompson Glacier, the exact distance differing slightly with each image pair. The first kilometer from the terminus of Thompson Glacier is fairly consistent among three (Figure 5-3 A to C) of the four image pairs and do not exceed 20 m a^{-1}, however, May 13th to June 6th (Figure 5-3D) reaches a velocity of 76 m a^{-1} within that first

kilometer. Figure 5-3 A, B and C are pretty consistent along the length of the glacier as well, reaching 35 m a^{-1} at 3 km from the terminus, then decreasing to below 30 m a^{-1} around 5 km. The motion starts increasing again to above 30 m a^{-1} at a distance of 8 km from the terminus and steadily increasing to around 75 m a^{-1} at about 24 km from the glacier terminus. The maximum velocities vary slightly by magnitude and location along the centerline with each image pair but reach 90 m a^{-1} around 20 km from the glacier tongue. The velocity product from May 13th to June 6th (Figure 5-3D) is missing some velocity data along the centerline, likely due to a loss of coherence between image acquisitions with the onset of the melt season. The velocity reaches a maximum of 76 m a^{-1} around 0.8 km from the terminus the slows to under 10 m a^{-1} around 2.5 km to increase again to a second maximum of 76 m a^{-1} at 18 km from the terminus.

White Glacier experiences velocities lower than 20 m a^{-1} within the first kilometer from the terminus, with the lowest velocities of under 10 m a^{-1} around 1 km. The velocity fluctuates between under 10 and 20 m a^{-1} then starts increasing around 7 km from the glacier tongue to reach a maximum velocity of 45 m a^{-1} around 8 km from the terminus. Similar to the image pairs of Thompson Glacier for these beam modes, May 13th to June 6th (Figure 5-3D) experiences a greater velocity of 61 m a^{-1} around 9 km, almost double that of the other beam modes at this location along the centerline.

Good results were derived from Figure 5-3 A to C. Less useable results were derived from Figure 5-3 D, which resulted in a greater velocity near the terminus compared to the other velocity products in this beam mode of Thompson Glacier, while also missing the greatest amount of data. This is possibly related to the start of the melt season in June (Müller and Iken, 1973).

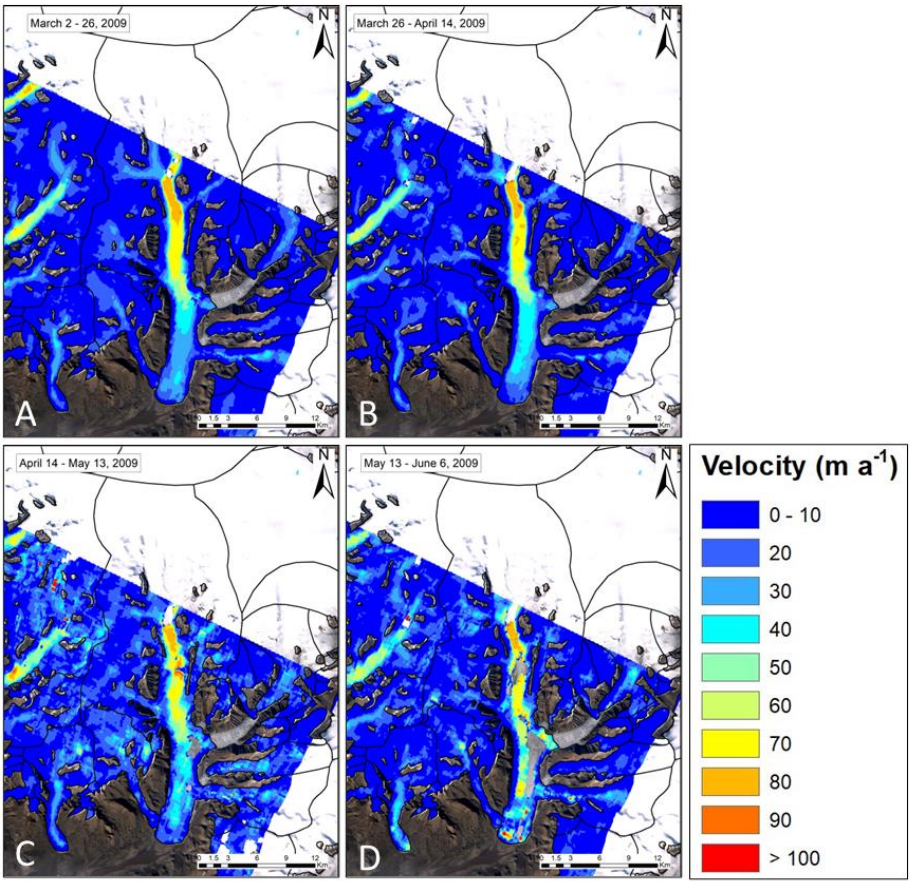

Figure 5-3. *Velocity structure of White and Thompson Glaciers derived from RADARSAT-2 Fine Beam F1N imagery from March 2nd to June 6th, 2009. Deep black lines on the figure indicate the glacier extents provided by version 6.0 of the Arctic Canada North shapefile of the Randolf Glacier Inventory. Background image is a cloud free Landsat image.*

The next R2 beam mode, F2 (Figure 5-4), has two image pairs from the accumulation season, April 16th to May 10th, 2009 (Figure 5-4A) and May 10th to June 3rd, 2009 (Figure 5-4B). Thompson Glacier experiences velocities under 22 m a^{-1} for the first kilometer then increases to 40 m a^{-1} around 6 km and reaching 45 m a^{-1} near 8 km upglacier from the terminus. A maximum velocity of 80 m a^{-1} is reached 20 km up glacier from the terminus, then decreases towards the ice cap interior.

White Glacier experiences a velocity under 20 m a^{-1} for the first few kilometers, then experiences velocity under 25 m a^{-1} near 4 km from the terminus. The velocity then varies between under 20 m a^{-1} and 30 m a^{-1} until the glacier reaches its maximum velocity of 60 m a^{-1} (Figure 5-4A) around 8 km from the glacier terminus and decreases slightly to under 30 m a^{-1} before increasing to 60 m a^{-1} at a distance of 9.2 km from the terminus, decreasing again to under 20 m a^{-1} further upglacier, towards the accumulation basin.

The R2 Fine Beam F2 derived velocity products, Figure 5-4, are poor results. The error of both image pairs were below the acceptable error limit, but there is a loss of coherence between images and greater velocity variability along the glacier trunks. The loss of coherence could be due to the start of the melt season, as the image pairs are from the end of accumulation season (Müller and Iken, 1973).

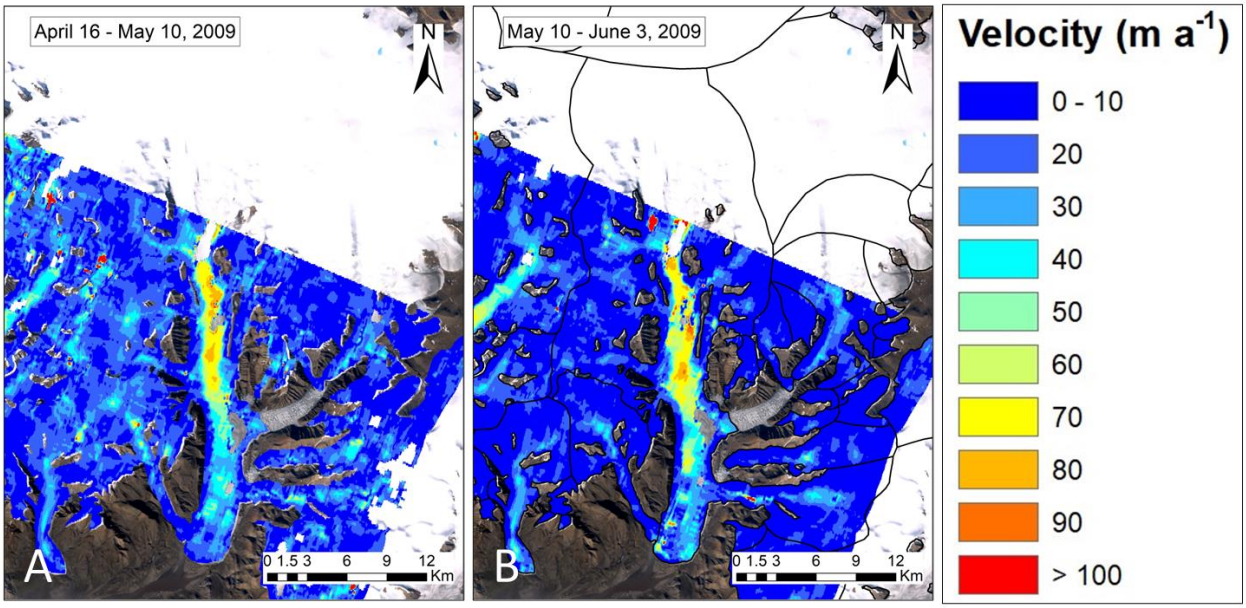

Figure 5-4. *Velocity structure of White and Thompson Glaciers derived from RADARSAT-2 Fine Beam F2 imagery April 16th to June 3rd, 2009. Deep black lines on the figure indicate the glacier extents provided by version 6.0 of the Arctic Canada North shapefile of the Randolf Glacier Inventory. Background image is a cloud free Landsat image.*

Figure 5-5 shows the velocity products of R2 Fine Beam F4 imagery. The three image pairs, March 3rd to 27th (Figure 5-5A), March 27th to April 20th (Figure 5-5B) and April 20th the May 14th (Figure 5-5C), show that Thompson Glacier experienced below 20 m a^{-1} for the first kilometer extending up from the terminus. The velocity then increases to 35 m a^{-1} around 3 km upglacier from the terminus then increases to a maximum velocity around 85 m a^{-1} at a distance of 23 km from the terminus.

White Glacier experienced velocities below 15 m a^{-1} for the first 3 km of the glacier. The velocity then increased to below 30 m a^{-1} around 3.5 km from the terminus. White Glacier then slows to under 10 m a^{-1} from 3.5 km further upglacier before reaching its velocity maximum of 60 m a^{-1} around 8 km from the terminus. The velocity decreases to below 25 m a^{-1} near the accumulation basin.

Figure 5-5 A and B are fairly good results, while Figure 5-5C provides less useable results. It shows White Glacier experiencing velocities upwards of 120 m a^{-1} in multiple locations along the glacier trunk

and a slight loss of coherence, likely errors that the GAMMA filtering code was unable to remove. Figure 5-5 D had a significant loss of velocity data along Thompson Glacier and was removed from further analysis of long and short-term changes in velocity structure of Thompson Glacier.

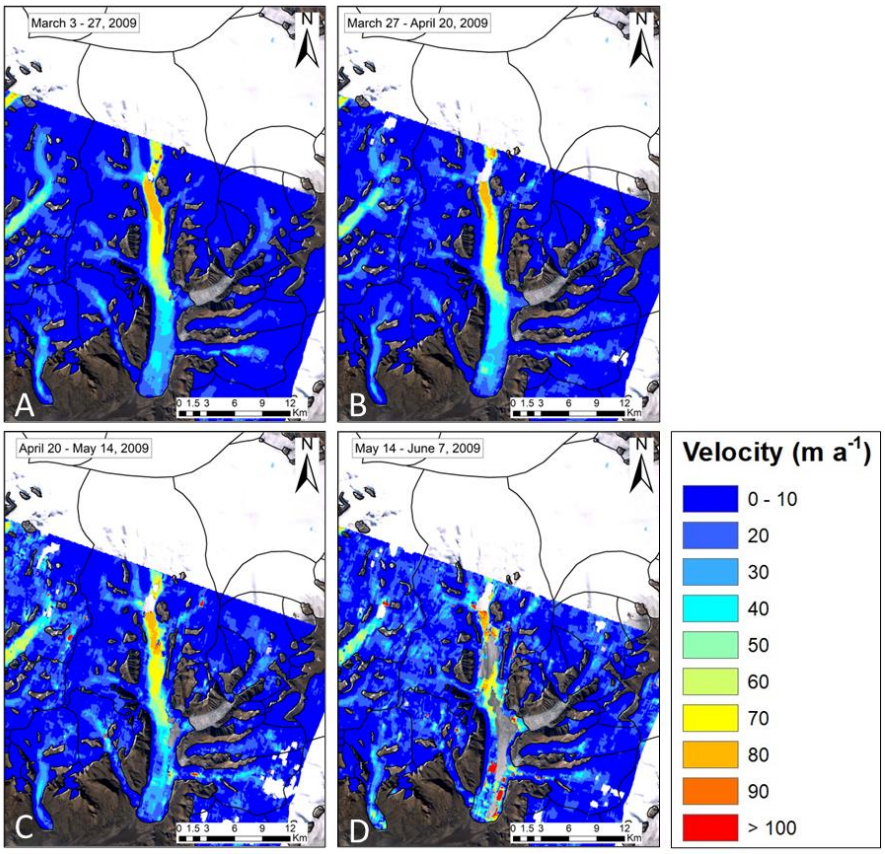

***Figure 5-5**. Velocity structure of White and Thompson Glaciers derived from RADARSAT-2 Fine Beam F4 imagery March 3rd to May 14th, 2009. Deep black lines on the figure indicate the glacier extents provided by version 6.0 of the Arctic Canada North shapefile of the Randolf Glacier Inventory. Background image is a cloud free Landsat image.*

Velocity products from R2 Fine Beam F5 are available for two image pairs in the spring of 2009, April 10th to May 4th and May 4th to 28th (Figure 5-6). Thompson Glacier experienced velocities below 20 m a^{-1} for the first kilometer from the terminus and increased to 45 m a^{-1} at 3.2 km from the terminus. The velocity decreased to under 40 m a^{-1} before increasing and exceeding 40 m a^{-1} around 9 km up glacier from the terminus. A maximum velocity of 90 m a^{-1} was reached near 24 km before decreasing again near the ice cap interior.

The first 0.5 km of White Glacier experienced a velocity below 30 m a^{-1} then decreased to below 10 m a^{-1} until the velocity increased slightly, staying below 20 m a^{-1} until 5 km from the terminus (Figure

5-6). White Glacier reached its maximum velocity of 30 m a^{-1} at a distance of 8 km from the terminus before slowly decreasing closer to the accumulation basin.

Both Figure 5-6 A and B had a significant loss of coherence along Thompson Glacier. Both A and B were removed from further velocity analysis due to both A and B having mean errors of 11 m a^{-1} and standard deviations of 10 m a^{-1} and 9 m a^{-1}, respectively. C and D are poorer results with a loss of coherence, possibly due to being close to the start of the melt season but were included in further analysis with errors below 10 m a^{-1}.

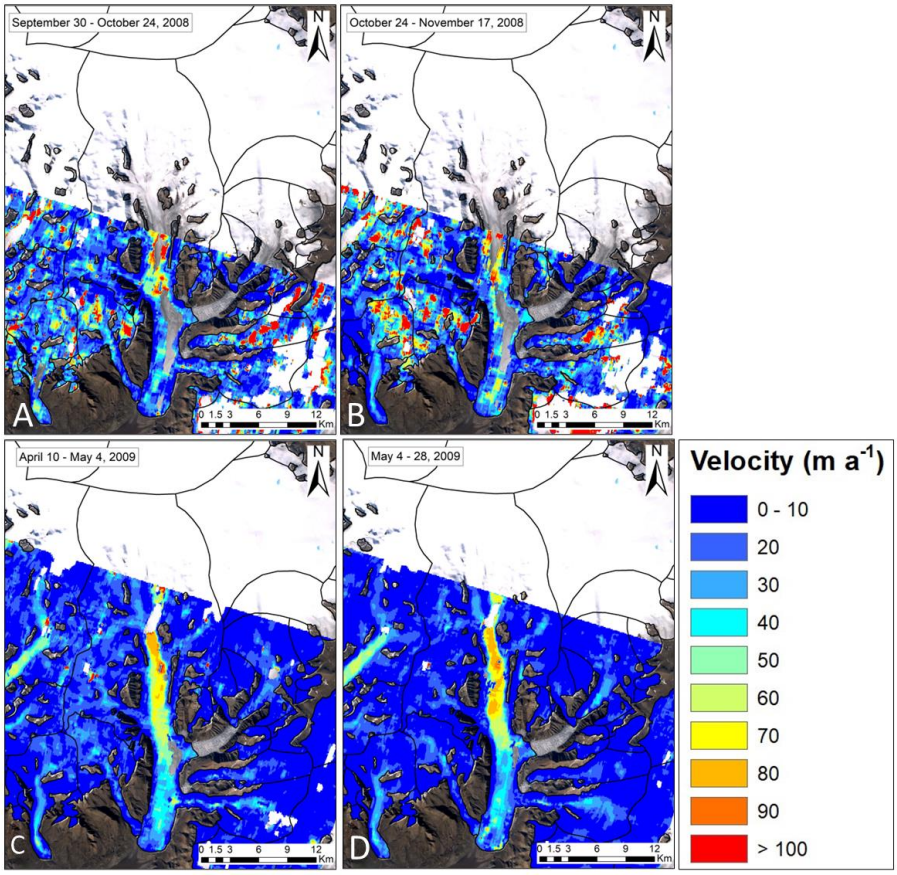

Figure 5-6. *Velocity structure of White and Thompson Glaciers derived from RADARSAT-2 Fine Beam F5 imagery from April 10th to May 28th, 2009. Deep black lines on the figure indicate the glacier extents provided by version 6.0 of the Arctic Canada North shapefile of the Randolf Glacier Inventory. Background image is a cloud free Landsat image.*

Fine Beam F6F data for the accumulation year 2008 to 2009 is presented in Figure 5-7. The first kilometer from the terminus of Thompson Glacier experienced velocities below 30 m a^{-1}, then stayed

under 40 m a^{-1} until a distance of 9.8 km from the terminus. The velocity then increased until Thompson Glacier experienced its maximum velocity of just under 90 m a^{-1} around 24 km from the terminus.

The first 4 km of White Glacier extending up from the terminus, experienced velocities below 15 m a^{-1}. The velocity increased to under 25 m a^{-1} around 5 km upglacier from the terminus. There is a slight decrease to under 15 m a^{-1} around 6 km, then the velocity of White Glacier increases to its maximum of 40 m a^{-1} at 8 km from the glacier tongue.

Good results were recorded in Figure 5-7 A to C, with a slight loss of coherence in Figure 5-7B and C, compared to A. Figure 5-7 D had a significant loss of coherence along Thompson Glacier and while this image pair had an error below 10 m a^{-1}, it was removed from further analysis as it was visually a poor result.

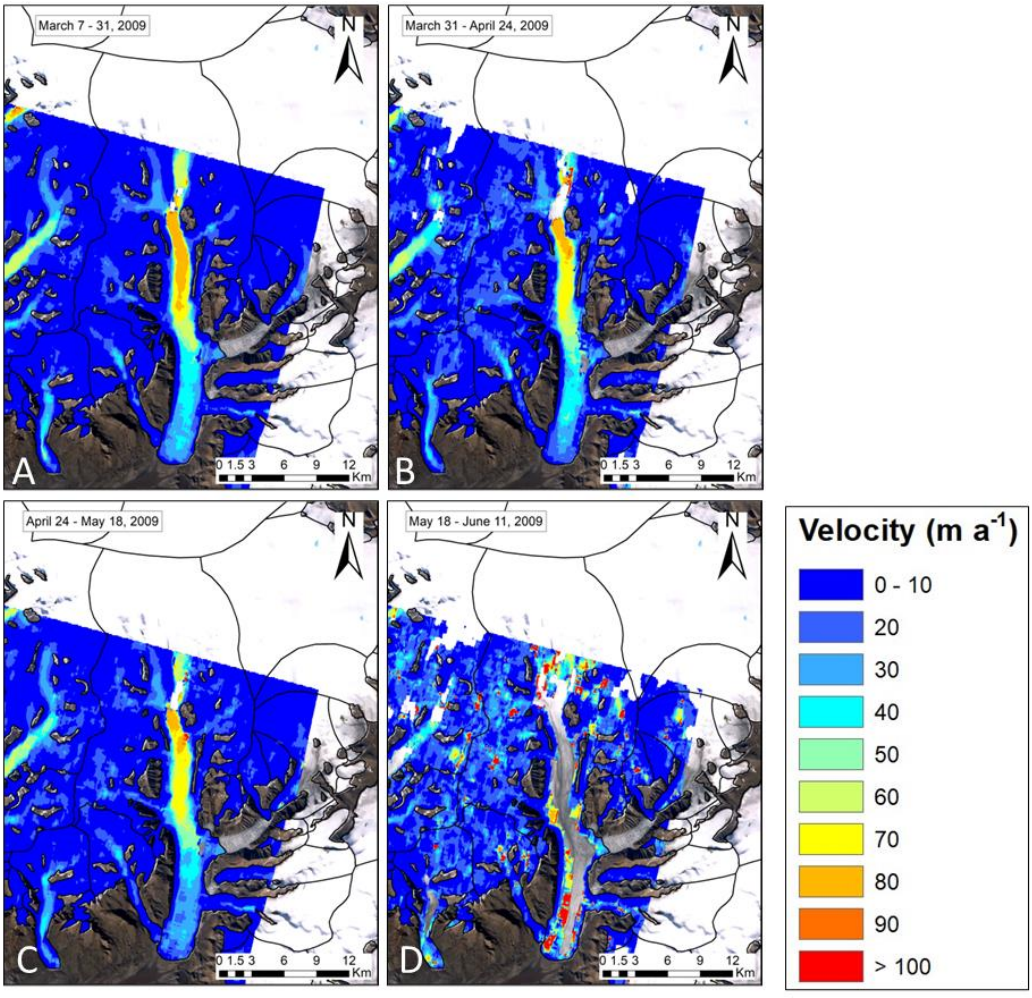

Figure 5-7. *Velocity structure of White and Thompson Glaciers derived from RADARSAT-2 Fine Beam F6F imagery from March 7th to May 18th, 2009. Deep black lines on the figure indicate the glacier extents provided by version 6.0 of the Arctic Canada North shapefile of the Randolf Glacier Inventory. Background image is a cloud free Landsat image.*

The last R2 beam mode with velocity data available for Thompson and White Glaciers for the accumulation year 2008 to 2009 is F6N (Figure 5-8). There were three image pairs available during the accumulation season: March 24 to April 17th (Figure 5-8A), April 17th to May 11th (Figure 5-8B) and May 11th to June 4th (Figure 5-8C). Velocities below 35 m a^{-1} were experienced along the first two kilometers extending from the glacier tongue of Thompson Glacier, with velocity increasing to below 50 m a^{-1} until 5 km from the terminus. The velocity decreased to under 35 m a^{-1} before steadily increasing along the trunk to a maximum velocity of 80 m a^{-1} around 22 km from the terminus.

White Glacier experienced velocities below 15 m a^{-1} from the terminus to 0.6 km upglacier. The velocity then decreased to below 10 m a^{-1} before increasing to velocities around 25 m a^{-1} around 1.5 km from the terminus. The velocity along the centerline decreased to below 10 m a^{-1} again around 3 km, before increasing to reach a maximum velocity of 40 m a^{-1} around 8.5 km from the terminus.

Poor results were recorded in Figure 5-8 B and C, while good results were recorded in Figure 5-8A. There are multiple lengths of the Thompson Glacier with no velocity information, particularly for Figures 5-8 B and C, likely due to a loss of coherence with the onset of the melt season. Figure 5-8 B also showed White Glacier experiencing velocities upwards of 160 m a^{-1} in different locations along the main trunk, which is likely incorrect and due to the GAMMA filtering code being unable to remove these errors.

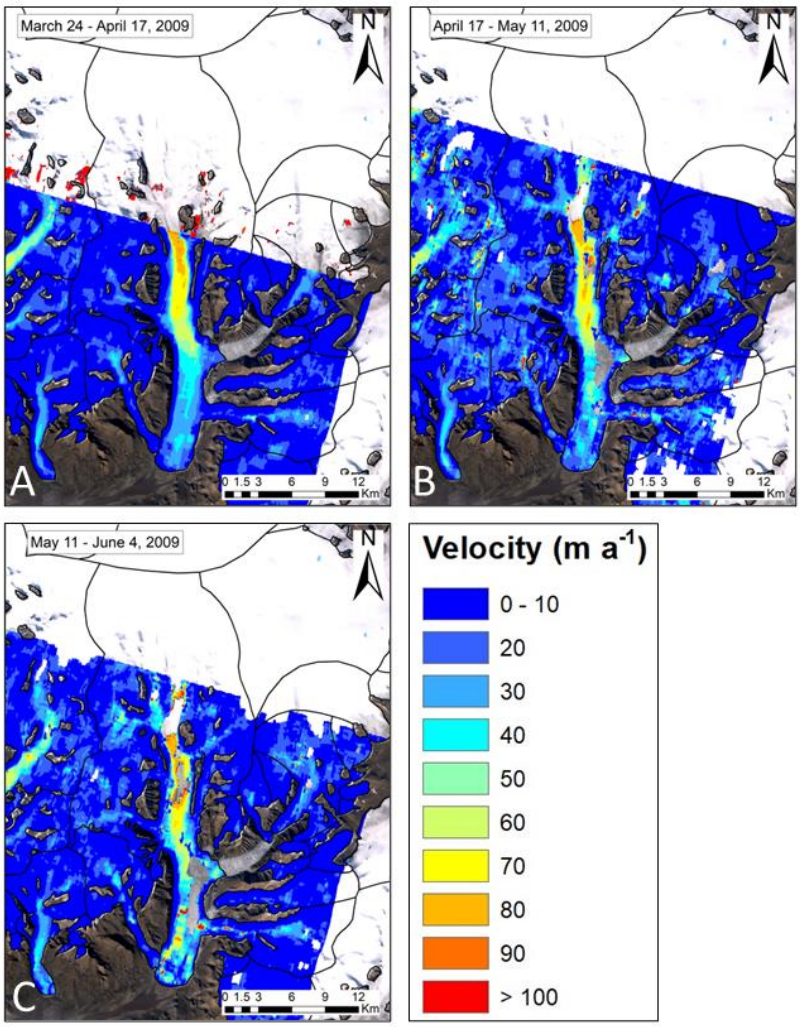

Figure 5-8. *Velocity structure of White and Thompson Glaciers derived from RADARSAT-2 Fine Beam F6N imagery from March 24th to June 4th, 2009. Deep black lines on the figure indicate the glacier extents provided by version 6.0 of the Arctic Canada North shapefile of the Randolf Glacier Inventory. Background image is a cloud free Landsat image.*

5.1.2 Accumulation year 2009 – 2010

There are only two beam modes available for R2 Fine Beam for the accumulation season of 2009 to 2010, F4 (Figure 5-9) and F5 (Figure 5-10). Beam mode F4 had four image pairs available for each season, resulting in nine velocity products (Figure 5-9). The first kilometer near the terminus of Thompson Glacier, experienced velocities under 20 m a^{-1}. The glacier velocity increased to around 30 m a^{-1} at a distance of 3 km from the terminus and stays around that magnitude of velocity until a distance of 6 km from the terminus, at which point the velocity increases to around 40 m a^{-1}. The glacier velocity slows

slightly to under 35 m a^{-1} until increasing again around 10 km, where the velocity increases upglacier to reach a maximum velocity of 85 m a^{-1} around 24 km from the glacier tongue.

White Glacier experienced velocities below 10 m a^{-1} from the terminus to 2 km upglacier. The centerline velocities then increased to around 20 m a^{-1} before decreasing to around 10 m a^{-1} at a distance of 6 km from the terminus. White Glacier experienced a maximum velocity of 50 m a^{-1} around 9 km before decreasing towards the accumulation basin.

Particularly good results were recorded in Figures 5-9 F, G and H, while poorer results were recorded in Figure 5-9 A to E and I. The loss of coherence experienced in Fig 5-9 I, could be explained by the onset of the melt season (Müller and Iken, 1973). Figure 5-9 A and B, during the fall, are at the start of the accumulation season. Figure 5-9 C to E are from the winter season. Typically, the winter season records good results (Van Wychen et al., 2016), but there was a loss of coherence in these images, despite low errors of 6 and standard deviation of 6 m a^{-1} (Figure 5-9C), mean error of 6 and standard deviation of 5 m a^{-1} (Figure 5-9D) and a mean error of 4 and standard deviation of 4 m a^{-1} (Figure 5-9E), possibly due to precipitation.

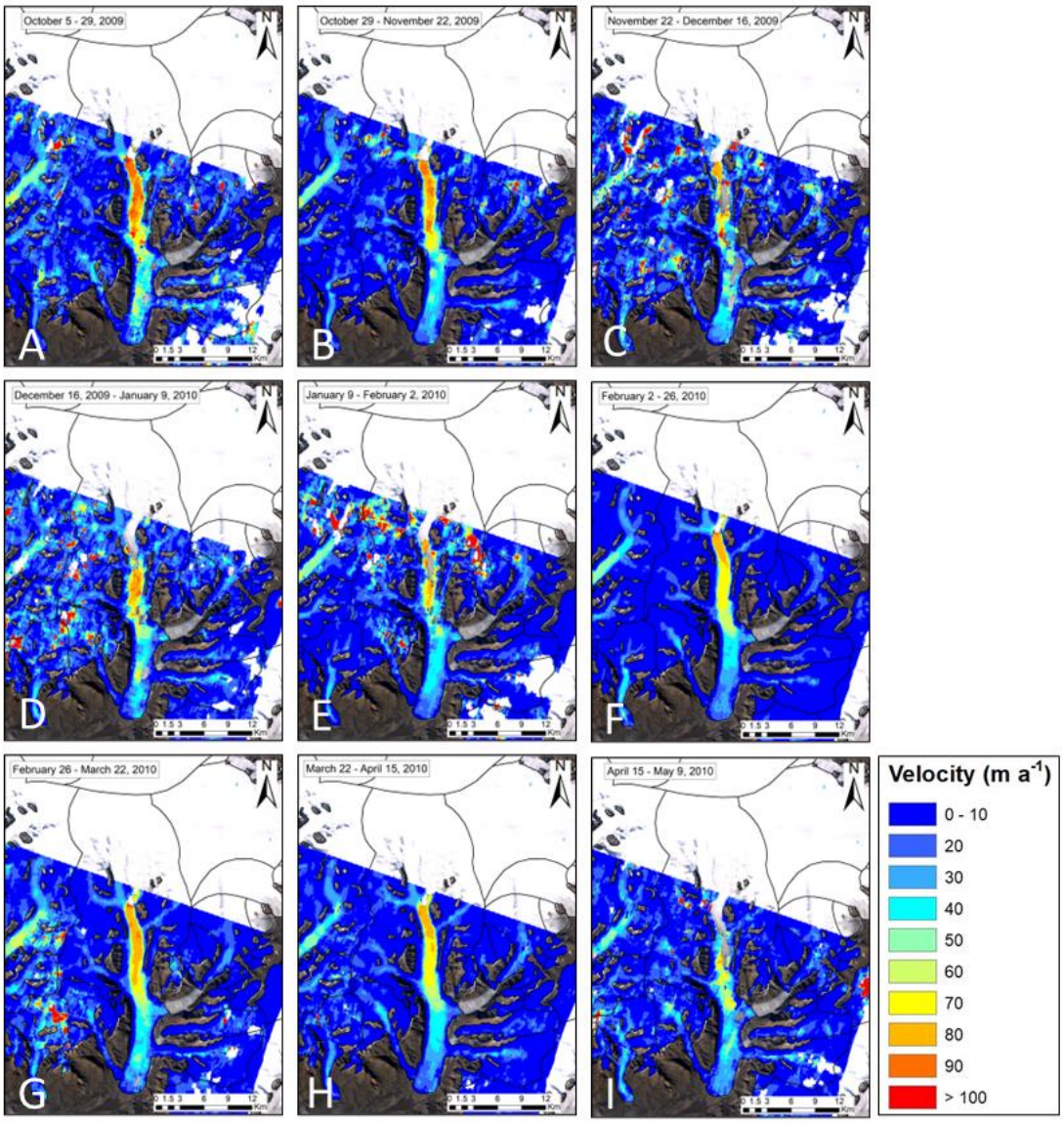

Figure 5-9. *Velocity structure of White and Thompson Glaciers derived from RADARSAT-2 Fine Beam F4 imagery from October 5th, 2009 to May 9th, 2010. Deep black lines on the figure indicate the glacier extents provided by version 6.0 of the Arctic Canada North shapefile of the Randolf Glacier Inventory. Background image is a cloud free Landsat image.*

Beam mode F5 (Figure 5-10) resulted in six image pairs across the accumulation season. The first kilometer from the terminus of Thompson Glacier experienced velocities below 15 m a^{-1}. The glacier then increased to under 35 m a^{-1} around 3 km from the terminus and extending upglacier. The velocity increased to above 40 m a^{-1} at a distance of 9 km from the terminus. The velocity of Thompson Glacier continued to increase until a maximum of 90 m a^{-1}, around 23.5 km from the glacier tongue, was reached, at which point the velocity decreased further upglacier towards the ice cap.

White Glacier experienced slower velocities of under 10 m a^{-1} for the first 2 km extending upglacier from the terminus. The velocity then increased slightly but stayed under 15 m a^{-1} until 4 km from the terminus, where velocities reached 20 m a^{-1} and continued to increase upglacier. At a distance of 6 km from the terminus, the velocity of White Glacier suddenly decreased for a short distance to velocities below 10 m a^{-1}. The glacier motion increased again around 6.5 km and continued to increase until a maximum velocity of 45 m a^{-1} was reached at 8.5 km from the terminus. The velocity slowly decreased towards the accumulation basin.

Figure 5-10 resulted in poor results, suggesting that a loss coherence was experienced; however Figure 5-10 G is slightly better than the rest. Figure 5-10 B, C, and J resulted in errors above the 10 m a^{-1} error limit of this study and were removed from further velocity analysis. Figure 5-10 D had an error below this limit but was removed from further analysis due to it being a poor result visually.

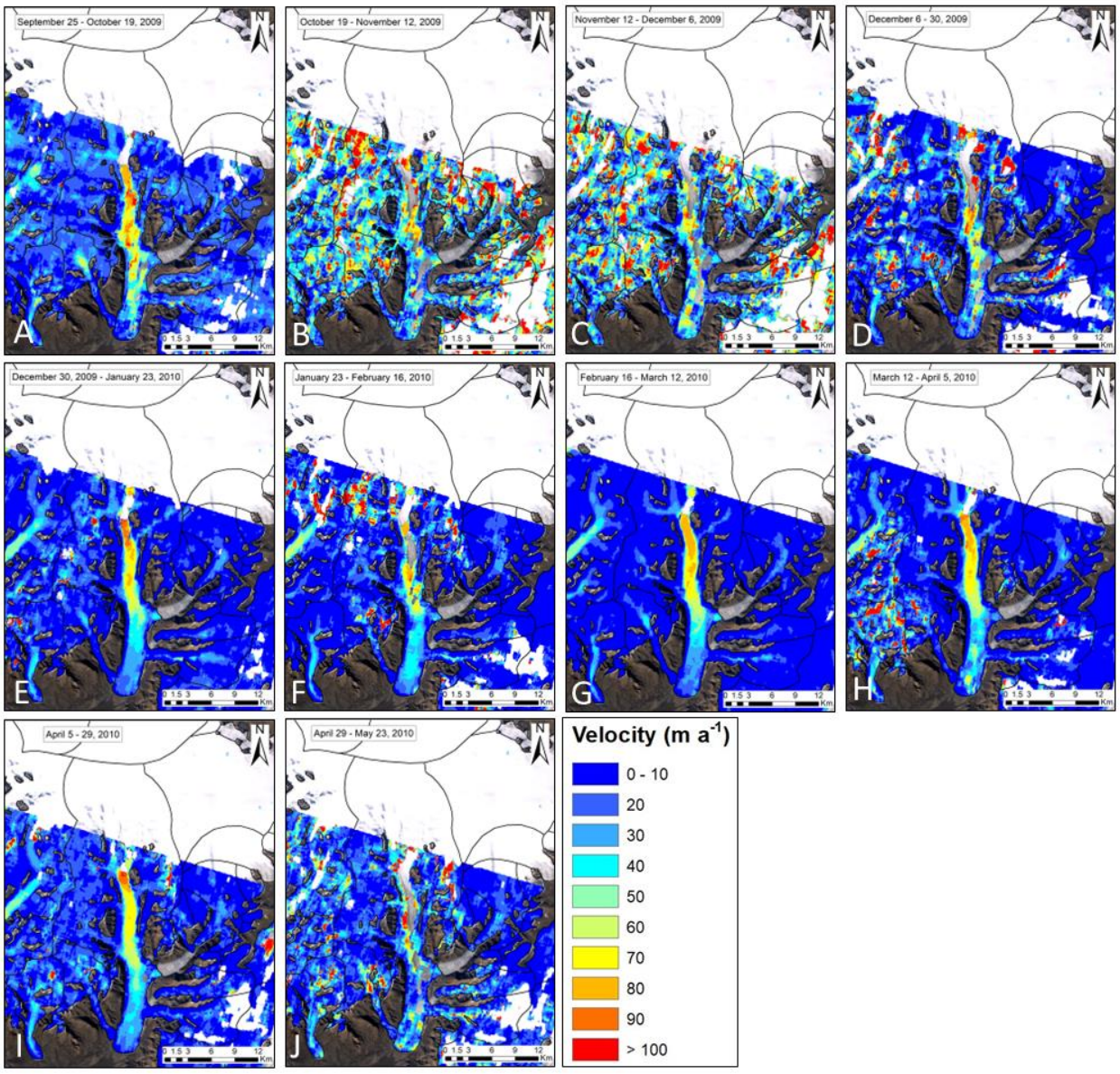

Figure 5-10. *Velocity structure of White and Thompson Glaciers derived from RADARSAT-2 Fine Beam F5 imagery from September 25th, 2009 to April 29th, 2010. Deep black lines on the figure indicate the glacier extents provided by version 6.0 of the Arctic Canada North shapefile of the Randolf Glacier Inventory. Background image is a cloud free Landsat image.*

5.1.3 Accumulation year 2010 – 2011

The 2010 to 2011 accumulation season includes data from R2 Fine Beam F4 (Figure 5-11) and R2 Yearly (Figure 5-12). This is the last accumulation season where there is R2 Fine Beam data available in this study for Thompson and White Glaciers. The Fine Beam F4 shows Thompson Glacier experienced velocities below 20 m a^{-1} for the first 2 km extending up from the terminus. The velocity then increased to

around 30 m a^{-1} until a distance of 7 km from the glacier tongue. The velocity gradually increased along the length of the glacier trunk before reaching its maximum velocity of 100 m a^{-1} at a distance of 21 km from the terminus before decreasing again upglacier.

The first 0.6 km of White Glacier experienced velocities below 20 m a^{-1}. The velocity then decreased to under 10 m a^{-1} before increasing further upglacier to under 20 m a^{-1} at 4 km. The velocity decreased to under 15 m a^{-1} around 5 km from the terminus before increasing to reach a maximum velocity of 30 m a^{-1}. The velocity then decreased from 30 m a^{-1} towards the accumulation basin. Good results were recorded in Figure 5-11 A compared to Figure 5-11 B.

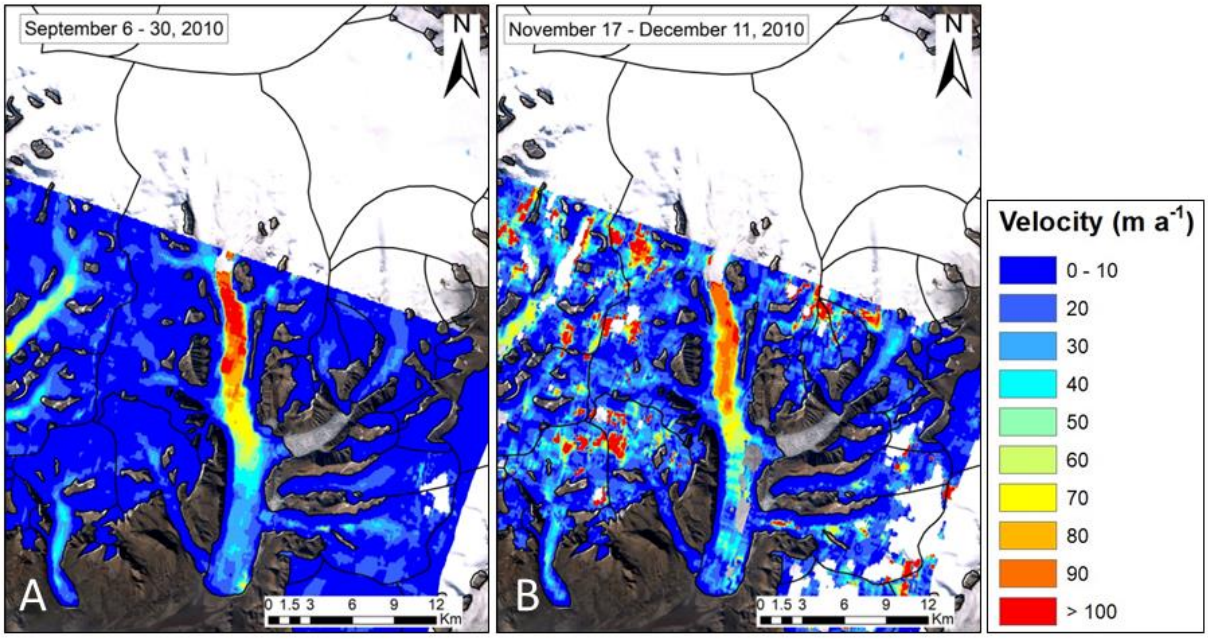

Figure 5-11. *Velocity structure of White and Thompson Glaciers derived from RADARSAT-2 Fine Beam F4 imagery from September 6th to December 11th, 2010. Deep black lines on the figure indicate the glacier extents provided by version 6.0 of the Arctic Canada North shapefile of the Randolf Glacier Inventory. Background image is a cloud free Landsat image.*

Figure 5-12 shows the pre-derived R2 Yearly velocity product that was created by averaging image pairs, February 1st to February 25th, 2011, and February 18th to March 14th, 2011. This averaged velocity product represented glacier motion for the 2010/11 accumulation season in the original study (Van Wychen et al., 2016). The velocity at the terminus of Thompson Glacier started around 15 m a^{-1} and increased to 40 m a^{-1} at 2 km from the terminus. The velocity along the glacier trunk then increased to 50 m a^{-1} at 6 km. The velocity then continued to increase along the length of Thompson Glacier before

reaching a maximum of 95 m a^{-1} around 23 km upglacier from the terminus. The velocity then decreased to below 20 m a^{-1} towards the ice cap interior.

White Glacier, Figure 5-12, experienced velocities below 20 m a^{-1} along the first 2 km then increased to 30 m a^{-1} until 6 km from the terminus, at which point, the velocity continued to increase until reaching a maximum velocity of 50 m a^{-1} around 8.5 km from the terminus.

The quality of these results are poorer, but comparable to the previous R2 Fine Beam velocity products.

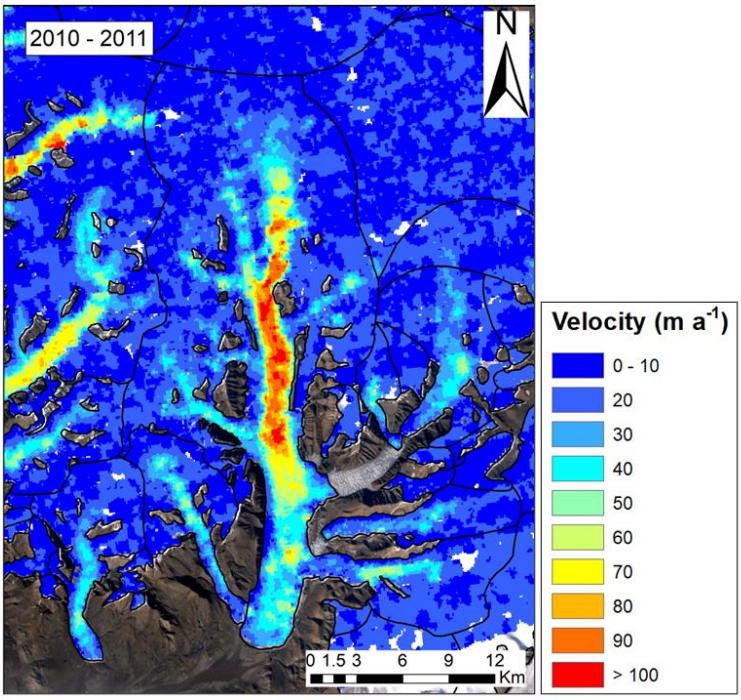

***Figure 5-12**. Velocity structure of White and Thompson Glaciers derived from Radarsat-2 Yearly imagery for the accumulation season 2010-2011 (the combination of reference image dates from February 1st and 18th, 2011 and secondary image dates of February 25th and March 14th, 2011 were averaged to create velocity representation). The thick black lines on the figure indicate the glacier extents provided by version 6.0 of the Arctic Canada North shapefile of the Randolf Glacier Inventory. Background image is a cloud free Landsat image.*

5.1.4 Accumulation year 2012 – 2013

This accumulation season consists of data from R2 Spotlight (Figure 5-13) and R2 Yearly (Figure 5-14) velocity products. The R2 Spotlight data only covers the terminus region of Thompson, so this data was used to focus on White Glacier.

White Glacier, based on R2 Spotlight, experienced a velocity of 10 m a^{-1} for the first 1.5 km from the terminus (Figure 5-13). The velocity then increased upglacier from the 1.5 km to 4.5 km where the velocity reached just below 30 m a^{-1}. The velocity then decreased to 20 m a^{-1} at a distance of 7 km, before increasing again to a maximum velocity of 30 m a^{-1}. The velocity then decreased to below 20 m a^{-1} at a distance of 10.5 km from the terminus, approaching the accumulation basin.

Particularly good results were recorded in Figure 5-13 A and B, better than the previous R2 Fine Beam (Figures 5-1 to 5-11) and Yearly (Figure 5-12) results presented. The R2 Spotlight data of Figure 5-13 has less variability in the velocities. Figure 5-13 produces a much cleaner velocity map than the previously R2 Fine Beam and Yearly products, which have greater noise.

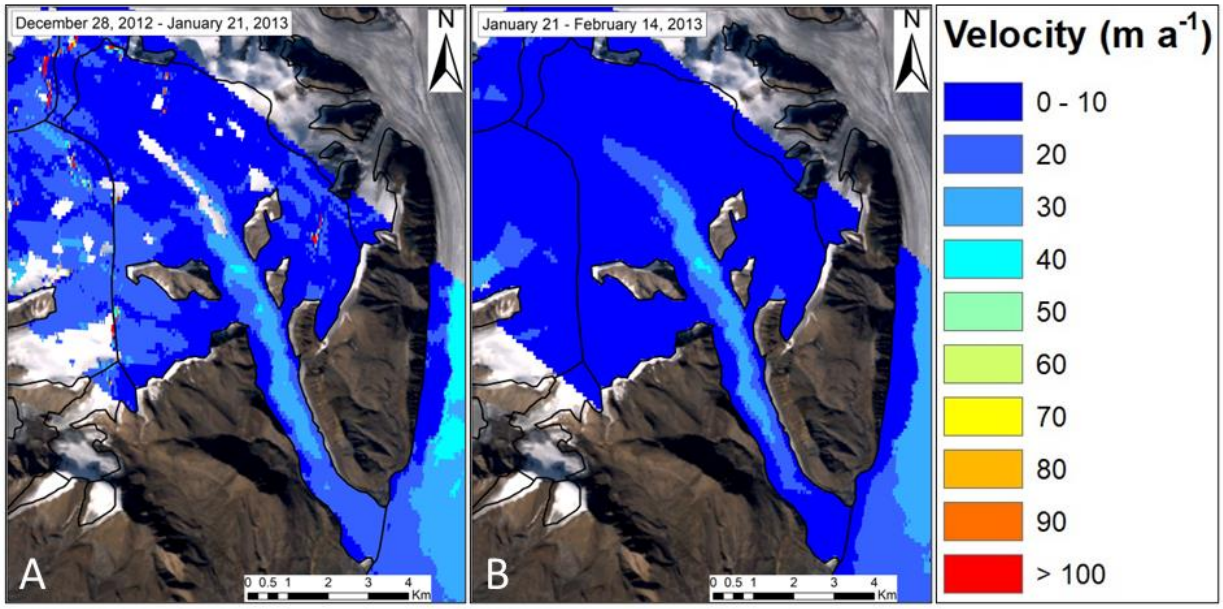

Figure 5-13. *Velocity structure of White Glacier derived from R2 Spotlight imagery from December 28th, 2012 to February 14th, 2013. Deep red line indicates the center of White Glacier. The thick black lines on the figure indicate the glacier extents provided by version 6.0 of the Arctic Canada North shapefile of the Randolf Glacier Inventory. Background image is a cloud free Landsat image.*

Figure 5-14 shows the pre-derived R2 Yearly velocity product with the acquisition dates of January 4th to 28th, 2013. Thompson Glacier experienced velocity below 10 m a^{-1} for the first kilometer extending up from the terminus, then increased to 25 m a^{-1} further upglacier after that first kilometer. The velocity increased to 75 m a^{-1} at a distance of 9 km from the terminus then decreased to below 40 m a^{-1} until the velocity increased again 11 km from the terminus until a maximum velocity of 80 m $a^{-1}$was reached at a

distance of 20 km from the glacier tongue. The velocity steadily decreased upglacier towards the ice cap after reaching its maximum.

White Glacier experienced velocity below 25 m a^{-1} for the first kilometer then decreased to below 10 m a^{-1} until 1.5 km from the terminus where the velocity increased to 20 m a^{-1}. The velocity then increased to 30 m a^{-1} at a distance of 6 km from the terminus. The velocity then dropped to below 5 m a^{-1} 7 km from the terminus until 10 km from the terminus, where the velocity increased to 20 m a^{-1}.

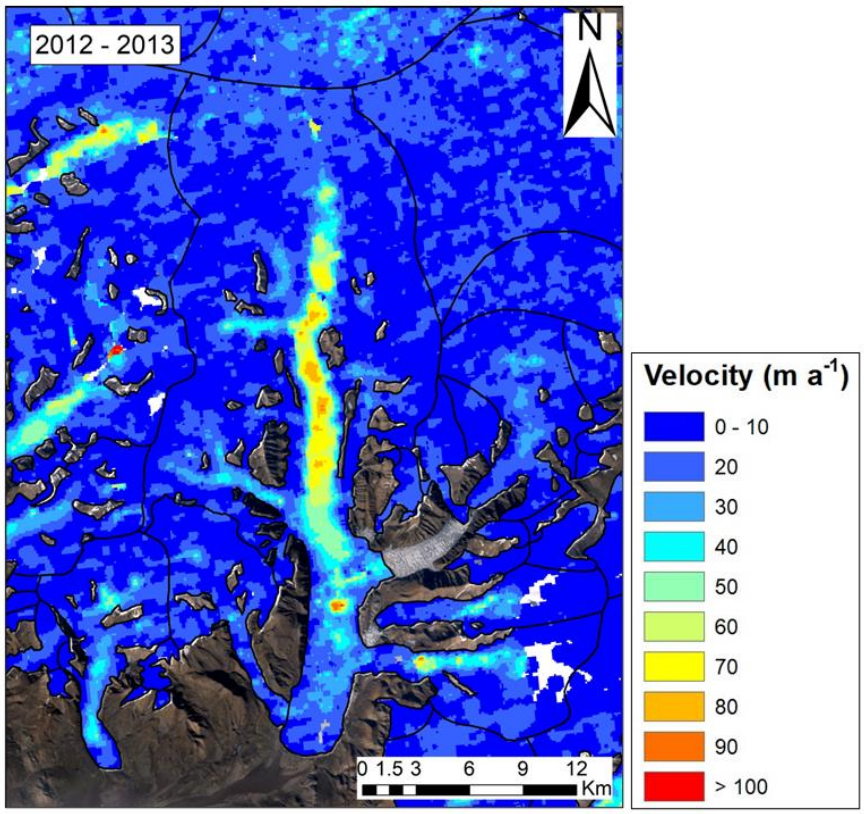

Figure 5-14. *Velocity structure of White and Thompson Glaciers derived from Radarsat-2 Yearly imagery for the accumulation season 2012-2013 (reference image from January 4th, 2013 and secondary image from January 28th, 2013). The thick black lines on the figure indicate the glacier extents provided by version 6.0 of the Arctic Canada North shapefile of the Randolf Glacier Inventory. Background image is a cloud free Landsat image.*

The R2 Spotlight (Figure 5-13) velocity product and the R2 Yearly (Figure 5-14) both have data available for January 2013. The R2 Yearly data has greater noise than the R2 Spotlight data. While both datasets show a maximum velocity of 30 m a^{-1}, there is greater variability in the R2 Yearly data along the glacier centerline compared to the R2 Spotlight data, particularly near the terminus region of White Glacier. R2 Spotlight data (Figure 5-13) shows the first 1.5 km from the terminus experienced velocity around 10 m a^{-1}, while Yearly data (Figure 5-14) shows the terminus experiencing velocities around 25 m

a^{-1} that decrease to 10 m a^{-1} then increase again to 20 m a^{-1}. Visually the R2 Spotlight data has less noise than the pre-derived R2 Yearly data.

5.1.5 Accumulation year 2013 – 2014

The velocity products from R2 Spotlight for White Glacier are presented in Figure 5-15. White Glacier experienced velocity below 15 m a^{-1} for the first kilometer extending up from the terminus. The velocity slightly decreased to below 10 m a^{-1} from 1 to 1.5 km from the terminus before steadily increasing to 25 m a^{-1} at a distance of 4 km from the terminus. The velocity stayed around 25 m a^{-1} upglacier until increasing to a maximum of 30 m a^{-1} at a distance of 7.5 km from the terminus. The velocity then decreased upglacier, towards the accumulation basin, to below 15 m a^{-1} at a distance of 10.5 km from the terminus.

Particularly good results were recorded in Figure 5-15, particularly A-E. There was very little loss of coherence between images and visually, the velocity products have less noise and better resolution than R2 Fine Beam and Yearly products. Figure 5-15F has a slight loss of coherence, likely due to the onset of the melt season (Müller and Iken, 1973).

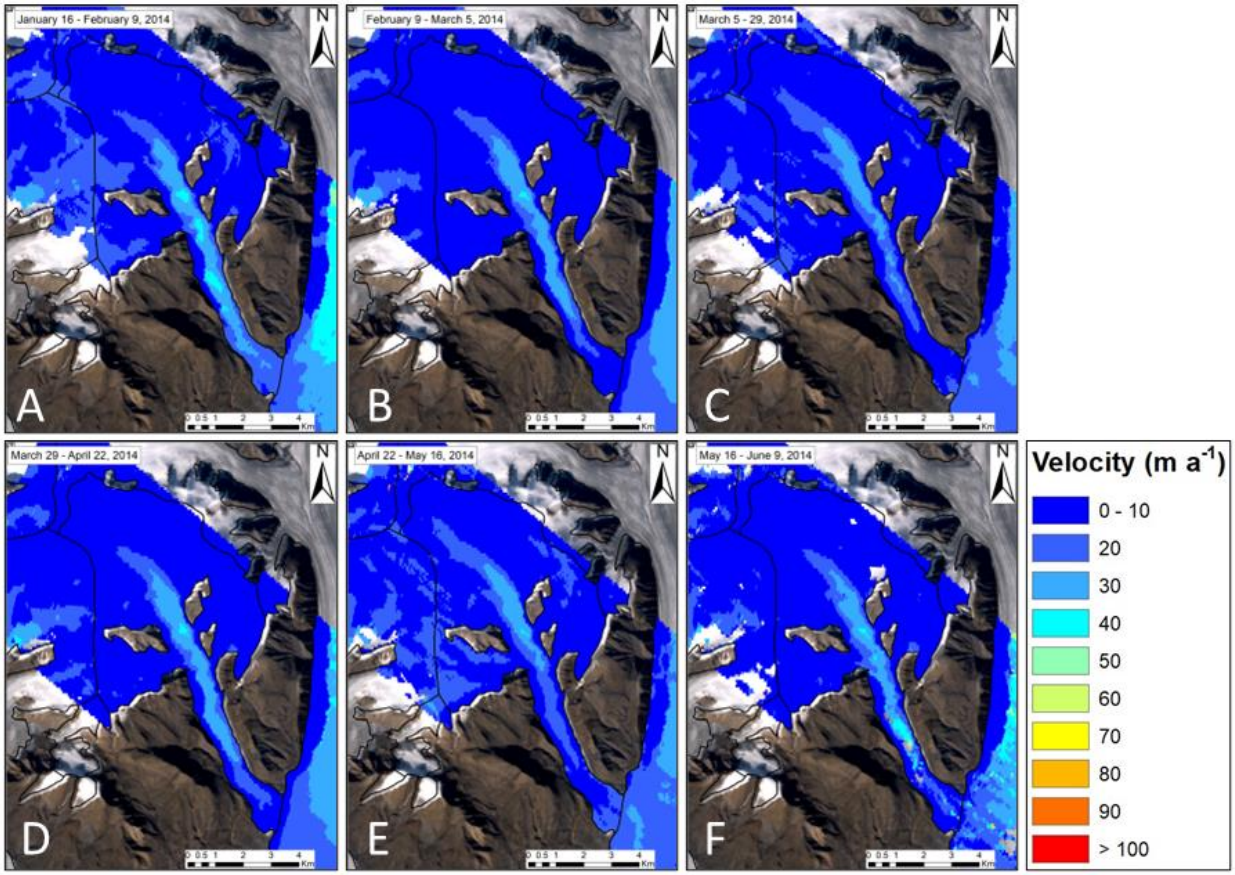

Figure 5-15. *Velocity structure of White Glacier derived from R2 Spotlight imagery from January 16th to June 9th, 2014. The thick black lines on the figure indicate the glacier extents provided by version 6.0 of the Arctic Canada North shapefile of the Randolf Glacier Inventory. Background image is a cloud free Landsat image.*

The pre-derived R2 Yearly velocity product is presented in Figure 5-16. The first 700 m from upglacier of the terminus of Thompson Glacier was missing. A velocity of 28 m a^{-1} was recorded at 0.8 km from the terminus. The velocity then decreased to below 20 m a^{-1} at 2.5 km from the terminus before increasing again to 30 m a^{-1} at a distance of 3 km from the terminus. The velocity then started increasing again after 7 km and reached a maximum velocity of 80 m a^{-1} at a distance of 22 km from the glacier tongue. The velocity decreased to below 40 m a^{-1} around 31 km from the terminus.

White Glacier experienced velocity just below 18 m a^{-1} at the terminus before decreasing to below 10 m a^{-1} at a distance of 0.5 km until 1.5 km from the terminus until. The velocity fluctuates a bit between under 20 m a^{-1} to under 10 m a^{-1} from 1.5 to 6 km from the terminus. At 6 km, the velocity starts increasing to 30 m a^{-1} at 6.5 km. The velocity reaches below 10 m a^{-1} for a few hundred meters between 7 and 7.3 km before steadily increasing to reach a maximum velocity of 45 m a^{-1} at 8 km from the terminus.

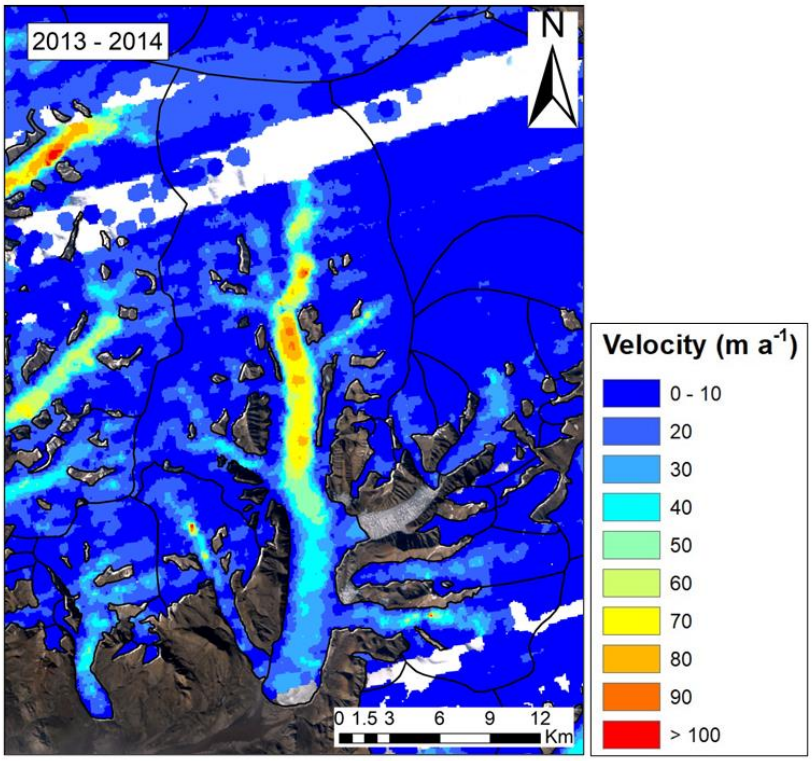

Figure 5-16. *Velocity structure of White and Thompson Glaciers derived from Radarsat-2 Yearly imagery for the accumulation season 2013-2014 (reference image from January 23rd, 2014, and secondary image from February 18th, 2014). The thick black lines on the figure indicate the glacier extents provided by version 6.0 of the Arctic Canada North shapefile of the Randolf Glacier Inventory. Background image is a cloud free Landsat image.*

The R2 Spotlight (Figure 5-15) has six image pairs available between January 16th (reference image date of first image pair) to June 9th (secondary image of last image pair), 2014. The R2 Yearly (Figure 5-16) for this accumulation season is from February 2014. The R2 Yearly data has greater noise than the R2 Spotlight data. The R2 Spotlight data shows a maximum surface velocity of 30 m a^{-1}, while the R2 Yearly has a maximum velocity of 45 m a^{-1}. Overall, R2 Spotlight shows slightly lower velocities along the length of the glacier, with the greatest difference being between the maximum velocities. Visually the R2 Spotlight (Figure 5-15) data has less noise than the pre-derived R2 Yearly (Figure 5-16) data.

5.1.6 Accumulation year 2014 – 2015

The R2 Spotlight data for White Glacier for the spring of 2015 is presented in Figure 5-17. White Glacier experienced velocities below 5 m a^{-1} for the first 0.7 km of the glacier extending up from the tongue. The velocity then stays below 10 m a^{-1} until 2 km from the terminus. The velocity then increases

with some variability to 30 m a^{-1} at a distance of 6.5 km from the terminus. The velocity then decreases to below 20 m a^{-1} between 6.7 km and 7 km from the terminus before reaching a maximum velocity of 30 m a^{-1} at a distance of 7.8 km from the terminus. The velocity then decreases further upglacier towards the accumulation basin.

Figure 5-17 recorded particularly good results. There is good coherence between image pairs and they visually look better than and the R2 Yearly (5-18).

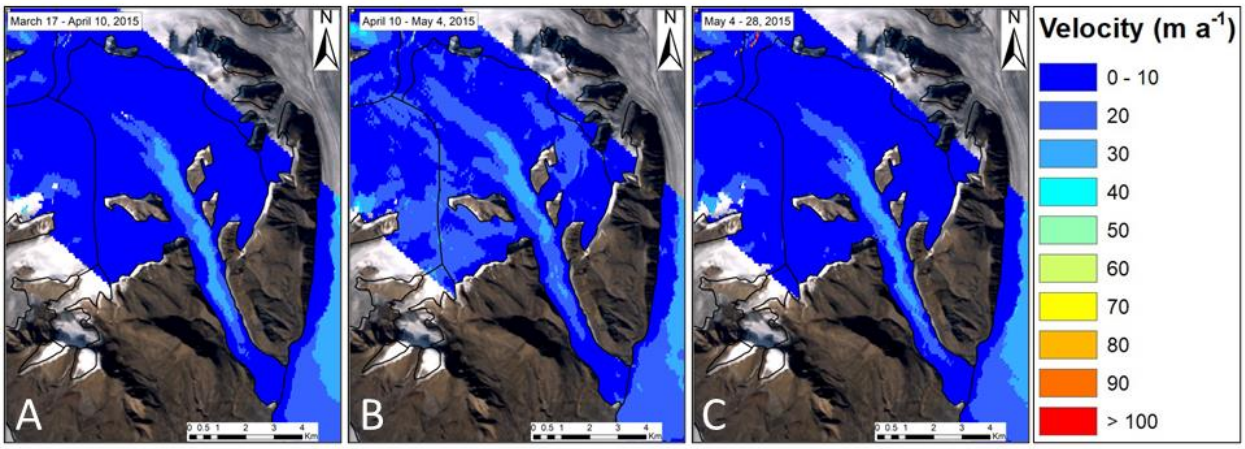

Figure 5-17. *Velocity structure of White Glacier derived from R2 Spotlight imagery from March 17th to June 21. Deep red line indicates the center of White Glacier. The thick black lines on the figure indicate the glacier extents provided by version 6.0 of the Arctic Canada North shapefile of the Randolf Glacier Inventory. Background image is a cloud free Landsat image.*

The R2 Yearly (Figure 5-18) was an image pair from the winter, January 18th to February 11th, 2015. Thompson Glacier experienced velocity below 10 m a^{-1} near the terminus until 0.6 km. The velocity then increased to 25 m a^{-1} at 0.6 km then decreased to below 15 m a^{-1} after 2 km from the terminus. The velocity started increasing again around 3.8 km from the terminus until reaching 40 m a^{-1} at a distance of 5 km from the terminus. At 6 km, the velocity decreased until reaching 20 m a^{-1} at 7.5 km from the terminus. The velocity started increasing again around 10 km until reaching a maximum velocity of 100 m a^{-1} from 21 km to 22.5 km, after which, the velocity decreased.

White Glacier experienced a velocity below 10 m a^{-1} for the first 500 m extending up from the terminus. The velocity fluctuated between 15 m a^{-1} and under 10 m a^{-1} until a distance of 6 km from the terminus, where the velocity reached 10 m a^{-1} and increased until a maximum of 45 m a^{-1} was reached 7.4 km from the terminus. The velocity then decreased after reaching the maximum to under 15 m a^{-1} at 10.5 km from the glacier tongue.

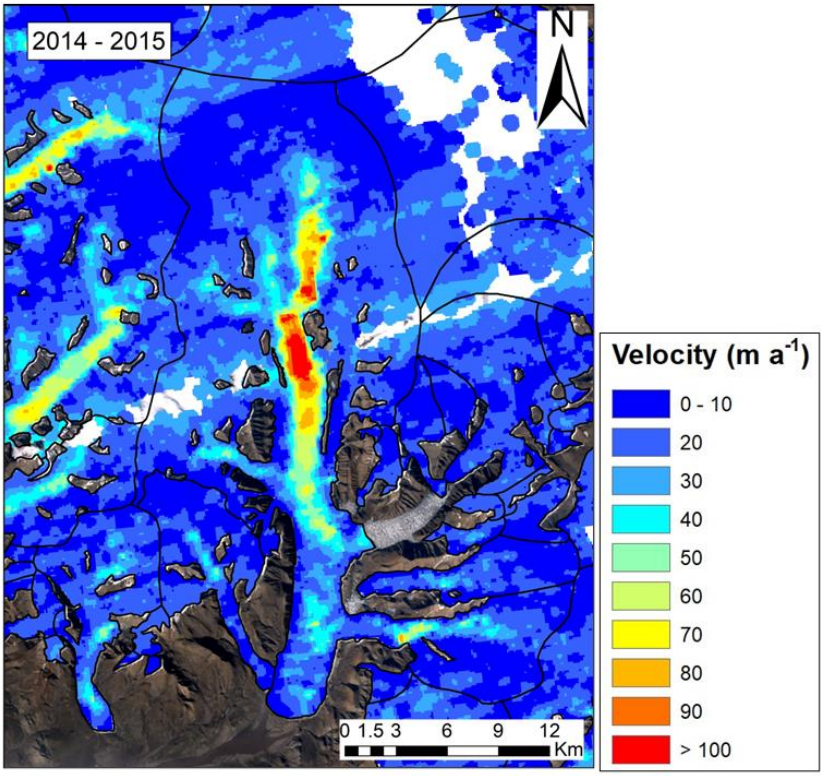

Figure 5-18. *Velocity structure of White and Thompson Glaciers derived from Radarsat-2 Yearly imagery for the accumulation season 2014-2015 (reference image from January 18th, 2015, and secondary image from February 11th, 2015). The thick black lines on the figure indicate the glacier extents provided by version 6.0 of the Arctic Canada North shapefile of the Randolf Glacier Inventory. Background image is a cloud free Landsat image.*

Figure 5-18, which presents the R2 Yearly data, provided less useable results, especially compared to the good results of the R2 Spotlight data (Figure 5-17). The R2 Yearly (Figure 5-18) data is from January 18th to February 11th, 2015. The R2 Spotlight (Figure 5-17) data is from March 17th to May 28th, 2015. Figure 5-18 should provide better results as it is from the middle of the winter season (Van Wychen et al., 2016), while the R2 Spotlight data is from the spring. There is more noise in the R2 Yearly data, possibly because it has a lower spatial resolution than the R2 Spotlight (Figure 5-17).

5.1.7 Accumulation year 2019 – 2020

TerraSAR-X data over Thompson and White Glaciers are available for this accumulation season, as well as the 2020/21 and 2021/22 accumulation seasons. During 2019/20, the first kilometer of Thompson Glacier is below 15 m a^{-1}, the velocity then increases to 20 m a^{-1} at 2 km (Figure 5-19). The

velocity then slowly increases and reaches 30 m a^{-1} at 8.5 km. The velocity then increases to reach a maximum of 75 m a^{-1} at a distance of 23.5 km from the terminus. After reaching its maximum velocity, the glacier slows towards the accumulation area and reaches 10 m a^{-1} at 36 km.

White Glacier has a velocity under 10 m a^{-1} until 3.5 km from the terminus, where it starts increasing and reaches 20 m a^{-1} at 4 km. A velocity around 25 m a^{-1} is then maintained until reaching 25 m a^{-1} at 7 km from the terminus. White Glacier then reaches its maximum velocity of 32 m a^{-1} at a distance of 8.5 km from the terminus. The velocity then decreases towards the accumulation basin, reaching below 10 m a^{-1} after 10.7 km.

The four velocity products in Figure 5-19 recorded particularly good results with good coherence between image pairs.

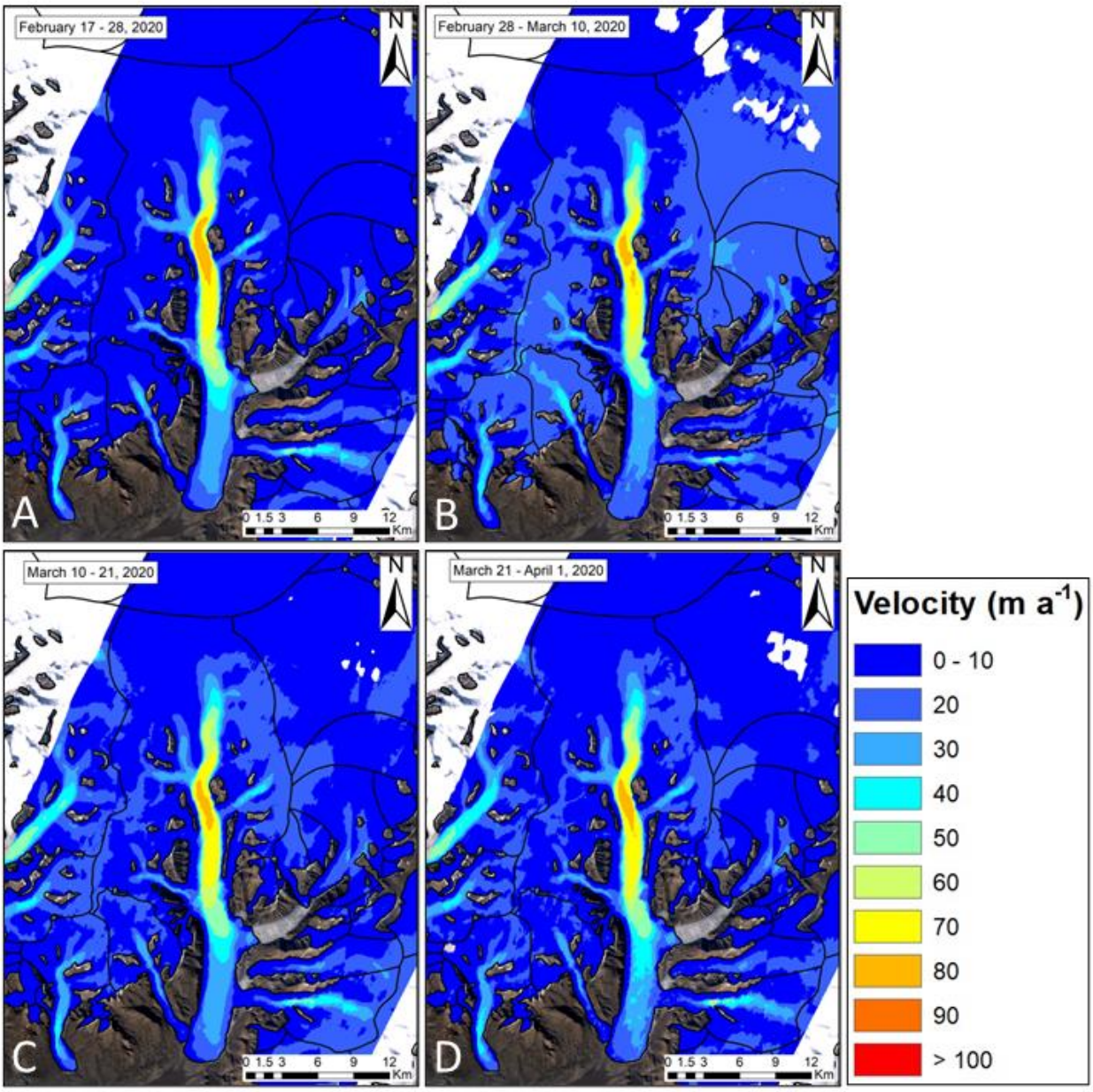

Figure 5-19. *Velocity structure of White and Thompson Glaciers derived from TerraSAR-X StripMap imagery from February 17th to March 21st, 2020. Deep black lines on the figure indicate the glacier extents provided by version 6.0 of the Arctic Canada North shapefile of the Randolf Glacier Inventory. Background image is a cloud free Landsat image. A, February 17th – 28th, 2020. B, February 28th – March 10th, 2020. C, March 21st – April 1st, 2020. D, March 10th – 21st, 2020.*

The pre-derived R2 Yearly for the 2019/20 accumulation season is presented in Figure 5-20. Thompson Glacier experienced velocities below 20 m a^{-1} from the terminus to 2 km upglacier from the terminus. At 2 km the velocity reached 20 m a^{-1} and increased to 30 m a^{-1} at 3 km. The velocity then

decreased slightly to 20 m a^{-1} around 4.5 km from the terminus before increasing again and reached 50 m a^{-1} at a distance of 10 km. The velocity continued to increase until reaching a maximum of 100 m a^{-1} at a distance of 24 km from the terminus, before decreasing to below 20 m a^{-1} around 35 km from the glacier tongue.

White Glacier experienced velocities below 10 m a^{-1} until 3 km from the terminus (Figure 5-20). At 3 km the velocity increased to 24 m a^{-1} before decreasing to just 16 m a^{-1} at 5.5 km. The velocity increased again to 30 m a^{-1} at 6.5 km before quickly decreasing to below 10 m a^{-1} at a distance of 7.1 km from the terminus. The velocity then increased and reached a maximum velocity of 46 m a^{-1} at 9.6 km from the glacier tongue. The velocity then decreased after reaching its maximum to under 10 m a^{-1} at 10.7 km.

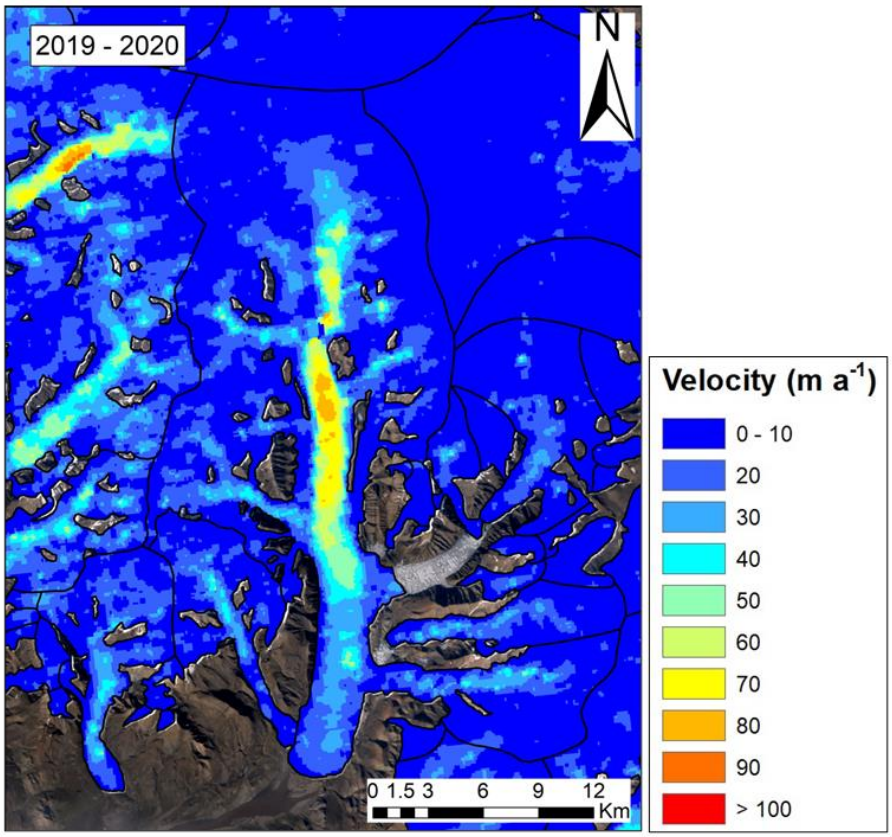

Figure 5-20. *Velocity structure of White and Thompson Glaciers derived from Radarsat-2 Yearly imagery for the accumulation season 2019-2020 (reference image from March 4, 2020, and secondary image from March 28, 2020). The thick black lines on the figure indicate the glacier extents provided by version 6.0 of the Arctic Canada North shapefile of the Randolf Glacier Inventory. Background image is a cloud free Landsat image.*

The S1 data available for the 2019/20 accumulation year are the February, March and April monthly mosaics (Figure 5-21). These results show that the terminus of Thompson Glacier experienced velocities of under 20 m a^{-1} from the terminus to 1 km from the terminus. The velocity then slowed slightly to under 15 m a^{-1} until a distance of 3 km, where the velocity increased to 40 m a^{-1} at 4 km from the terminus. After 4 km the velocity slowed to under 25 m a^{-1} and maintained that velocity until 10 km from the terminus, where the velocity started increasing again, until reaching a maximum velocity of 75 m a^{-1} at 23 km before decreasing as it extends towards the accumulation area.

The velocity of White Glacier near the terminus is below 20 m a^{-1} until 0.6 km from the terminus, where it decreases to below 10 m a^{-1}, increasing slightly to 15 m a^{-1} until 3 km. The velocity fluctuates between 10 and 15 m a^{-1} until 6 km from the terminus, where the velocity starts increasing until it reaches a maximum of 40 m a^{-1}at 9.7 km from the terminus. The velocity then decreases again, towards the accumulation basin.

Good results were recorded in Figure 5-21A, during February, which can be expected as winter is typically when better results are obtained. Less useable results were recorded in Figure 5-21 B and C, where there was a loss of coherence between images.

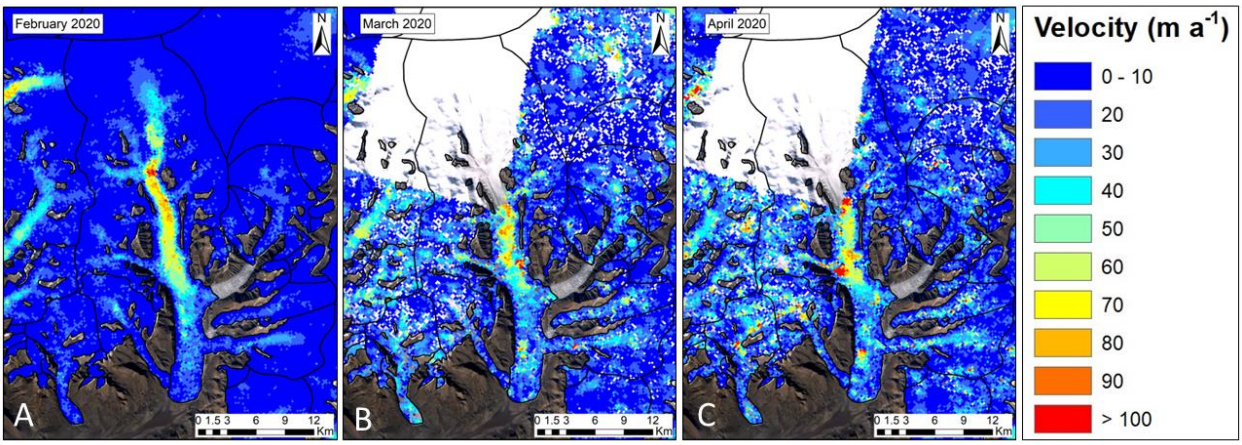

Figure 5-21. *Velocity structure of White and Thompson Glaciers derived from Sentinel-1 monthly mosaics from the FAU university portal. Deep black lines on the figure indicate the glacier extents provided by version 6.0 of the Arctic Canada North shapefile of the Randolf Glacier Inventory. Background image is a cloud free Landsat image. (A) February 2020 monthly mosaic. (B) March 2020 monthly mosaic. (C) April 2020 monthly mosaic.*

5.1.8 Accumulation year 2020 – 2021

This accumulation season contains TSX (Figure 5-22) and pre-derived S1 monthly mosaics (Figure 5-23). Figure 5-22 contains 14 image pairs, from fall, winter and spring. The three seasons combined for the TSX data (Figure 5-22) result in Thompson Glacier experiencing a velocity below 20 m a^{-1} near the terminus. At 1 km, the velocity decreases slightly to below 15 m a^{-1} before increasing at 1.5 km. The velocity increases to 25 m a^{-1} at 3.5 km from the terminus then decreases to 20 m a^{-1} at 4.8 km before slowly increasing to reach a maximum velocity of 71 m a^{-1} at a distance of 24 km from the terminus. The velocity decreases and reaches 10 m a^{-1}at 36 km.

White Glacier experiences velocity below 10 m a^{-1} from the terminus to 3.5 km, at which point, the velocity increases and reaches 20 m a^{-1} at 4.5 km. This velocity is maintained upglacier until 6 km, where the velocity falls below 15 m a^{-1} at 6.6 km before increasing to reach a maximum velocity of 32 m a^{-1} at 8.2 km from the terminus. The velocity then decreases further upglacier towards the accumulation basin.

Particularly good results were recorded in Figure 5-22 B, E to L. There was a slight loss of coherence recorded in Figure 5-22 C, D, M and N. This can be expected of Figure 5-22 M and N, as those image pairs are from the end of the accumulation season, late spring, and may be influenced by the start of the melt season. Figure 5-22 A experienced a loss of coherence has an error of 10 m a^{-1} and standard deviation of 11 m a^{-1}, this error is above the threshold for this study and was remove from further analysis of long-term or short-term changes in velocity structure.

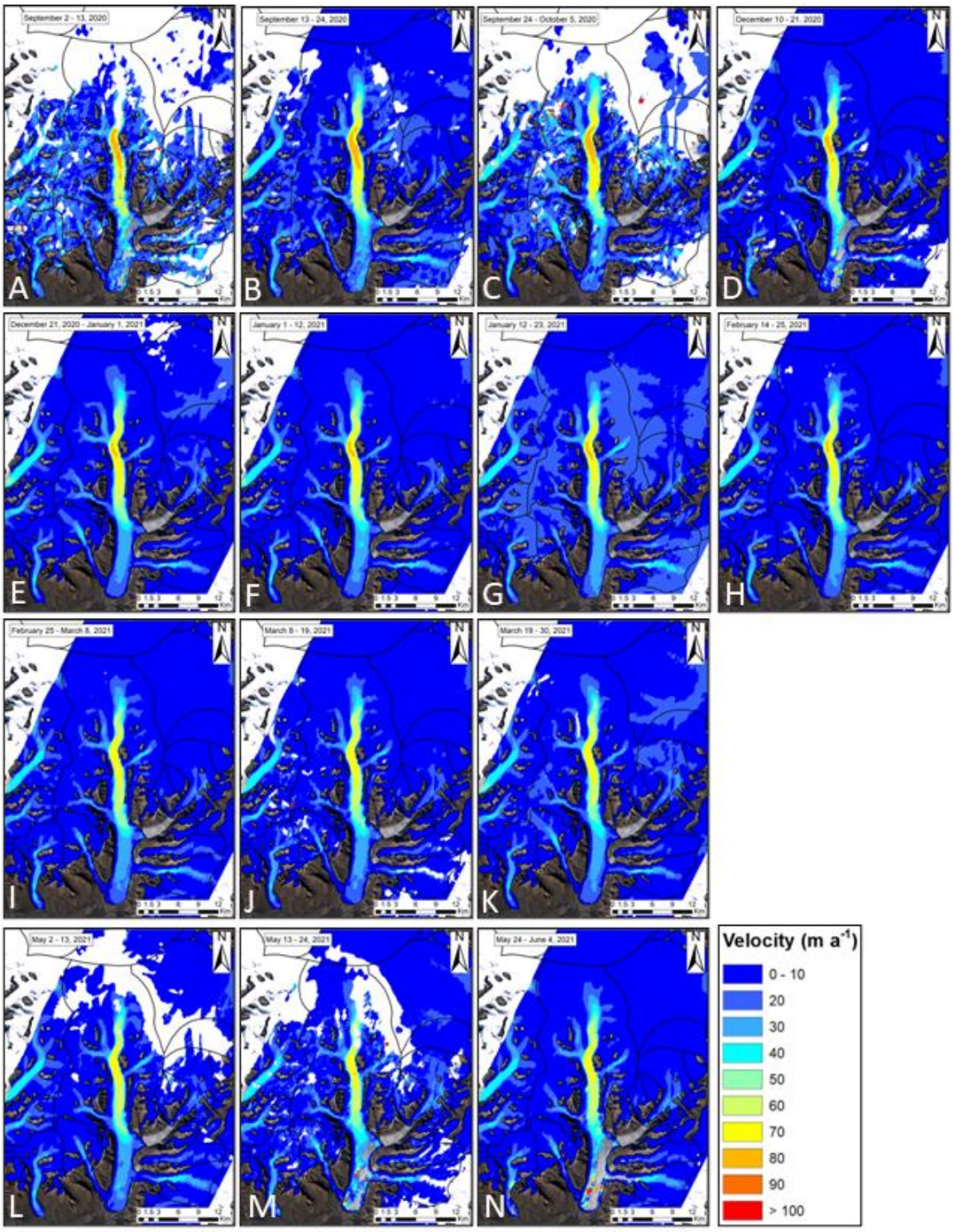

***Figure 5-22**. Velocity structure of White and Thompson Glaciers derived from TerraSAR-X StripMap imagery from September 13th, 2020 to June 4th, 2021. Deep black lines on the figure indicate the glacier extents provided by version 6.0 of the Arctic Canada North shapefile of the Randolf Glacier Inventory. Background image is a cloud free Landsat image.*

Figure 5-23, the pre-derived S1 monthly mosaics shows Thompson Glacier experienced an increased velocity starting from 10 m a^{-1} at the terminus and reached 30 m a^{-1} at 1 km from the terminus. The velocity then slowed to around 20 m a^{-1} from 1 km until 2.5 km from the terminus where velocity started increasing to 30 m a^{-1}. This 20 m a^{-1} velocity was maintained until a distance of 4 km from the terminus, where velocity increased to 35 m a^{-1}. The surface velocity then decreased to below 20 m a^{-1} at 6.5 km. Thompson Glacier reached its maximum of 75 m a^{-1} at 20 km from the terminus. The velocity gradually decreased towards the ice cap after reaching its maximum.

White Glacier experienced velocities below 15 m a^{-1} until 0.6 km from the terminus, where velocity decreased to below 10 m a^{-1}. This velocity fluctuated a bit but maintained 10 m a^{-1} until 4 km where velocity increased to 35 m a^{-1} at 4.6 km. Velocity decreased to below 20 m a^{-1} at 5.5 km before increasing to reach a maximum velocity of 40 m a^{-1}at 8.4 km from the glacier terminus.

Less useable results were recorded in Figure 5-23, there was a loss of coherence between images, particularly A and E, at the start and end of the accumulation seasons, respectively. These results are poor compared to the previous TSX results in Figure 5-22.

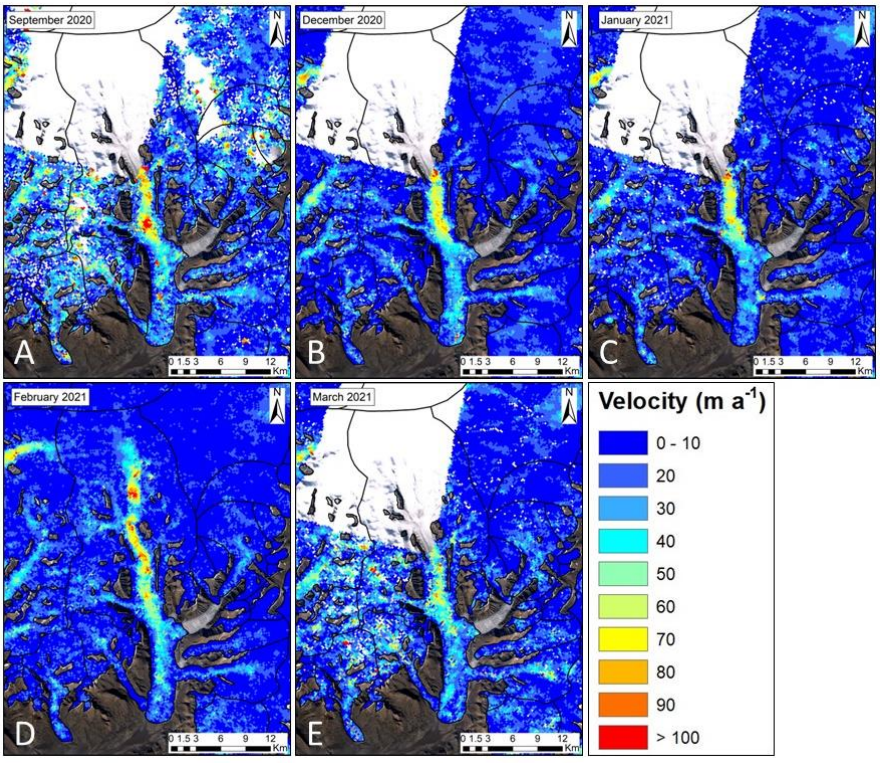

***Figure 5-23**. Velocity structure of White and Thompson Glaciers derived from Sentinel-1 monthly mosaics from the FAU university portal. Deep black lines on the figure indicate the glacier extents provided by version 6.0 of the Arctic Canada North shapefile of the Randolf Glacier Inventory. Background image is a cloud free Landsat image.*

5.1.9 Accumulation year 2021 – 2022

This last accumulation season contains only TSX data (Figure 5-24). The first kilometer of Thompson Glacier experienced velocities below 10 m a^{-1}. At 1 km, the velocity increased from 10 m a^{-1} to 25 m a^{-1} at 4 km. This velocity of 25 m a^{-1} was maintained until 7 km from the terminus, where the velocities increased, reaching 30 m a^{-1} at 8 km and continuing until 9 km. The velocity of Thompson Glacier then increased and reached its maximum of 85 m a^{-1} at 21 km before decreasing towards the ice cap interior.

White Glacier experienced a velocity below 10 m a^{-1} from the terminus until 2 km upglacier from the terminus. Velocity increased to 15 m a^{-1} at 2 km and reached 25 m a^{-1} at 4.5 km. The velocity around 25 m a^{-1} was maintained until it started increasing around 6.8 km to reach a maximum velocity of 35 m a^{-1} at a distance of 8 km from the terminus. The surface velocity then decreased upglacier towards the accumulation basin.

Good results were recorded in Figure 5-24 and visually look better than the R2 Fine Beam, R2 Yearly and R2 Spotlight datasets of previous accumulation seasons. Particularly good results were recorded in Figure 5-24 E-H and J.

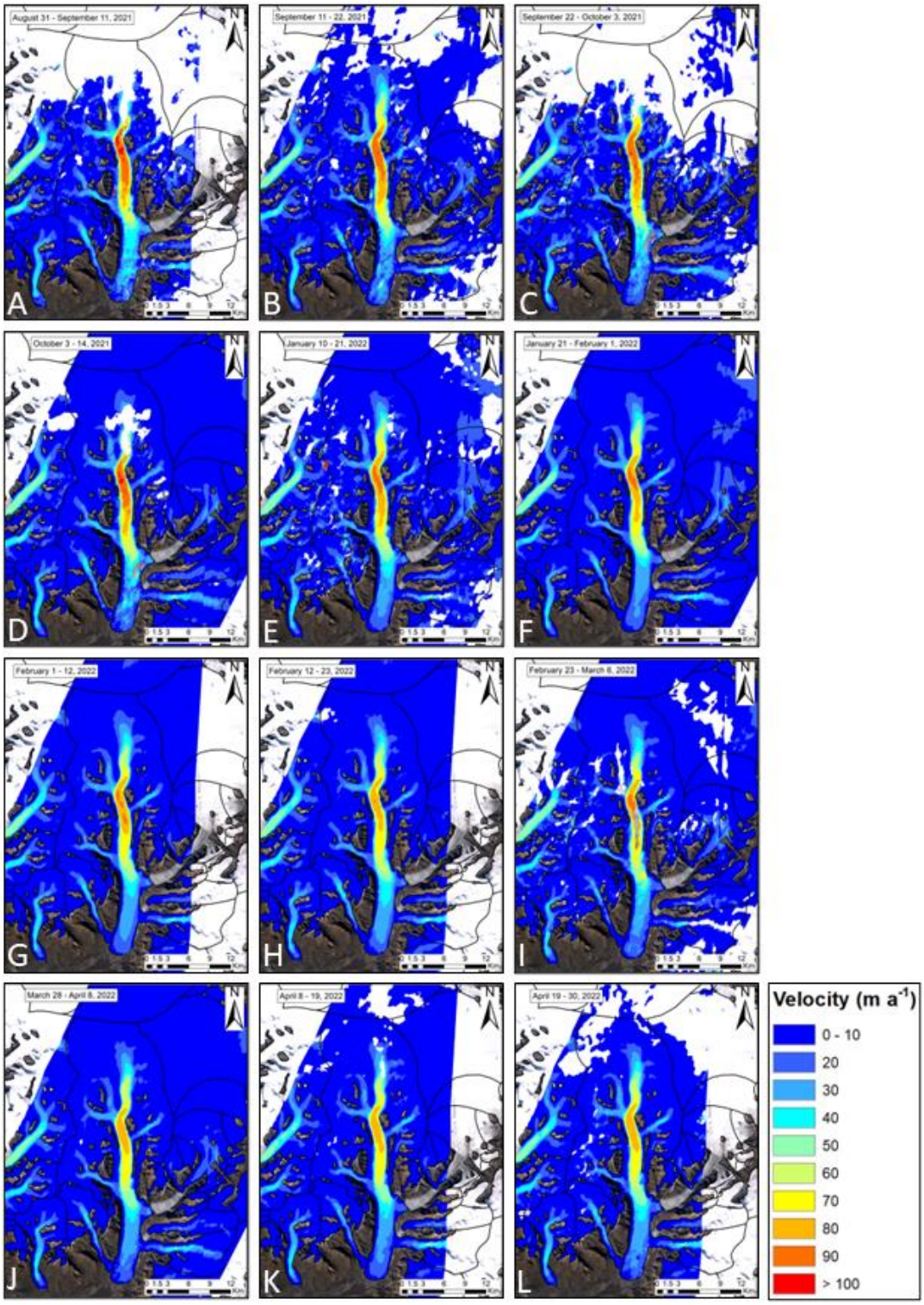

Figure 5-24. *Velocity structure of White and Thompson Glaciers derived from TerraSAR-X StripMap imagery from August 31st, 2021 to April 30th, 2022. Deep black lines on the figure indicate the glacier extents provided by version 6.0 of the Arctic Canada North shapefile of the Randolf Glacier Inventory. Background image is a cloud free Landsat image.*

5.1.10. Discussion of results for section 5.1

White and Thompson Glaciers experienced consistent velocities between 2008 and 2022, with slight variations from year to year, as seen in the velocity products in section 5.1. Both glaciers follow the expected velocity structure of previous research for land terminating glaciers, with slower velocities below 20 m a^{-1} approaching the terminus and near the accumulation area (Short and Gray, 2005; Van Wychen et al., 2016). Land terminating glaciers reach a maximum velocity along the main trunk of the glacier, as described previously by (Van Wychen et al., 2016, Milan et al., 2017). This study shows that White Glacier has an average velocity below 20 m a^{-1} until a distance of ~3.5 km from the terminus, with exact distance from the terminus varying between years while the lowest velocity is observed at the terminus. White Glacier then reaches its maximum velocity between 30 and 40 m a^{-1} around 8 km from the terminus, before slowing to below 20 m a^{-1} as it approaches its accumulation basin. Thompson Glacier experiences average velocities below 20 m a^{-1} for the first 4 km from the glacier tongue. The velocity then increases to reach a maximum velocity ~85 m a^{-1} between ~21 and ~24 km from the terminus, the location where the maximum velocity is experienced varied between image pairs and sensors. The surface velocity of Thompson Glacier then decreased to below 20 m a^{-1} as it approached the interior of the ice cap around 36 km from the glacier terminus.

The results of this study are consistent with previous research and maintain that both White and Thompson Glacier are slow flowing (Short and Gray, 2005; Van Wychen 2016). As the surface velocity of both White and Thompson Glaciers are consistent and do not show a drastic increase or decrease over this study period, neither glacier displays signs of being either a surge-type or pulse-type glacier. The use of the additional datasets of R2 Fine Beam, R2 Spotlight and TSX aids previous research by augmenting data over the same period, with an additional 71 images. The results are largely like results of previous studies and show the expected velocity structure of land terminating glaciers. This study used a multitude of available data of different sensors that had not been utilized to its full extent previously, and results in a dense record of surface velocities for both Thompson and White Glaciers. While previous research used a slightly different method of offset tracking, Gray method in Matlab (Short and Gray, 2005; Van Wychen et al., 2014; 2016; Schellenberger et al., 2016; Medrzycka et al., 2019), there was no major difference in results by using GAMMA offset tracking method in this study.

Typically, surface velocity of land terminating glaciers rarely exceeds 75 m a^{-1} (Van Wychen et al., 2016). White Glacier has a maximum velocity well below this upper limit, between 30 and 40 m a^{-1}.

Thompson Glacier experiences velocity around this limit but has an average maximum velocity of 85 m a^{-1}. In this case, it can be due to a physical constraint from the glacier moving into a narrower channel of ~2.1 km at a distance of ~22 km to 24 km from the glacier tongue. This section of the main trunk of Thompson Glacier is where the maximum velocity occurs. Below 22 km from the terminus, the glacier widens to ~ 2.5 to 3km.

The velocity data used in the earlier years of this study, 2008 to 2011, were comprised of R2 Fine Beam of different beam modes (F1, F1F, F1N, F2, F4, F5, F6F and F6N). The different beam modes were comparable to one another, in terms of spatial resolution of the final velocity product and quality of the data. For future studies, the choice of R2 Fine Beam mode acquired for investigations into glacier surface velocity studies in the CAA does not have a huge impact on the results and as such does not likely need to be considered when selecting datasets. These different Fine Beam modes of R2 were similar to the R2 Yearly data the was pre-derived in previous work (Van Wychen et al., 2016; 2021). The pre-derived S1 monthly mosaic velocity products are similar in quality to the R2 Fine Beam and R2 Yearly. Visually, both R2 Spotlight and TSX data produced better velocity results than R2 Fine Beam, R2 Yearly and S1. This can also be seen in the presented velocities, where R2 Spotlight and TSX data have less variability than the other sensors and beam modes. R2 Spotlight and TSX data also have the lowest error values (see section 5.2) of the sensors used in this study.

TSX and R2 Spotlight sensors resulted in better velocity products, visually with less noise and smaller error values (see section 5.2), compared to R2 Fine Beam and Yearly and S1. For all sensors and beam modes in this study the time of year of acquisition influences that quality of the velocity product, better results were obtained in the winter months, with poorer results in the early fall and late spring due to loss of coherence from the presence of water during the summer melt season (McNairn, 2021a). A loss of coherence is caused by too much change between image acquisitions. Change can be due to increased melt or snowfall – some change on the surface of the glacier – that is large enough to not be recognized by the sensor resulting in a poor calculation of displacement between acquisitions (McNairn, 2021a). As the majority of melt in the CA occurs in the summer season, it is expected for there to be less useable SAR data due to loss of coherence as the pattern of pixels are not consistent between image pairs. As less melt is expected in the winter months, with colder temperatures, winter is less likely to have loss of coherence between image pairs. This can be seen in the data presented here, image acquisitions from the early fall or late spring show more of a loss of coherence than velocity products derived from winter. For example,

TSX velocity products (Figure 5-24) A-D, may be experiencing a slight loss of coherence, as there are locations along White Glacier where velocity data is missing, compared to winter months.

5.2 Error derived from different SAR sensors and comparison with GPS data

This section presents the error over bedrock for each sensor used in this study and provides comparisons between datasets More specifically, an intercomparison of the TSX, R2 Yearly and S1 derived glacier velocities during March 2020, and a comparison between R2 Spotlight and in situ GPS data over White Glacier.

5.2.1 Derived SAR error

A bedrock error analysis was performed on each processed image pair over Thompson and White Glaciers for R2 Fine Beam, R2 Spotlight and TSX velocity results (Table 5-1). The average mean error (m a^{-1}) and standard deviation (SD in m a^{-1}) of all images was extracted from displacement maps determined over bedrock. As bedrock areas should have no motion, any motion that is recorded represents an estimate of the error of that image pair. The mean and SD of R2 Yearly used in this study was obtained from the original studies that processed the data (Van Wychen et al., 2016; 2021) and is presented in Table 5-1. The S1 error used was used from a study by Strozzi et al. (2017), that estimated a range of uncertainty of 20 – 30 m a^{-1} over mid-glacier areas.

Table 5-1. *Total error estimates of datasets R2 Fine Beam, R2 Spotlight and R2 Yearly (pre-derived, Van Wychen et al., 2014; 2016; 2021)), TSX and S1 (pre-derived, Strozzi et al., 2017).*

Sensor	Mean Error (m a^{-1})	SD (m a^{-1})	# image pairs
R2 Fine Beam	7	19	53
R2 Spotlight	4	4	12
R2 Yearly	6	5	12
TSX	6	29	30
S1	20-30		
		Total	107

The R2 Spotlight derived velocity products resulted in the lowest mean error over bedrock of 4 m a^{-1} and SD of 4 m a^{-1} (Table 2), while R2 Yearly was not far behind with an error of 6 m a^{-1} and SD of 5 m a^{-1} (Table 2). R2 Fine Beam (7 m a^{-1} and SD of 19 m a^{-1}) and TSX (6 m a^{-1} and a SD of 29 m a^{-1}) image pairs

resulted in a greater error. However, this is not an accurate comparison of error, as the R2 Spotlight and Yearly image pairs provided were during the accumulation season, either fall, winter, or spring, while the total error calculated for both R2 Fine Beam and TSX include image pairs from summer months. The inclusion of summer velocity pairs skews the results, since it is expected that there will be a loss of coherence between images (from melt and rain events) during the ablation season and, therefore, likely results in a greater error. The summer and non-summer average errors were then calculated for R2 Fine Beam and TSX for a more accurate comparison with R2 Spotlight and R2 Yearly (Table 5-2).

Both R2 Fine Beam (7 m a^{-1} and SD of 47 m a^{-1}) and TSX (11 m a^{-1} and SD of 79 m a^{-1}) have large summer errors (Table 5-2), which is to be expected due to loss of coherence from increased velocity and surface melt, which likely impacted the total mean error and SD. The summer error of 11 m a^{-1} and SD of 79 m a^{-1} contributed to the total TSX mean error and SD being much higher than expected. The non-summer error of TSX (4 m a^{-1} and SD of 4 m a^{-1}) is comparable to the R2 Spotlight data. Both TSX and R2 Spotlight data have lower errors than the R2 Fine Beam and S1 (Table 5-1). Fine Beam resulted in a slightly higher non-summer error of 6 m a^{-1} and SD of 9 m a^{-1}. By removing summer error from R2 Fine Beam, the mean error was reduced from 7 m a^{-1} to 6 m a^{-1} and the SD decreased from 19 m a^{-1} to a non-summer SD of 9 m a^{-1}.

Table 5-2. *Summer and non-summer error of R2 Fine Beam and TSX datasets*

Season	Sensor	Mean Error (m a^{-1})	SD	# image pairs
Summer	R2 Fine Beam	7	47	19
	TSX	11	79	15
Non-summer	R2 Fine Beam	6	9	53
	TSX	4	4	18

Based on this error analysis (Tables 5-1 and 5-2), R2 Spotlight (4 m a^{-1} and SD of 4 m a^{-1}) and TSX (4 m a^{-1} and SD of 4 m a^{-1}) provide the results with the lowest error and are comparable to one another. The pre-derived R2 Yearly data has an error of 6 m a^{-1} and SD of 5 m a^{-1} which is comparable to the error over bedrock derived in this study for R2 Fine Beam 7 m a^{-1} and SD of 10 m a^{-1}. Based on the error analysis and variability seen in the derived velocity products (section 5.1), TSX and R2 Spotlight would be the best sensors to use for more in-depth analysis where more detail is desired, like seasonality. While R2 Fine

Beam may not be the best option to investigate seasonality, it can still be useful for investigation of changes in long term velocity or for velocity studies over large areas or on a regional scale.

Figure 5-25 below, compares the derived glacier velocities for March 2020 from TSX data, the pre-derived velocities from S1 (FAU University: http://retreat.geographie.uni-erlangen.de/search) and R2 Yearly (Van Wychen et al., 2021) for Thompson Glacier. This direct comparison was performed as it was the only timeframe where these three glacier velocity datasets all nearly overlapped temporally. All results follow the same velocity trend along the length of the glacier, as is typical of land terminating glaciers in the CA. However, the S1 and R2 data have more variability and the TSX derived results are much smoother along the length of the glacier, notably at 6.6 km from the terminus where R2 increases to 50 m a^{-1} and S1 decreases to 5 m a^{-1}, while the TSX velocity is consistent around 28 m a^{-1}. This could be because the TSX data used for the comparison was an average of two images (22 days) and does not represent the exact same time period as the S1 data (6 or 12 days combined into a monthly composite) or R2 (24 days). It could also be due to the different range and azimuth image resolutions of the input imagery: R2 Fine Beam (~5 m x ~5 m), R2 Spotlight (1 m x 1 m), R2 Yearly (~5 m x ~ 8 m), S1 (~3 m x ~25) and TSX (~1.5 m x ~1.8 m). S1 has a spatial resolution of ~25 m in the azimuth direction, more than 5 times the resolution in the range direction (~3 m), compared to the other datasets that have similar resolutions in the range and azimuth directions. This leads to S1 having less information to resolve, resulting in less accurate velocities.

Another possibility is the temporal resolution, as the TSX data is collected every 11 days, while R2 is every 24 days, and S1 data can be from every 6 or 12 days, but the poor resolution degrades the results. The longer the time period between acquisitions, the more likely it is for coherence to be lost. The 11 days between TSX acquisitions is less likely to lose coherence compared to R2 imagery which is acquired 24 days apart. Additionally, these datasets used different window sizes: R2 Fine Beam (128 m x 256 m), R2 Spotlight (128 m x 256 m), R2 Yearly (370 m x 450 m), S1 (128 m x 128 m) and TSX (256 m x 512 m). The different studies used different offset tracking procedures. All of which may explain some of the observed differences. TSX is the best to use out of S1 and R2 Yearly (comparable to R2 Fine Beam) for smaller glaciers or areas or for investigating velocity structure over shorter periods, like seasonality, where more detail and accuracy may be needed and desired. That is not to say there is no place for S1 or R2 Yearly in velocity analysis over glaciers, but these datasets may be best for coarser analysis, either over long term or on a larger, regional scale.

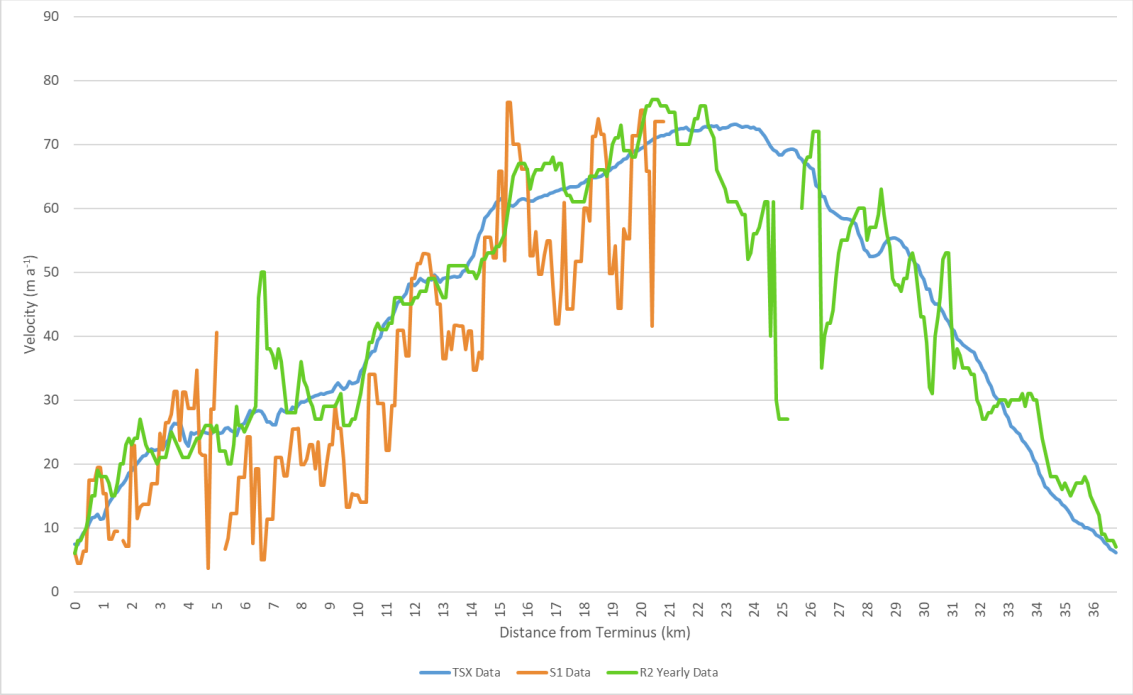

Figure 5-25. *SAR dataset comparison between TSX, S1 and R2 for March 2020. TSX (blue) an average of two images (March 10 and 21, 2020). S1 (orange) from a pre-derived monthly velocity mosaic. R2 Yearly (green) a single image from previous research (March 4-28, 2020).*

5.2.2 SAR error comparison with in-situ dGPS

The GPS results will now be presented then discussed and compared to the derived SAR error over bedrock. There were 9 dates where dGPS data was available that coincided with R2 Spotlight data. The locations of the three GPS stations along White Glacier can be seen in Figure 5-26 for May 4th, 2015. The GPS station data is being compared to the closest available pixel of SAR derived displacement. It should be noted that slow flowing glaciers may have a small difference between the GPS displacement and SAR derived displacement which will result in a large percent difference. The absolute difference seen in Table 5-3 below, shows an average absolute difference close to 10 m a^{-1}, which is good agreement between the in situ and SAR derived error of displacement over bedrock.

The differential GPS collected data over the three profiles of White Glacier resulted in good agreement compared to the SAR derived velocity products. Certain dates seemed to be in better agreement, May 4th to 28th, 2015 at the Lower and Middle profiles with an absolute difference of 1.81 m a^{-1} and 2.08 m a^{-1}, respectively, between GPS and SAR velocities where they are well below the combined error. The greatest difference between the GPS and R2 Spotlight derived velocity product of 22.88 m a^{-1}

at the Middle profile on the date May 28th to June 21st, 2015. This was at the one location that had the closest available SAR data at a distance of 30 m away from the GPS location.

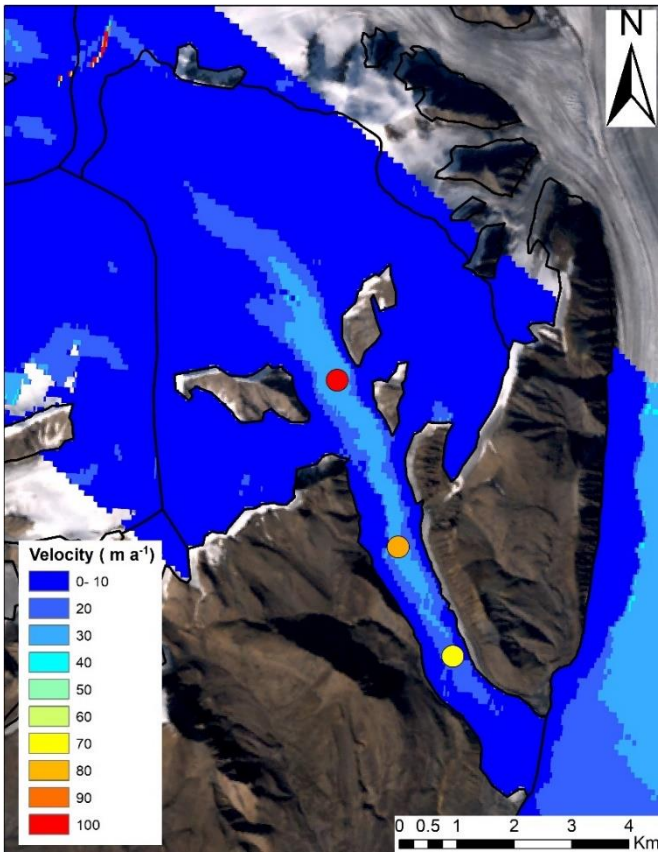

***Figure 5-26**. dGPS station locations along White Glacier. Red circle is the Upper profile GPS location from May 4th, 2015. The orange circle is the Middle profile GPS location from May 4th, 2015. The yellow circle is the lower profile GPS location from May 4th, 2015. The velocity product show is the direct comparison, reference from May 4th, 2015 and secondary image from May 28th, 2015. Base map is a cloud free Landsat image.*

The GPS data was mostly available during the summer months as it uses solar power. This means most GPS data is collected during the summer with some data during the shoulder seasons (mid to end of spring and early to mid fall), depending on the equipment and sunlight conditions. No GPS data would be collected during the polar night, which is when the best SAR derived velocity products and better coherence between image pairs is available. It is likely that the difference between the GPS and R2 Spotlight derived velocity product of 22.88 m a^{-1}, is due to the SAR image pair being mostly from June, the beginning of the melt season in addition to the closest available pixel of SAR data to the GPS station was 30 m away. The R2 Spotlight data for the May 28th to June 21st, 2015 image pair had an error of 3 ± 19 m a^{-1}.

Table 5-3. *Shows the comparisons between in situ GPS measurements and SAR derived displacement where the SAR image acquisition date overlaps with dates of GPS measurements. The asterisk for Middle profile on May 28th to June 21st is because that is the only image pair where SAR data was not available right at the location of the GPS station. The SAR displacement for this date is 30 m away and was the closest available pixel.*

Date 1	Date 2	White Glacier Profile	dGPS displacement (m a^{-1})	SAR derived displacement (m a^{-1})	Difference (%)	Absolute Difference (m a^{-1})
2014-05-16	2014-06-09	Upper	16.34	31.9	95.28	15.56
2015-05-04	2015-05-28	Upper	15.81	27	70.73	11.19
2015-05-28	2015-06-21	Upper	21.36	28.5	33.43	7.14
2015-05-04	2015-05-28	Middle	25.8	23.72	-8.05	2.08
2015-05-28	2015-06-21	Middle*	30.68	7.8	-74.58	22.88
2014-04-22	2014-05-16	Lower	16.23	10.5	-5.73	35.29
2014-05-16	2014-06-09	Lower	16.34	8.1	-50.42	8.24
2015-05-04	2015-05-28	Lower	15.81	14	-11.47	1.81
2015-05-28	2015-06-21	Lower	21.36	13.6	-36.3	7.76
		Average total	19.97	18.35	1.43	12.44

Van Wychen et al. (2012) compared dGPS displacement with SAR derived velocity products on Belcher Glacier (Devon Ice Cap) and had very good agreement between the datasets and was well within the determined error over bedrock. In that study, there were two dGPS stake positions, one further downglacier which had a displacement difference of +4.99%, while the second stake positioned upglacier had a displacement difference of -0.44%. Another study, Schellenberger et al. (2016), also compared SAR derived velocity products with dGPS measurements and found good agreement between the GPS displacement with both GAMMA and the offset tracking method utilized in Van Wychen et al, (2012).

The combined absolute difference of the dates and profiles from the GPS comparison with R2 Spotlight data resulted in an average absolute difference of 12.44 m a^{-1}, which is still in fair agreement for the slow flowing White Glacier and is close to the 10 m a^{-1} threshold that is typically expected. It is similar to the GPS error derived in a previous study by Van Wychen, et al. (2012). While these datasets show a slightly worse agreement than what has been previously recorded (Van Wychen et al., 2012), it is likely more realistic as this study used a greater number of comparisons than the previous study. The study by Van Wychen et al. (2012), on Belcher Glacier used a different methodology of Matlab speckle tracking compared to the GAMMA offset tracking used in this study. Belcher Glacier is also a large tidewater glacier compared to the small, land terminating White Glacier. The agreement between the in situ data and SAR data means that the SAR data is a trustworthy dataset. There will always be a need for in situ data for

validation, but SAR data has been proven to be a reliable source of data for glacier velocity studies and can be use for remote locations that may be difficult or dangerous to access.

5.3 Glacier velocities changes over Thompson and White Glaciers (seasonality and long-term changes)

5.3.1 Detection of long-term velocity change

This section explores long term changes in the velocity structure of both Thompson and White Glaciers. This is not a direct comparison of the different datasets, but rather an investigation of changes in the velocity structures of each glacier from 2008 to 2021 using non-summer averages and comparing the velocity structures of the glaciers over multiple years. Starting with R2 Fine Beam, which has a large quantity of data from 2008 – 2010, then R2 Spotlight to look at the velocity structure between 2010 – 2015 and lastly, looking at the dense velocity data from TSX between 2020 – 2022 for both Thompson Glacier (Figures 5-26 and 5-27) and White Glacier (Figures 5-28 and 5-29). Tables 5-4 and 5-5 summarizes the number of image pairs that were averaged for each accumulation season for both Thompson and White Glaciers, respectively. All datasets show that White and Thompson Glaciers follow the general expected velocity structure of land terminating glaciers in the CA (Van Wychen et al., 2016; Short and Gray, 2005).

Table 5-4. Number of image pairs used for each non-summer velocity average of Figures 5-27 and 5-28 of Thompson Glacier.

Accumulation year	Sensor	# images
2008-2009	R2 Fine Beam	24
2009-2010	R2 Fine Beam	16
2010-2011	R2 Fine Beam	2
2012-2013	R2 Spotlight	2
2013-2014	R2 Spotlight	6
2014-2015	R2 Spotlight	3
2019-2020	TSX	4
2020-2021	TSX	13
2021-2022	TSX	12

5.3.1.1 Thompson Glacier

Data spanning over a decade (2008/09 – 2021/22) was used to create annual velocity composites of Thompson Glacier for each accumulation year where data was available (Figures 5-27 and 5-28). The earlier years of 2008-2011, are a compilation of R2 Fine Beam velocity averages of non-summer months which have more noise and variability within the datasets. The 2008/09, 2009/10 and 2010/11 velocity composites were created from 25, 16 and 2 image pairs, respectively (Table 5-4). When averaging datasets, the greater the sample number, the more likely the variability will be minimized by reducing the effect of any outliers. These earlier accumulation years from 2008/09 and 2009/10 used the greatest quantity of images used to create the annual composites compared to later years that used R2 Spotlight and TSX sensors. Despite this, the R2 Fine Beam velocity product still had greater variability compared to R2 Spotlight and TSX data (Figure 5-27). More variability occurred from R2 Fine Beam up-glacier during times when there should be good coherence between images, the variability is most likely due to the lower resolution and accuracy of the dataset, compared to TSX and R2 Spotlight. General long-term changes across the full length of the glacier, comparing R2 Fine Beam and TSX, will be discussed first. Then a closer look at the terminus region will take place and will include the R2 Spotlight data in the comparison.

The velocities from 2008/09 to 2009/10 (R2 Fine Beam) follow a similar flow pattern to the other sensors before experiencing great variability after 24 km (Figure 5-27). The centerline velocities for the R2 Fine Beam after a distance of 24 km was removed from further analysis as the noise was too great. There are a few locations, however, where there are differences beyond the error limits, particularly for Fine Beam data in accumulation year 2010/11. At 2 km, Fine Beam 2010/11 show Thompson Glacier experienced a velocity of 10 m a^{-1}, while the previous years velocities close to 30 m a^{-1}. From 20 km until 24 km, Fine Beam 2010/11 experiences velocities above 90 m a^{-1}, while the previous years experience velocities below 80 m a^{-1} along the same length, with the difference between Fine Beam 2008/09 and 2010/11 being beyond the combined error (Figure 5-27). The greater variability of the Fine Beam 2010/11 is most likely due to only 2 images being combined for the composite, so any error in the velocities will have a greater impact, compared to the 24 and 16 image pairs creating the composites for 2008/09 and 2009/10, respectively (Table 5-4).

The TSX data has less variability than the R2 Fine Beam and more cleanly show the velocity structure over the length of Thompson Glacier, with decreased velocities near the terminus (< 20 m a^{-1}) that slowly increase and reach the maximum velocity (of around 70 m a^{-1} at ~24km) before decreasing again close to the ice cap interior (decreasing to below 20 m a^{-1}). At 21 km, TSX 2021/22 has a velocity of

82 m a^{-1} while 2020/21 has a velocity of 68 m a^{-1}, and TSX 2019/20 is has a maximum velocity of 72 m a^{-1}. The majority of velocities along the length of Thompson Glacier are within the combined error limits of the sensors or at the error limits.

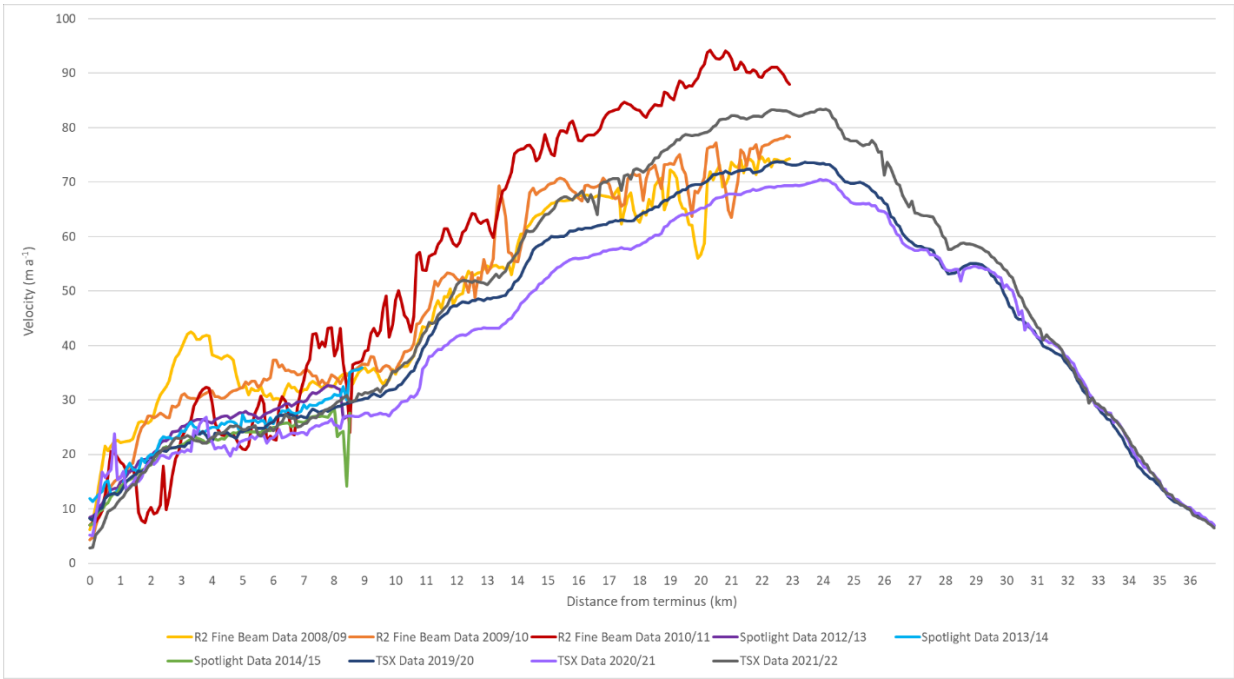

Figure 5-27. *Velocity structure of Thompson Glacier from 2008 to 2022, using non-summer yearly averages from R2 Fine Beam, R2 Spotlight and TSX datasets. Fine Beam data covers 2008/09, 2009/10 and 2010/11. R2 Spotlight data covers 2012/13, 2013/14, 2014/15. TSX data covers 2019/20, 2020/21 and 2021/22. While the error bars were no included for legibility, R2 Fine Beam has an error of 6 m a^{-1} and both R2 Spotlight and TSX have an error of 4 m a^{-1}.*

Unfortunately, the R2 Spotlight data obtained did not cover the entire length of the glacier and only reaches up to ~ 9 km from the terminus of Thompson Glacier, Figure 5-28 presents changes over time of the near the terminus region, extending 9 km upglacier. With persistent negative mass balance, it is likely that the terminus region would slow down the most and is cause for closer examination of the terminus region (Heid and Kääb, 2012). The centerline velocities included in this study from 2008/2009 to 2020/2021 from the R2 Fine Beam, R2 Spotlight and TSX datasets are included. A closer examination of the terminus of Thompson Glacier, shows that there is more variability in R2 Fine Beam compared to R2 Spotlight and TSX. R2 Spotlight from 2012/13 to 2014/15 does not experience any significant change when compared to itself. R2 Spotlight and TSX follow velocity trends more closely than the Fine Beam, there is little significant change between R2 Spotlight and TSX. Fine Beam data from 2008/09 and 2009/10 experience greater velocities along certain lengths of the terminus compared to R2 Spotlight and TSX. At 3 km, Fine Beam 2008/09 experiences 40 m a^{-1}, almost double that of R2 Spotlight and TSX, which experienced between 21 and 25 m a^{-1}, beyond the combined error (Figure 5-28). Fine Beam 2008/09 velocity continues to be significantly greater than R2 Spotlight and TSX until about 6 km from the terminus. At 4 km from the terminus, Fine Beam 2009/10 experiences velocity of 32 m a^{-1} while the accumulation years of TSX 2019/20, 2020/21 and 2021/22, experience 22 m a^{-1}, 22 m a^{-1} and 23 m a^{-1}, respectively, just within the error limits.

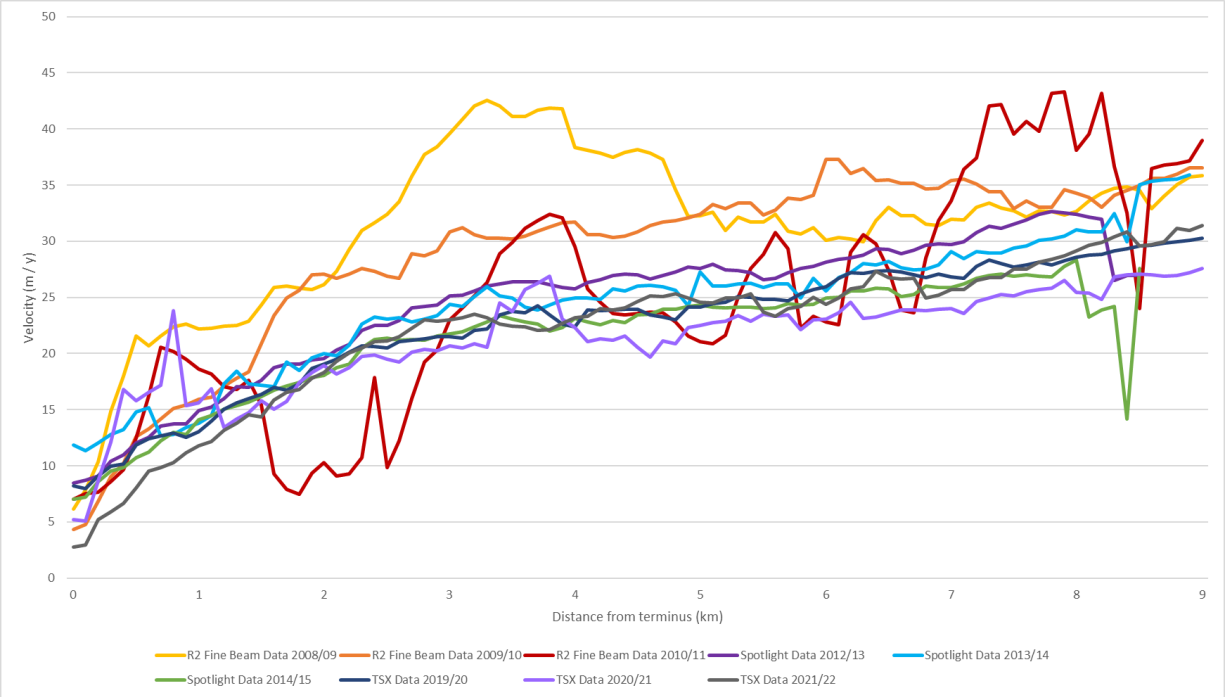

***Figure 5-28**. Velocity structure of the terminus (up to 9 km upglacier) of Thompson Glacier from 2008 to 2021, using non-summer yearly averages from each dataset. Fine Beam data covers 2008/09, 2009/10 and 2010/11. R2 Spotlight data covers 2012/13, 2013/14, 2014/15. TSX data covers 2019/20 and 2020/21. R2 Fine Beam has an error of 6 m a^{-1} and both R2 Spotlight and TSX have an error of 4 m a^{-1}.*

5.3.1.2 White Glacier

Data from the accumulation seasons from 2008/09 – 2021/22 was also used to create annual velocities of White Glacier (Figures 5-29 and 5-30; Table 5-5). The earlier years of 2008/09, 2009/10 and 2010/11, are a compilation of R2 Fine Beam velocities.

Figure 5-29 shows the surface ice velocities of R2 Fine Beam, R2 Spotlight and TSX datasets for White Glacier. There is a lot of variability in velocity across the length of the White Glacier between the different years. The surface velocity of R2 Spotlight data for 2012/13 is significantly higher from 0.8 km to 2.6 km, while the data only extends 4.3 km from the terminus (Figure 5.30). At 2 km from the terminus, R2 Spotlight data from the 2012/13 accumulation year has a velocity of 26 m a^{-1}, while the other datasets have velocities of 11 m a^{-1} and below at that same distance from the terminus (Figure 5-29 and Figure 5-30). At 3.3 km from the terminus, all three accumulation years of R2 Spotlight are greater than R2 Fine Beam and TSX data, 29 m a^{-1}, 25 m a^{-1} and 19 m a^{-1} compared to 14 m a^{-1} for TSX data from 2021/22, while the remaining datasets show velocities below 10 m a^{-1}.

The R2 Spotlight data is more variable in the first 4 km from the terminus, while the R2 Fine Beam data has the greatest variability, particularly further up-glacier, at a distance of 7 km from the terminus and continuing upglacier, beyond the error margins. The Fine Beam data for accumulation year 2010/11 is a composite of 2 image pairs from early in the fall (Figure 5-29) and could be the cause for it having greater variability.

Table 5-5. *Number of image pairs used for each non-summer velocity average of Figures 5-29 and 5-30 for White Glacier.*

Accumulation year	Sensor	# images
2008-2009	R2 Fine Beam	25
2009-2010	R2 Fine Beam	17
2010-2011	R2 Fine Beam	2
2012-2013	R2 Spotlight	2
2013-2014	R2 Spotlight	6
2014-2015	R2 Spotlight	3
2019-2020	TSX	4
2020-2021	TSX	13
2021-2022	TSX	12

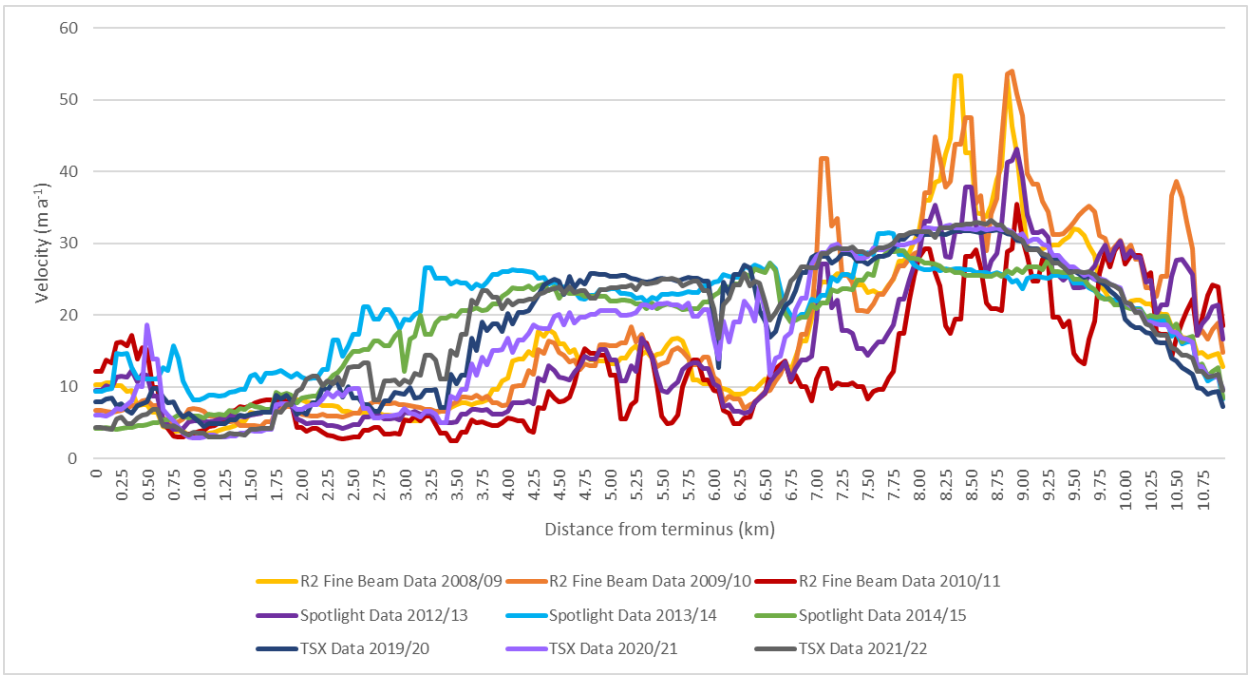

Figure 5-29. *Velocity structure of White Glacier from 2008 to 2021, using non-summer yearly averages from each dataset. Fine Beam data covers 2008/09, 2009/10 and 2010/11. R2 Spotlight data covers 2012/13, 2013/14, 2014/15. TSX data covers 2019/20 and 2020/21. No error bars were included in the graph for legibility; however, R2 Fine Beam has an error of 6 m a^{-1} and both R2 Spotlight and TSX have an error of 4 m a^{-1}.*

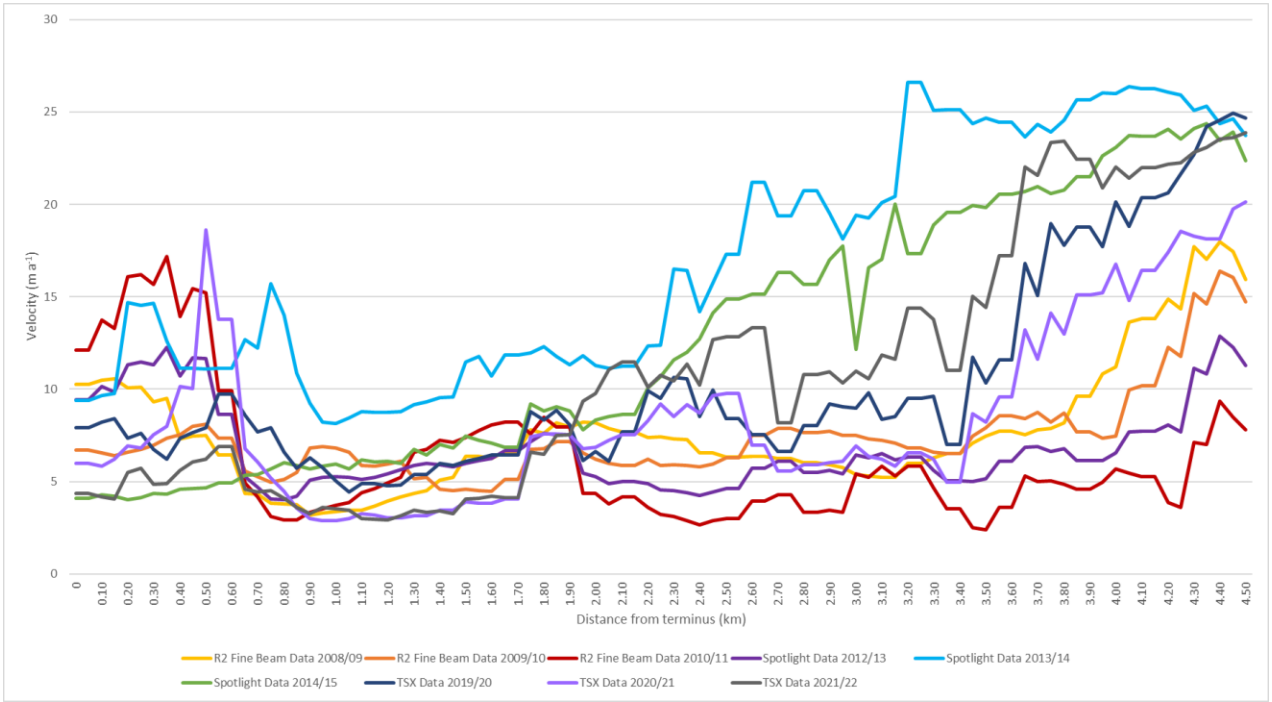

Figure 5-30*. Velocity structure of the terminus (up to 4.5 km upglacier) of White Glacier from 2008 to 2021, using non-summer yearly averages from each dataset. Fine Beam data covers 2008/09, 2009/10 and 2010/11. R2 Spotlight data covers 2012/13, 2013/14, 2014/15. TSX data covers 2019/20 and 2020/21. Error bars of 4 m a^{-1} for R2 Spotlight are included for the 2014/15 and 2012/13 accumulation seasons for the R2 Spotlight datasets. The error bars for R2 Fine Beam (6 m a^{-1}) and TSX (4 m a^{-1}) were not included for legibility of the graph.*

5.3.1.3 Discussion of long-term velocity changes

There is no long-term change in velocity for either Thompson or White Glacier based on the data available for this study, as would be expected with the negative mass balance regime in the CAA (Derksen et al., 2019). Glaciers respond to a negative mass balance by thinning and receding as less ice is transported downglacier and is particularly evident in lower parts of the glacier (Heid and Kääb, 2012). The time it takes for the glacier to start being affected by a change in mass balance is the reaction time, which can be rapid, compared to the response time of glaciers, the time it takes for the glacier to adjust its terminus position and velocity, which that takes place over tens to several thousand years (Heid and Kääb, 2012). Both Thompson and White Glaciers are dynamically stable (Van Wychen et al., 2016; Thomson and Copland 2017b) – they do not undergo surge-type or pulse-type behavior – so changes in velocity over time would be due to changes in mass balance.

Although there is variability of the surface velocity on White Glacier, there is no visible trend of an increase or decrease in velocity over time. While there are some differences beyond the error limits from 2.5 to 4.5 km from the terminus, there is no continuous deceleration over the years as would be expected with a negative mass balance. With a negative mass balance being experienced, less ice mass is being accumulated and less ice is transported downglacier, resulting in a slowdown of glacier motion, particularly in the terminus region (Heid and Kääb, 2012). Typically, glaciers respond by thinning and retreating (Benn and Evans, 2010; Heid and Kääb, 2012). White Glacier has experienced a negative mass balance since the 1970s (Cogley et al., 2011). A previous study (Thomson and Copland, 2017b) used dGPS data to show that there was a reduced mean annual velocity at the lower elevations of White Glacier. There was no detectable change upglacier, which the SAR velocity data in this study agrees with, particularly upglacier of 9 km. The GPS data shows that White Glacier has experienced a slowdown in the terminus region (Thomson and Copland, 2017b), likely due to the glacier being frozen to the bed and moving by decreased internal deformation at the terminus region (Heid and Kääb, 2012) and reduced basal motion from an increased hydraulic efficiency (Thompson and Copland, 2017b). These changes are likely too small to be determined by the SAR data of this study. Upglacier, Thomson and Copland (2017b) found no detectable change in glacier motion and expected their result to be due to decreased internal deformation from thinning of White Glacier being offset by in basal motion in the summer and winter. This is likely due to water accessing an inefficient subglacial system (Thomson and Copland 2017b), where the water is more likely to have an effect on glacier motion by reducing friction at the ice-bed interface.

There is however a change in velocity over the time period of this study that occurs over the same length of Thompson Glacier but is not a continuous increase or decrease. There is no real change below 9 km, however, differences beyond the error limits of surface velocity Thompson Glacier are seen between ~16 and 24 km from the terminus. The datasets that show these changes are R2 Fine Beam and TSX, as R2 Spotlight does not extend this far upglacier. There is no pattern of which accumulation year will have a greater or lower maximum velocity. The greatest velocity occurred in the 2010/11 accumulation season (R2 Fine Beam). The TSX velocity from 2021/22 was the next greatest velocity of Thompson Glacier. The accumulation seasons of 2008/09 and 2009/10 (R2 Fine Beam data) were within the error limits. TSX data for the 2019/20 accumulation season had the second lowest surface velocity along the ~16 to 24 km distance, while TSX data for the 2020/21 accumulation season had the lowest velocity (Figure 5-26). The seemingly random but significant differences in velocity along this section of the main trunk of Thompson Glacier could be explained by annual changes in the efficiency of the subglacial hydrology.

As there is no pattern to which year has a greater surface velocity on Thompson Glacier, subglacial hydrology and the amount of melt that reaches the bed in the summer is likely what influences the velocity during the accumulation season. The supraglacial system is composed of the movement and storage of water on the glacier surface, while the englacial system transports water on the surface of the glacier to the bed. The subglacial system impacts glacier velocity based on the quantity of water at the ice-bed interface. If there is increased melt during the summer, it is likely that the subglacial hydrology will switch to an efficient or channelized system, reducing the lubricating effect and resulting in a slower velocity. If the amount of water in the subglacial system is not substantial enough to cause a switch from inefficient to an efficient system, the water in the subglacial system will reduce the friction at the ice-bed interface and cause greater motion. For Thompson Glacier the amount of melt and water in the subglacial system is possibly what is causing the difference in surface velocity between accumulation years (Figure 5-26).

The difference in velocity between years would be continuously decreasing if the changes in velocity were caused by changing dynamics from a negative mass balance regime (Heid and Kääb, 2012). Therefore, it is likely that difference in magnitude of velocity between accumulation years on Thompson Glacier (Figure 5-27) is likely due to the amount of melt formed and transported to the glacier bed during the melt season that remains at the ice-bed interface and stays into the winter, particularly due to the persistence of an inefficient subglacial hydrology system through the summer melt season. The summers that have a stronger melt can impact the motion during following accumulation seasons. A melt season that does not cause enough melt to switch to an efficient subglacial system will likely form pockets of

water at the glacier bed that will persist further into the winter season than years of lower melt. The smaller pockets of water created during a weaker melt season will freeze faster in the winter and not have as much impact on the total winter accumulation velocity. Potentially, a summer melt season with stronger melt, although not enough to switch to an efficient system that rapidly evacuates water, will continue to impact glacier velocity into the winter and cause greater motion by acting as a lubricant at the ice-bed interface.

The expected change that the velocity of both glaciers should be slowing down over time because they are stable and therefore controlled by mass balance (Heid and Kääb, 2012), is not seen here. This could be due to the fact that the change in glacier velocity may be too small to be picked up with the resolution of the SAR data or the glaciers are too small for this change to be noticeable. While there was an interesting change in the velocity of Thompson Glacier over the years, it is likely due to the persistence of an inefficient subglacial system and not a continual decrease in velocity of the years as would be expected from a negative mass balance regime.

5.3.2 Detection of short-term velocity change – seasonality

One of the main goals of this research is to properly identify and understand the drivers of seasonality on AHI. First, investigation into any seasonality on Thompson Glacier will be explored then intra-annual variability of White Glacier will be investigated. The investigation into seasonality was performed using the dense record of TSX data over both glaciers for the 2020/21 and 2021/22 accumulation seasons (Table 5-6). R2 Spotlight data is not used for this analysis, as there is no fall data provided for the accumulation seasons. Fine Beam data was not used for this investigation as it is not consistent enough as it had the greatest error and variable distribution of image pairs across the seasons. The majority of R2 Fine Beam acquisitions were from the spring, and some beam modes only had data for the spring and not fall or winter. TSX data had a similar number of acquisitions for each non-summer season for the 2020/21 and 2021/22 accumulation seasons.

Table 5-6. *Number of images used to represent the average velocity of each year for each season of Figures 43 and 47 for both Thompson and White Glaciers.*

Season	Year	# image pairs
Fall	2020	2
	2021	4
Winter	2020/21	5
	2021/22	4
Spring	2021	6
	2022	4

5.3.2.1 Thompson Glacier

Early research found consistent glacier flow speeds throughout the entire year in high Arctic regions, but seasonal changes in glacier velocity structure were later observed and it has become well known that glaciers within the Canadian Arctic experience seasonality in flow (Müller and Iken, 1973; Thomson and Copland, 2017b). This section will first present and discuss seasonal trends in velocity structure from the TSX data for Thompson Glacier.

Figures 5-31 and 5-32 shows the seasonal (fall, winter and spring) average centerline velocities of Thompson Glacier using TSX data for the 2020 to 2021 and 2021 to 2022 accumulation seasons, respectively. Table 5-6 provides the number of images used for Thompson Glacier's seasonal average centerline velocities for Figures 5-31 and 5-32. The error bars, using the mean error for TSX data of 4 m a^{-1} (Table 5-2), were placed on all series, representing the fall, winter and spring velocities.

The velocities for Thompson Glacier follow the same trend along the length of the glacier with winter and spring velocities being most similar. For a short distance in the first kilometer of the terminus of Thompson Glacier, the spring 2021 velocity reaches 23 m a^{-1} at 0.5 km from the terminus, while the fall and winter velocities for the accumulation year reach 18 and 12 m a^{-1}, respectively, around 1 km from terminus. Approaching 4 km from the terminus, the spring velocity is greater than fall and winter for a short distance. At 3.8 km, spring reaches 31 m a^{-1}, while fall and winter reach 16 and 25 m a^{-1}. At 3.9 km, spring velocity decreases to 20 m a^{-1}, while fall and winter (19 and 25 m a^{-1}, respectively).

At 12 km from the terminus, the fall surface velocity is 45 m a^{-1}, while winter is 43 m a^{-1} and spring is 40 m a^{-1}. The fall velocity continues to be greater than the spring velocity, although not beyond the error limits, until 27.7 km from the terminus, where the fall velocity is 60 m a^{-1} and the spring velocity is 56 m a^{-1}. At 17.7 km, the fall velocity is above the error limit compared to the winter velocity, 63 and 59 m a^{-1}, respectively, until 21.7 km. At 21.7 km, the winter velocity is 70 m a^{-1} while the fall velocity is 74 m a^{-1}. From 27.7 km further upglacier, the surface velocities between seasons are in good agreement. At a distance of 32 km from the terminus, fall experiences an average velocity of 40 m a^{-1}, while both winter and spring experience a velocity of 37 m a^{-1}. The seasonal velocities are mostly within the combined error limits along the length of the glacier.

The following accumulation year, 2021 to 2022 (Figure 5-32), shows a similar trend of the fall velocity being greater and beyond the error limits for short sections along a similar length of Thompson Glacier. The fall surface velocity is at the error limits of winter and spring from 13 km until 26 km from the terminus and is beyond the error limit for shorter sections between 20 to 21.2 km and 22.1 to 23 km from the terminus. At 13 km, fall velocity is 57 m a^{-1}, while the winter velocity is 51 m a^{-1} and spring is 45 m a^{-1}. At 26 km, the fall velocity falls to 68 m a^{-1}, while winter and spring maintain velocities of 74 and 71 m a^{-1}. Further upglacier from 26 km, the winter and spring surface velocities are very consistent, while there is no available velocity data for fall beyond 27 km.

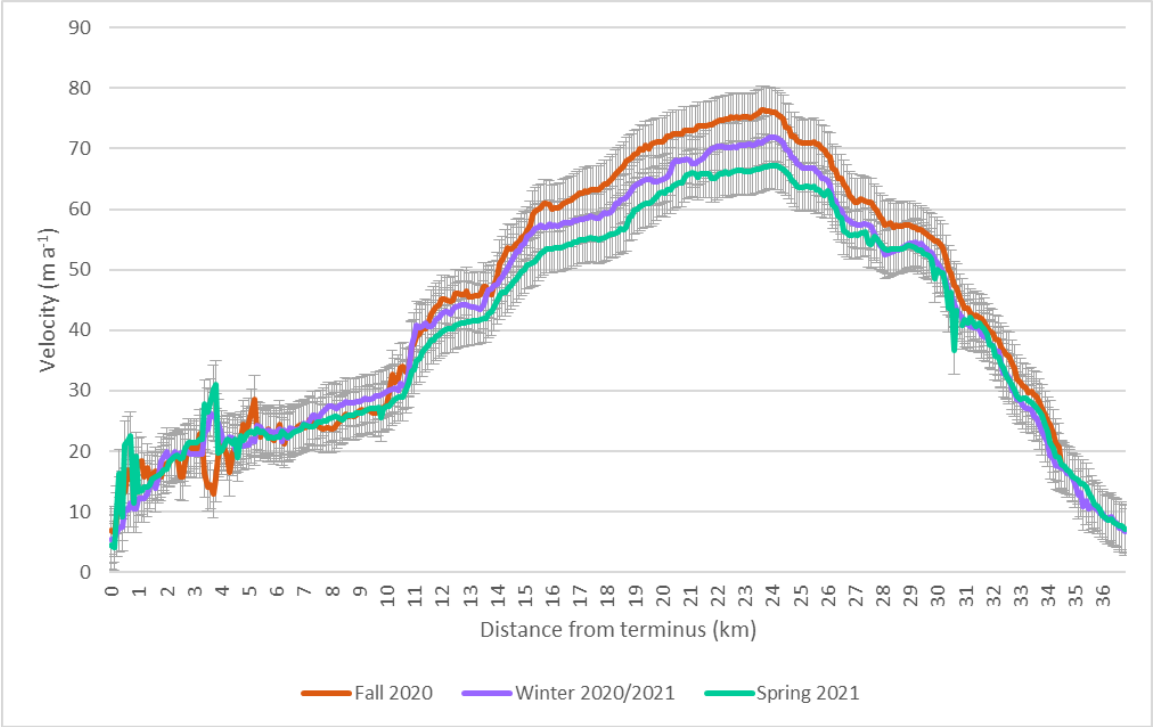

***Figure 5-31**. Average seasonal velocities for accumulation year 2020 - 2021 TSX data of Thompson Glacier. Error bars of 4 m a^{-1} were included on each series representing the non-summer seasons.*

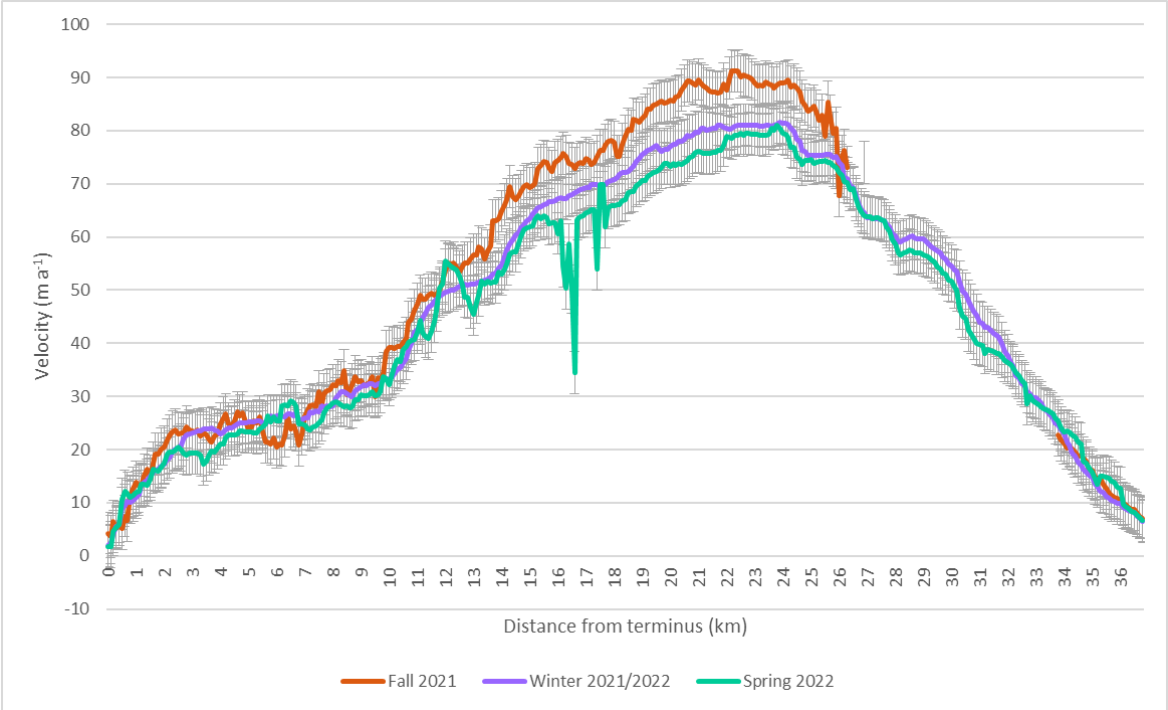

***Figure 5-32.** Average seasonal velocities for accumulation year 2021 – 2022 TSX data of Thompson Glacier. Error bars of 4 m a^{-1} were included on each series representing the non-summer seasons.*

5.3.2.2 White Glacier

For White Glacier, there were no significant differences in TSX velocities between seasons, but the most variability can be seen in the fall (Figure 5-33 and 5-34). Table 5-6 shows the number of image pairs used for each season of each accumulation year of TSX data used to investigate seasonality. While there are some locations along White Glacier during the 2020/21 accumulation season where fall has a greater velocity compared to winter and spring, beyond error limits (Figure 5-33). However, the following accumulation season (Figure 5-34) does not show the same trend. Both accumulation seasons show variability in glacier motion around 6 km from the terminus (Figure 5-33 and 5-34), as previously seen in Figure 5-29, likely indicating a physical obstruction to glacier flow however there is lack details of bed topography to know this for sure. Greater variability is seen along the terminus, particularly in Figure 5-34, compared to the rest of the glacier, which is where the greatest sliding typically occurs (Ben and Evans, 2010).

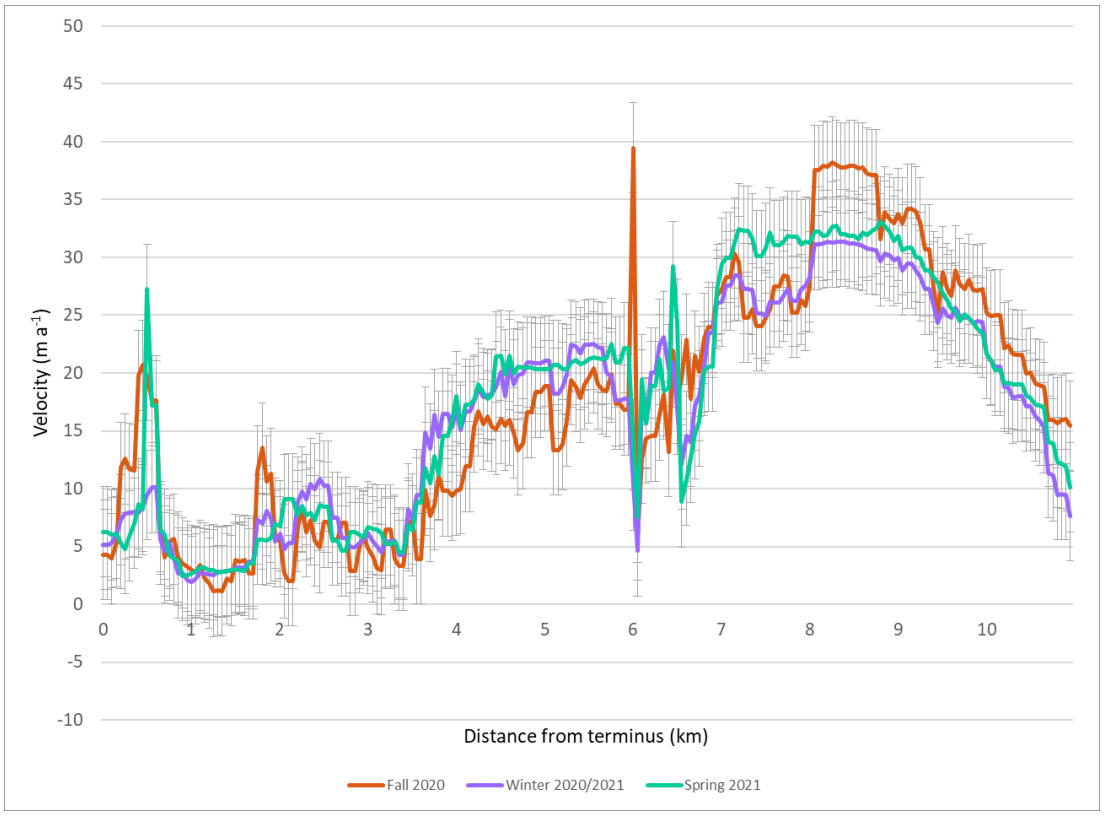

Figure 5-33. *Average seasonal velocities for accumulation year 2020 - 2021 TSX data of White Glacier. Error bars of 4 m a^{-1} were included on each series representing the non-summer seasons.*

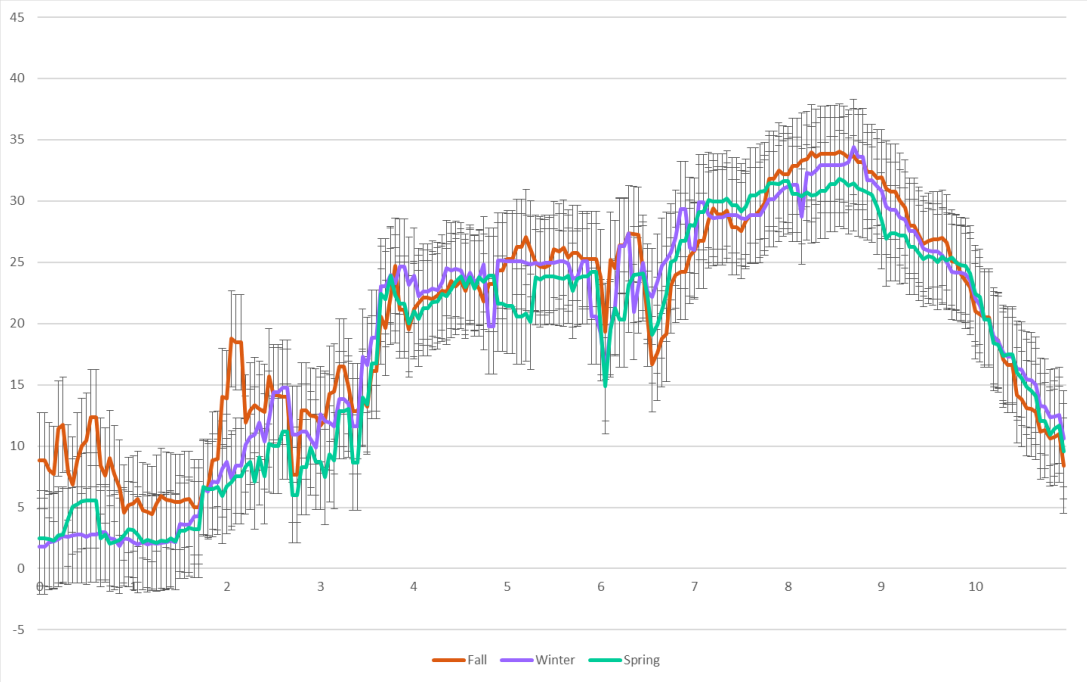

Figure 5-34. *Average seasonal velocities for the accumulation year of 2021 to 2022 for White Glacier. Error bars of 4 m a^{-1} were included on each series representing the non-summer seasons.*

5.3.2.3 Discussion of seasonality

There are two accumulation seasons, 2020 to 2021 and 2021 to 2022, that show the fall velocity being greater than both winter and spring surface velocities, for at least a part of the length of Thompson Glacier, from ~15 km to 26 km from the glacier terminus. This shows that the greater velocity experienced in the fall is most likely real change and indicative of seasonality and not just error. However, this pattern of seasonality is not expected. As previously described, the fall surface velocity should be slowest, particularly after the summer melt season when all the subglacial water is being efficiently evacuated due to the switch to an efficient subglacial drainage system. This does not seem to be the case for Thompson Glacier. It is possible that the subglacial hydrological system does not have enough meltwater during the summer months to switch the subglacial hydrology from an inefficient system to an efficient one. With no major evacuation of subglacial water in the summer months, a large enough amount of water may remain in pockets along the ice-bed interface the fall, assisting the glacier flow, resulting in the faster velocity being experienced in the fall. In the winter months, the remaining meltwater that remains in the subglacial hydrological system, would start to refreeze due to the decreased temperature and Thompson Glacier being a thin glacier. By the middle to end of winter, all remaining water underneath the glacier would most likely be frozen, explaining why the velocity is lowest during the spring.

The maximum fall surface velocity experienced during the 2020 to 2021 accumulation season is 76 m a^{-1} at 24 km from the terminus (Figure 5-31), while the maximum velocity experienced in the fall of the 2021 to 2020 accumulation season is 91 m a^{-1} at 22.3 km from the terminus (Figure 5-32). The 15 m a^{-1} difference between maximum velocities could be explained by the difference in summer melt between the years, a weak compared to a strong melt experienced in the prior summer. Therefore, it is possible that the summer of 2020 had weaker melt, with smaller pockets of water that remained into the accumulation season. The smaller amount of water would refreeze faster than larger areas of water in the subglacial system, reducing its impact on glacier velocity earlier in the year. The summer of 2021 could have then experienced strong melt, where larger pockets of water remained into the fall, causing greater velocities than the previous fall. The larger water pockets would take longer to refreeze in the winter, resulting in more glacier motion later into the accumulation year. As this pattern of fall velocity being greater than both winter and spring surface velocities are consistent between the years, it is likely an indication of some seasonality and not random error.

For White Glacier (Figures 5-33 and 5-34) there is no obvious pattern or sign of seasonality. There is greater variability of velocity on White Glacier compared to Thompson Glacier (Figures 5-31 and 5-32). Seasonality was expected to be seen on White Glacier, as there are studies going back to the 1960s that first proved glaciers undergo seasonal changes to their velocity structure using in situ data (Müller and Iken, 1973). White Glacier has continued to be a glacier of interest because of the dense in site mass balance and velocity measurements. However, the results of this study do not show signs of seasonality on this small, land terminating glacier. It is possible the glacier is too small for these seasonal changes to be picked up by the SAR sensors.

5.4 Summary of Results and Discussion

The main findings of section 5.1 are that the surface velocities of both Thompson and White Glaciers are consistent and follow the expected velocity structure of land terminating glaciers (Short and Gray 2005; Van Wychen et al., 2016). Despite slightly different methodologies, the results of the velocity products derived in this study are in agreement with previous research (Short and Gray 2005; Van Wychen et al., 2016; 2017). Section 5.1 satisfies the first objective of this study, which was to utilize a large catalogue of previously unused SAR data to produce velocity maps by processing 71 useable images from R2 Fine Beam and TSX.

Section 5.2 provided an error analysis of derived velocity products, compared different SAR datasets and compared R2 Spotlight with in situ GPS data. TSX and R2 Spotlight had the best results and lowest error of 4 m a^{-1}, R2 Yearly had an average error of 6 m a^{-1} and R2 Fine Beam had an error of 7 m a^{-1}. The direct comparison between TSX, S1 and R2 Yearly showed that S1 and R2 both have much greater variability and noise in the velocity products, while TSX provided more consistent results. The comparison with GPS data showed a pretty good agreement close to 10 m a^{-1}. This section satisfied the second research objective of this study, error analysis and comparison of SAR datasets.

Section 5.3 investigated both long and short-term changes in the velocity structure of White and Thompson Glaciers. These glaciers did not show the expected decrease in velocity over time. There was subtle display of seasonality and long-term changes in the velocity structure of Thompson Glacier, interestingly, both were along the same section of the main trunk, likely due to the persistence of an inefficient subglacial system through the summer. White Glacier did not show evidence of seasonality based on the SAR data, likely from the small size of the glacier and SAR resolution not being high enough to determine any change. This section satisfied the third objective of investigating seasonality and long-term changes in velocity structure of both White and Thompson Glaciers.

Chapter Six – Conclusions and Significance

6.0 Thesis overview

The CAA is experiencing warming at rates that are twice the global average (Derksen et al., 2019). Glaciers in the CAA have been experiencing a negative mass balance that can influence the velocity structure of glaciers over time. As such, building large catalogues of glacier motion over a variety of glaciers, and characterizing variations in glacier flow over time, is important to know how these glaciers are changing with a warming climate. White and Thompson Glaciers on AHI were the main glaciers of interest in this study, both glaciers are known to be dynamically stable and do not undergo surge or pulse type behavior and thus provide a good site to determine how ice motion is evolving for smaller, land terminating glaciers in the Canadian Arctic. Given this, the purpose of this thesis was to do an in-depth analysis of the flow of these two glaciers, which have a large amount of SAR data available to enable this work. The specific research objects of this study were:

1) Utilize a large catalogue (71 image pairs) of SAR datasets (R2 Fine Beam, R2 Spotlight and TSX) that have not previously been used to its full extent and create a dense record of velocity maps for Thompson and White Glaciers over the 2008 to 2022 period;

2) Provide an assessment of different SAR datasets (R2 (Fine Beam, Spotlight and Yearly), S1 and TSX) for deriving glacier monitoring of Thompson and White Glaciers on Axel Heiberg Island;

3) Use the record created in objective 1, to investigate long-term and short-term (seasonality) velocity variability from the derived velocity products for Thompson and White Glaciers on AHI and explore drivers of observed changes

The purpose of this section is to recap the objectives and main findings of this thesis and review the significance of the results based on the main goals of this research.

6.1 Thesis summary

Research objective 1

With regard to research objective 1, the outcomes of this research satisfy the goal of rescuing a large volume of SAR data that has not been previously used to measure glacier velocity for this region. The dense time series of 71 images, has improved the amount of data available to understand ice dynamics of AHI and adds to previous studies that only used a few image pairs to represent an entire year of ice motion (Van Wychen et al., 2016; 2021). The velocities derived in this study are in agreement with

previous studies (Short and Gray, 2005; Van Wychen et al., 2016; 2017) and show that both White and Thompson Glaciers follow the expected velocity structure of land terminating glaciers, with a slower velocity below 20 m a^{-1} near the terminus then increasing to reach its maximum along the main trunk before decreasing again to below 20 m a^{-1} near the accumulation basin. These velocity products will be made openly available for future studies in the area, which will help investigations into long term changes in velocity structure.

Research objective 2

In terms of research objective two, an assessment of the SAR datasets used in this research, this study found that TSX and R2 Spotlight are comparable with calculated bedrock errors of 4 ± 3 m a^{-1} and 4 ± 4 m a^{-1}, respectively. These datasets are better used for velocity investigations where finer details may be desired, such as studying a smaller glacier or shorter time-periods, like seasonality. The R2 Fine Beam velocity products derived in this study produced an error of 7 ± 10 m a^{-1}. This was comparable to the pre-derived velocity products from Van Wychen et al., (2016; 2020), where the error was found to be 6 ± 5 m a^{-1}. The R2 Fine Beam and R2 Yearly would be better for a regional scale analysis of velocity or for studies that span a longer time period, where there is less need for fine details. It was found that it is better to average the error by accumulation season as opposed to averaging the entire year, as the loss of coherence during the summer months skews the error over bedrock. The SAR derived error over bedrock for R2 Spotlight (mean error of 4 m a^{-1} and SD of 4 m a^{-1}) was in good agreement with the GPS station data and largely within 10 m a^{-1}, based on the 9 R2 Spotlight image pairs that had corresponding GPS data available. The results of the GPS comparison were in good agreement with previous studies that compared GPS to SAR derived velocities (Schellenberger et al., 2016; Van Wychen et al., 2012).

Research objective 3

In terms of research objective three, the determination of long-term and short-term change, this research found that there was no continuous deceleration for the past decade for either Thompson or White Glaciers, as was expected based on previous studies that show a deceleration due to a negative mass balance (Thompson and Copland, 2017b; Heid and Kääb, 2012). There is a change in the velocity over a section of the main trunk of Thompson Glacier beyond the error limits when investigating both long term and seasonal trends, from ~16–24 km from the terminus. The inter and intra-annual differences

in velocity are likely due to the development and efficiency of the subglacial hydrology system. There was no continuous deceleration of White Glacier detected for the near decade of SAR data available for this study, however, there was a significant difference near the terminus, between 2.5 and 4.5 km. The SAR data did not show seasonality for White Glacier, although there is evidence from previous research using in situ data (Müller and Iken, 1973; Thomson and Copland, 2017a) that show there is seasonality that occurs on White Glacier. It is likely that seasonality was not detected because the glacier is too small for SAR resolution to pick up these changes.

The velocity records that were previously unused, provide a dense surface velocity dataset over White and Thompson Glacier that will be important for future research looking at long term changes. The best data to use to investigate seasonality and inter-annual changes in velocity structure over small and medium sized glaciers would be either TSX or R2 Spotlight. This may also indicate that SAR may not be able to detect seasonality on small and medium sized land terminating glaciers in the CA. This is useful as most of the previous research on seasonality focused on larger land terminating or tidewater terminating glaciers and have primarily utilized spatially limited in situ methods. Previous research has also not done an assessment of seasonality using only SAR data. The approach used may be useful for other glaciers in areas where in situ data is unavailable, particularly since the velocity products will be openly available for future research.

This study accomplished the three research objectives that were initially set out. The main findings of the investigation into long term and seasonal changes in velocity structure were that the results were consistent with findings of previous remote sensing-based studies (Van Wychen et al., 2017) but were less consistent compared to in situ based studies (Thomson and Copland, 2017a and b). The was no continuous deceleration visible for White Glacier, while Thompson Glacier had subtle but consistent differences between accumulation years possibly due to subglacial hydrology. There was no seasonality detected over White Glacier, while it is known that this glacier does experience seasonality as proven with in situ data by previous research (Müller and Iken 1973; Thomson and Copland 2017a). Seasonality was detected on Thompson Glacier, but it was not what was expected, as fall had the greatest velocity, followed by winter and spring. It was expected that fall would have the slowest velocity since it follows the summer melt season where typically, meltwater is drained through an efficient subglacial system, reducing the impact that water along the ice-bed interface has on glacier motion. This is not the case based on the SAR data in this study, suggesting a different subglacial process is occurring for this glacier.

6.2 Outlook

The major dataset for deriving ice motion in the Canadian Arctic over the last decade was R2 data, but it is now largely unavailable. However, since ~2015, S1 data has become freely available and is regularly collected over the CA but has a much greater error than other available datasets, like R2 Spotlight and TSX. Going forward, R2 Spotlight and TSX sensors should be considered for use of glacier monitoring in the CA, due to less noise and variability, lower error and uncertainty and increased accuracy compared to other available data. However, S1 being freely available over the area may be beneficial to some, depending on the aim of the research.

Future work can add on to this dense time series over White and Thompson Glaciers. Another possibility for future work that may be able to determine seasonality would be interferometric SAR (inSAR), that can provide up to millimetre accuracy. This may be a better option to investigate seasonality over small and medium sized glaciers like White and Thompson Glaciers. The addition of summer velocities using optical imagery may gain further insight into why Thompson Glacier experiences the greatest velocity in the fall, as opposed to spring, since what happens during the summer season can influence velocity structure during the following accumulation season.

6.3 Thesis significance

This research augments previous datasets of glacier velocity research in the Canadian Arctic by adding a dense time series of velocity products (71 images) for Thompson and White Glaciers. The velocity products produced in this study are in agreement with previous studies, that Thompson and White Glaciers follow the expected velocity structure of land terminating glaciers and that both glaciers are dynamically stable and slow moving. The use of GAMMA offset tracking in this study, compared to previous studies that used a Matlab speckle tracking algorithm, show largely the same results. These velocity products were in pretty good agreement with the in-situ GPS data available over White Glacier. Future studies investigating seasonality may prefer to use R2 Spotlight or TSX data as they have a higher spatial resolution and lower error than the other SAR datasets (R2 Yearly, R2 Fine Beam and R2 Spotlight) used in this study.

The SAR data currently available was not able to show seasonality on either Thompson or White Glacier, as any changes are largely within the error limits. However, there was a difference between seasons on Thompson Glacier along the same length where long term changes were experienced. As these are along the same length of the glacier, it is likely not error and some real change due to the amount of melt produced, strong or weak, during the summer with the continuation of an inefficient subglacial

system. This is an interesting finding that should be further explored. Having a dense velocity record is helpful for future studies to follow changes or trends.

The majority of previous studies that investigated the variability of ice motion have concentrated on larger tidewater terminating glaciers (Short and Gray, 2005; Van Wychen et al., 2016; Medzrycka et al., 2019). Research that investigated smaller glaciers used either in situ data or a few SAR image pairs to represent ice motion for an entire year. (Thomson and Copland 2017a; Thomson and Copland 2017b; Van Wychen et al., 2016; Van Wychen et al., 2017). This study addresses a research gap and is the first that does a deep dive into the variability of smaller, land terminating glaciers using a dense record of SAR data. This study also is a first to do a comparison of multiple SAR datasets used for deriving ice motion in the region. The study adds to previous research of these glaciers and augments the velocity data for Thompson and White Glaciers. This study will help future research as the derived velocity products will be made openly available for long-term preservation and dissemination.

References

ASF. (n.d.). *What is SAR?* ASF. Retrieved September 6, 2021, from https://asf.alaska.edu/information/sar-information/what-is-sar/

Banks, S. (2021, August 9). *Synthetic Aperture Radar and Remote Sensing* [Online lecture]. Zoom @ Carleton University. https://curesearch.sharefile.com/Authentication/Login

Benn, D. I. & Evans, D. J. A. (2010). *Glaciers & glaciation*. 2nd ed. Hodder Education.

Blatter, H. (1987). Stagnant Ice at the Bed of White Glacier, Axel Heiberg Island. N.W.T., Canada. *Annals of Glaciology*, *9*, 35–38. https://doi.org/10.3189/S0260305500200724

Blatter, H. (1987). On the Thermal Regime of an Arctic Valley Glacier: A Study of White Glacier, Axel Heiberg Island, N.W.T., Canada. *Journal of Glaciology*, *33*(114), 200–211. https://doi.org/10.3189/S0022143000008704

Chandler, B. M. P., & Evans, D. J. A. (2021). Glacial Processes and Sediments. In D. Alderton & S. A. Elias (Eds.), *Encyclopedia of Geology (Second Edition),* 830–856. Academic Press. https://doi.org/10.1016/B978-0-12-409548-9.11902-5

Cogley, J. Graham, et al. (1996). Mass Balance of White Glacier, Axel Heiberg Island, N.W.T., Canada, 1960–91. *Journal of Glaciology*, *42*(142), 548–563. doi:10.3189/S0022143000003531.

Cogley, J. G., Adams, W. P., & Ecclestone, M. A. (2011). Half a Century of Measurements of Glaciers on Axel Heiberg Island, Nunavut, Canada. *ARCTIC*, *64*(3), 371–375. https://doi.org/10.14430/arctic4127

Copland, L., Sharp, M. J., & Dowdeswell, J. A. (2003). The distribution and flow characteristics of surge-type glaciers in the Canadian High Arctic. *Journal of Glaciology*, *36*, 73–81. https://doi.org/10.3189/172756403781816301

Copland, L., 2013. Classification of ice masses. In: Shroder, J. (Editor in Chief), Giardino, R., Harbor, J. (Eds.), *Treatise on Geomorphology.* Academic Press, San Diego, CA, vol. 8, Glacial and Periglacial Geomorphology, pp. 45–52. https://doi.org/10.1016/B978-0-12-374739-6.00193-7

Cress, P., Wyness, R., (1961). The Devon Island expedition, observations of glacial movements. *Arctic 14*, 247–259.

Dalton, A., Van Wychen, W., Copland, L., Gray, L., & Burgess, D. (2022). Seasonal and Multiyear Flow Variability on the Prince of Wales Icefield, Ellesmere Island: 2009–2019. *Journal of Geophysical Research: Earth Surface*, *127*(4). https://doi.org/10.1029/2021JF006501

Danielson, B., & Sharp, M. (2013). Development and application of a time-lapse photograph analysis method to investigate the link between tidewater glacier flow variations and supraglacial lake drainage events. *Journal of Glaciology*, *59*(214), 287–302. https://doi.org/10.3189/2013JoG12J108

Derksen, C., Burgess, D., Duguay, C., Howell, S., Mudryk, L., Smith, S., Thackeray, C. and Kirchmeier-Young, M. (2019). Changes in snow, ice and permafrost across Canada; Chapter 5 in Canada's Changing Climate Report. E. Bush and D.S. Lemmen (Eds.). p.194-260. Government of Canada, Ottawa, Ontario,

Dowdeswell, J. A., et al. (1997). The mass balance of circumarctic glaciers and recent climate change. *Quaterly Research. 48*(1), 1–14

European Space Agency. (n.d.). *Level-1 Interferometric Wide Swath SLC Products*. Retrieved November 2, 2022, from https://sentinels.copernicus.eu/web/sentinel/technical-guides/sentinel-1-sar/products-algorithms/level-1/single-look-complex/interferometric-wide-swath

Fisher, D., Zheng, J., Burgess, D., Zdanowicz, C., Kinnard, C., Sharp, M., & Bourgeois, J. (2012). Recent melt rates of Canadian arctic ice caps are the highest in four millennia. *Global and Planetary Change*, *84–85*, 3–7. https://doi.org/10.1016/j.gloplacha.2011.06.005

Friedl, P., Seehaus, T., & Braun, M. (2021). Global time series and temporal mosaics of glacier surface velocities derived from Sentinel-1 data. *Earth System Science Data*, *13*(10), 4653–4675. https://doi.org/10.5194/essd-13-4653-2021

Government of Canada (n.d.). *RADARSAT satellites: Technical comparison*. Canadian Space Agency. (Accessed 2022, November 12). https://www.asc-csa.gc.ca/eng/satellites/radarsat/technical-features/radarsat-comparison.asp

Heid, T., & Kääb, A. (2012). Repeat optical satellite images reveal widespread and long term decrease in land-terminating glacier speeds. *The Cryosphere*, *6*(2), 467–478. https://doi.org/10.5194/tc-6-467-2012

Iken, A., (1974) Velocity fluctuations of an Arctic valley glacier, A study of the White Glacier, Axel Heiberg Island, Canadian Arctic Archipelago. *Axel Heiberg Island Research Reports, Glaciology.* No. 5, 123 pp.

Jiskoot, Hester, et al. (2000). Controls on the Distribution of Surge-Type Glaciers in Svalbard. *Journal of Glaciology*, 46(154), 412–22. https://doi.org/10.3189/172756500781833115.

Koerner, R. M. (2005). Mass balance of glaciers in the Queen Elizabeth Islands, Nunavut, Canada. *Annals of Glaciology*, *42*, 417–423. https://doi.org/10.3189/172756405781813122

Koerner, R. M. (1979). Accumulation, ablation, and oxygen isotope variations on the Queen Elizabeth Islands ice caps. Canada. *Journal of Glaciology, 22,* 25–41.

Lenaerts, J. T. M., Angelen, J. H. van, Broeke, M. R. van den, Gardner, A. S., Wouters, B., & Meijgaard, E. van. (2013). Irreversible mass loss of Canadian Arctic Archipelago glaciers. *Geophysical Research Letters*, *40*(5), 870–874. https://doi.org/10.1002/grl.50214

McNairn, H. (2021a, August 9). *Synthetic Aperture Radar and Remote Sensing* [Online lecture]. Zoom @ Carleton University. https://curesearch.sharefile.com/Authentication/Login

McNairn, H. (2021b, August 10). *Synthetic Aperture Radar and Remote Sensing* [Online lecture]. Zoom @ Carleton University. https://curesearch.sharefile.com/Authentication/Login

Medrzycka, D., Copland, L., Wychen, W. V., & Burgess, D. (2019). Seven decades of uninterrupted advance of Good Friday Glacier, Axel Heiberg Island, Arctic Canada. *Journal of Glaciology*, *65*(251), 440–452. https://doi.org/10.1017/jog.2019.21

Meier, M.F., Post, A. (1969). What are glacier surges? *Canadian Journal of Earth Sciences 6*(4), 807-817.

Müller, Fritz (1962). Zonation in the Accumulation Area of the Glaciers of Axel Heiberg Island, N.W.T., Canada. *Journal of Glaciology 4*(33), 302-311. DOI: 10.3189/S0022143000027623.

Müller, F., Iken, A. (1973). Velocity fluctuations and water regime of Arctic valley glaciers. International Association of Scientific Hydrology Publication (95 g., S. 165-182.).

Murray, T., Strozzi, T., Luckman, A., Jiskoot, H. and Christakos, P. (2003). Is there a single surge mechanism? Contrasts in dynamics between glacier surges in Svalbard and other regions. *Journal of Geophysical Research* 108, B5 2237, doi:10.1029/2002JB001906.

Nienow, P. W., Sole, A. J., Slater, D. A., & Cowton, T. R. (2017). Recent Advances in Our Understanding of the Role of Meltwater in the Greenland Ice Sheet System. *Current Climate Change Reports*, *3*(4), 330–344. https://doi.org/10.1007/s40641-017-0083-9.

Ommanney, C. (1969): A study in glacier inventory: The ice masses of Axel Heiberg Island, Canadian Arctic Archipelago. (Axel Heiberg Island Research Reports Glaciology 3)/

Pfeffer, W. T., et al. (2014). The Randolph Glacier Inventory: a globally complete inventory of glaciers. *Journal of Glaciology 60*:537-552.

Schellenberger, T., Van Wychen, W., Copland, L., Kääb, A., & Gray, L. (2016). An Inter-Comparison of Techniques for Determining Velocities of Maritime Arctic Glaciers, Svalbard, Using Radarsat-2 Wide Fine Mode Data. *Remote Sensing*, *8*(9), 785. https://doi.org/10.3390/rs8090785

Raymond, C. F. (1983). Deformation in the vicinity of ice divides. *Journal of Glaciology, 29*(103), 357–73.

Raymond, C. F. (1987). How do glaciers surge? A review. *Journal of Geophysical Research, 92*(91), 21–34.

Rohner, C., Small, D., Beutel, J., Henke, D., Lüthi, M. P., & Vieli, A. (2019). Multisensor validation of tidewater glacier flow fields derived from synthetic aperture radar (SAR) intensity tracking. *The Cryosphere*, *13*(11), 2953–2975. https://doi.org/10.5194/tc-13-2953-2019

Sevestre, Heïdi, and Douglas I. Benn. (2015). Climatic and Geometric Controls on the Global Distribution of Surge-Type Glaciers: Implications for a Unifying Model of Surging. *Journal of Glaciology*, *61(*228), 646–662. https://doi.org/10.3189/2015jog14j136.

Sevestre, H., Benn, D. I., Luckman, A., Nuth, C., Kohler, J., Lindbäck, K., & Pettersson, R. (2018). Tidewater glacier surges initiated at the terminus. *Journal of Geophysical Research: Earth Surface, 123*, 1035–1051. https://doi.org/10.1029/2017JF004358

Sharp, M., Burgess, D. O., Cawkwell, F., Copland, L., Davis, J. A., Dowdeswell, E. K., et al. (2014). in J. S. Kargel et al. (eds.). Remote sensing of recent glacier changes in the Canadian Arctic. *Global Land*

Ice Measurements from Space. (chap. 9, pp. 205–228). Praxis-Springer, Berlin, doi:10.1007/978-3-540-79818-7_9.

Sharp, M., Burgess, D. O., Cogley, J. G., Ecclestone, M., Labine, C., & Wolken, G. J. (2011). Extreme melt on Canada's Arctic ice caps in the 21st century. *Geophysical Research Letters*, *38*(11). https://doi.org/10.1029/2011GL047381

Short, N. H., & Gray, A. L. (2005). Glacier dynamics in the Canadian High Arctic from RADARSAT-1 speckle tracking. *Canadian Journal of Remote Sensing*, *31*(3), 225–239. https://doi.org/10.5589/m05-010

Strozzi, T., Paul, F., Wiesmann, A., Schellenberger, T., and Kääb, A. (2017). Circum-Arctic Changes in the Flow of Glaciers and Ice Caps from Satellite SAR Data between the 1990s and 2017. *Remote Sensing. 9*, 947, https://doi.org/10.3390/rs9090947

Sturm, M. (1987). Observations on the distribution and characteristics of potholes on surging glaciers. *J. Geophysical Research Letters, 92*(B9), 9015-9022.

Thomson, L. I., Osinski, G. R., & Ommanney, C. S. L. (2011). Glacier change on Axel Heiberg Island, Nunavut, Canada. *Journal of Glaciology*, *57*(206), 1079–1086. https://doi.org/10.3189/002214311798843287

Thomson, L. I., & Copland, L. (2017a). Changing contribution of peak velocity events to annual velocities following a multi-decadal slowdown at White Glacier. *Annals of Glaciology*, *58*(75pt2), 145–154. https://doi.org/10.1017/aog.2017.46

Thomson, L. I., & Copland, L. (2017b). Multi-decadal reduction in glacier velocities and mechanisms driving deceleration at polythermal White Glacier, Arctic Canada. *Journal of Glaciology*, *63*(239), 450–463. https://doi.org/10.1017/jog.2017.3

Van Wychen, W., Copland, L., Gray, L., Burgess, D., Danielson, B., & Sharp, M. (2012). Spatial and temporal variation of ice motion and ice flux from Devon Ice Cap, Nunavut, Canada. *Journal of Glaciology*, *58*(210), 657–664. https://doi.org/10.3189/2012JoG11J164

Van Wychen, W., Burgess, D. O., Gray, L., Copland, L., Sharp, M., Dowdeswell, J. A., & Benham, T. J. (2014). Glacier velocities and dynamic ice discharge from the Queen Elizabeth Islands, Nunavut, Canada. *Geophysical Research Letters*, *41*(2), 484–490. https://doi.org/10.1002/2013GL058558

Van Wychen, W., Davis, J., Burgess, D. O., Copland, L., Gray, L., Sharp, M., & Mortimer, C. (2016). Characterizing interannual variability of glacier dynamics and dynamic discharge (1999-2015) for the ice masses of Ellesmere and Axel Heiberg Islands, Nunavut, Canada: GLACIER DYNAMICS OF THE CANADIAN ARCTIC. *Journal of Geophysical Research: Earth Surface*, *121*(1), 39–63. https://doi.org/10.1002/2015JF003708

Van Wychen, W., Davis, J., Copland, L., Burgess, D. O., Gray, L., Sharp, M., Dowdeswell, J. A., & Benham, T. J. (2017). Variability in ice motion and dynamic discharge from Devon Ice Cap, Nunavut, Canada. *Journal of Glaciology*, *63*(239), 436–449. https://doi.org/10.1017/jog.2017.2

Van Wychen, W., Copland, L., & Burgess, D. (2020). Ice Masses of the Eastern Canadian Arctic Archipelago. In O. Slaymaker & N. Catto (Eds.), *Landscapes and Landforms of Eastern Canada* (pp. 297–314). Springer International Publishing. https://doi.org/10.1007/978-3-030-35137-3_13

Wychen, W. V., Burgess, D., Kochtitzky, W., Nikolic, N., Copland, L., & Gray, L. (2021). RADARSAT-2 Derived Glacier Velocities and Dynamic Discharge Estimates for the Canadian High Arctic: 2015–2020. *Canadian Journal of Remote Sensing*, *46*(6), 695–714. https://doi.org/10.1080/07038992.2020.1859359

Williamson, S., Sharp, M., Dowdeswell, J. & Benham, T. (2008). Iceberg calving rates from northern Ellesmere Island ice caps, Canadian Arctic, 1999-2003. *Journal of Glaciology*, *54*(186).

Wohlleben, T., Sharp, M. and Bush, A. (2009). Factors influencing the basal temperatures of a High Arctic polythermal glacier. *Annals of Glaciology,50*(52), pp.9-16.